Conservation and divergence of UVR8-COP1/SPA-HY5 signaling in UV-B responses of *Marchantia polymorpha*

Yuanke Liang[1,l,#], Roman Podolec[1,¶,#], Richard Chappuis[1], Emmanuel Defossez[2], Gaétan Glauser[3], Johannes Rötzer[4,5], Sara Christina Stolze[6], Liam Dolan[4], Hirofumi Nakagami[6], Emilie Demarsy[1], Roman Ulm[1,7,*]

[1]Department of Plant Sciences, Section of Biology, Faculty of Sciences, University of Geneva, 1211 Geneva 4, Switzerland

[2]Institute of Biology, University of Neuchâtel, 2000 Neuchâtel, Switzerland

[3]Neuchâtel Platform of Analytical Chemistry, University of Neuchâtel, 2000 Neuchâtel, Switzerland

[4]Gregor Mendel Institute of Molecular Plant Biology (GMI), Austrian Academy of Sciences, 1030 Vienna, Austria

[5]Vienna BioCenter PhD Program, Doctoral School of the University of Vienna and Medical University of Vienna, 1030 Vienna, Austria

[6]Max-Planck Institute for Plant Breeding Research, D-50829, Cologne, Germany

[7]Institute of Genetics and Genomics of Geneva (iGE3), University of Geneva, 1211 Geneva 4, Switzerland

[l]Present address: Max-Planck-Institute of Molecular Plant Physiology, Potsdam-Golm, Germany

[¶]Present address: Whitehead Institute for Biomedical Research, Cambridge, MA, USA

[#]Y.L. and R.P. contributed equally to this work.

*Author for correspondence: roman.ulm@unige.ch (R.U.)

ABSTRACT

Ultraviolet-B radiation (UV-B) poses a major challenge to all forms of plant life. The liverwort *Marchantia polymorpha* (Marchantia) serves as a key model organism to study signaling pathways and to infer their evolution throughout the green lineage. Marchantia expresses key components of UV-B signaling, including the photoreceptor UV RESISTANCE LOCUS 8 (MpUVR8), the

WD40-repeat protein REPRESSOR OF UV-B PHOTOMORPHOGENESIS (MpRUP), the E3 ubiquitin ligase complex CONSTITUTIVELY PHOTOMORPHOGENIC 1 / SUPPRESSOR OF phyA-105 (MpCOP1/MpSPA), and the transcriptional regulator ELONGATED HYPOCOTYL 5 (MpHY5). Here, we show that MpUVR8 exists as a homodimer in its ground-state in vivo, then monomerizes and accumulates in the nucleus upon UV-B activation. Activated MpUVR8 interacts with MpCOP1, triggering growth inhibition, gene expression changes, biosynthesis of UV-absorbing metabolites, and photoprotection, which overall contributes to UV-B stress tolerance. MpRUP facilitates redimerization of MpUVR8 and Mp*rup* null mutants show enhanced UV-B photomorphogenesis, indicating that MpRUP efficiently represses MpUVR8 signaling. Unlike the case in Arabidopsis and in contrast to the strong Mp*cop1* mutant phenotype, Mp*spa* mutants develop only a weak constitutive photomorphogenesis phenotype, indicating that COP1 function is more independent of SPA in Marchantia than in Arabidopsis. Interestingly, however, Mp*spa* is linked with a hyper-responsive UV-B phenotype, suggesting that MpSPA is a negative regulator of MpUVR8 signaling. Our findings demonstrate that core components of UV-B signaling existed in the last common ancestor of extant land plants; however, regulatory interactions have diversified in different lineages since their divergence more than 400 million years ago.

INTRODUCTION

Photoautotrophic plants have a “love/hate relationship” with light. Whereas plant life is unable to survive with too little light, excessive sunlight also poses a major challenge, in part because it contains potentially damaging ultraviolet-B radiation (UV-B; 280–315 nm) (Demarsy et al., 2018). Plants have a unique and conserved UV-B photoreceptor UV RESISTANCE LOCUS 8 (UVR8) that is crucially important for UV-B acclimation, tolerance, and survival (Kliebenstein et al., 2002; Rizzini et al., 2011; Tilbrook et al., 2016; Li et al., 2018; Soriano et al., 2018; Rai et al., 2019; Podolec et al., 2021; Hu et al., 2024; Stockenhuber et al., 2024). The UVR8 signaling pathway has mainly been outlined in Arabidopsis, with UVR8 being a homodimer in its ground state, which exhibits monomerization after absorption of UV-B photons by intrinsic tryptophan (Trp) residues, followed by accumulation in the nucleus (Kaiserli and Jenkins, 2007; Rizzini et al., 2011; Christie et al., 2012; Wu et al., 2012; Yin et al., 2016; Li et al., 2020; Qian et al., 2020; Podolec et al., 2021; Fang et al., 2022). Activated UVR8 then interacts with CONSTITUTIVELY PHOTOMORPHOGENIC 1 (COP1) (Favory et al., 2009; Yin et al., 2015; Wang et al., 2022).

63 COP1 forms an E3 ubiquitin ligase complex together with SUPPRESSOR OF phyA-105 proteins
64 (SPA1–4 in Arabidopsis) (Laubinger et al., 2004; Chen et al., 2010). The COP1/SPA complex
65 represses photomorphogenesis by ubiquitinating photomorphogenesis-promoting factors, directing
66 them to degradation by the 26S proteasome (Podolec and Ulm, 2018; Ponnu and Hoecker, 2021).
67 UV-B-activated UVR8 inhibits the activity of the COP1-SPA complex through a cooperative, high-
68 affinity binding mechanism that displaces substrate proteins from COP1, thus allowing the
69 stabilization of key transcription factors, including the basic leucine zipper (bZIP) transcriptional
70 regulators ELONGATED HYPOCOTYL 5 (HY5) and HY5 HOMOLOG (HYH) (Holm et al.,
71 2002; Ulm et al., 2004; Oravecz et al., 2006; Binkert et al., 2014; Lau et al., 2019). This ultimately
72 leads to broad changes in gene expression upon UV-B exposure (Brown et al., 2005; Favory et al.,
73 2009; Tavridou et al., 2020). COP1/SPA together with HY5/HYH thus represents a major
74 regulatory hub in light signaling in Arabidopsis (Holm et al., 2002; Ulm et al., 2004; Ponnu et al.,
75 2019). In Arabidopsis, the two WD-40 repeat proteins REPRESSOR OF UV-B
76 PHOTOMORPHOGENESIS 1 (RUP1) and RUP2 act as negative feedback regulators of the UVR8
77 photocycle by facilitating UVR8 redimerization, thereby repressing UV-B signaling (Gruber et al.,
78 2010; Heijde and Ulm, 2013; Podolec et al., 2021; Wang et al., 2023).
79 The core of UVR8 signaling seems to be evolutionarily conserved in the green lineage,
80 since it is present in the alga *Chlamydomonas reinhardtii* (hereafter Chlamydomonas) (Allorent et
81 al., 2016; Tilbrook et al., 2016; Tokutsu et al., 2019; Dannay et al., 2025) and the liverwort
82 *Marchantia polymorpha* (hereafter Marchantia) (Clayton et al., 2018; Soriano et al., 2018; Kondou
83 et al., 2019). Notably, Marchantia has minimal gene redundancy in many signaling pathways, and
84 many studies in the past decade have contributed to our understanding of the origins and evolution
85 of major plant regulatory pathways (Bowman et al., 2017; Liang et al., 2022; Frangedakis et al.,
86 2024). The Marchantia genome indeed possesses single homologs for genes encoding the known
87 UVR8 signaling-related components, such as MpUVR8, MpRUP, MpCOP1, MpSPA, and MpHY5.
88 Although a few studies have explored the role of some of these components in UV-B (Clayton et
89 al., 2018; Soriano et al., 2018; Kondou et al., 2019) and visible light signaling (Zhang et al., 2021;
90 Yelina et al., 2024), a deeper understanding of their activities and roles in UV-acclimation is
91 warranted because it remains largely unknown to what extent the precise molecular mechanisms
92 by which these components mediate UV acclimation and tolerance are conserved or divergent

93 throughout the plant kingdom, thus limiting our ability to fully explain how plants sense, respond
94 to, and survive in environments with fluctuating UV levels.
95 We investigated if the major UVR8 signaling components have functionally diverged
96 during plant evolution, and how mechanisms underlying UV-B tolerance may have evolved during
97 the colonization of land by plants. We extend our understanding of the crucial role of MpUVR8 in
98 UV-B acclimation and survival in Marchantia, and provide unequivocal evidence clarifying
99 conservation of the UVR8 photocycle in Marchantia: MpUVR8 forms UV-B-responsive
100 homodimers, then monomerizes, interacts with MpCOP1, and accumulates in nuclei in response to
101 UV-B. MpRUP facilitates MpUVR8 redimerization to repress signaling, with Mp*rup* mutants
102 showing extreme dwarfism specifically under UV-B. Although Mp*cop1* mutants exhibited
103 enhanced constitutive photomorphogenesis and extreme dwarfism comparable to UV-B-grown
104 Mp*rup* mutants, Mp*spa* mutants showed only a weak constitutive photomorphogenesis phenotype
105 in visible light; however, Mp*spa* mutants were surprisingly hyper-responsive to UV-B, suggesting
106 that MpSPA plays a divergent role from that in Arabidopsis. Notably, our transcriptome data
107 revealed that only a few UV-B-regulated genes were entirely MpHY5-dependent. This is different
108 from Arabidopsis, where HY5/HYH serves as a major regulator in the UV-B signaling pathway.
109 Moreover, we provide a genome-wide view of MpUVR8-mediated transcriptional responses in
110 Marchantia and identify UV-B-regulated gene clusters and metabolites key to UV-B protection.
111

112 RESULTS

113 MpUVR8 is homodimeric in its ground state, and monomerizes and accumulates in nuclei in 114 response to UV-B

115 In Marchantia, UVR8 is encoded by a single locus, but alternative splicing of the 11th intron
116 produces two transcripts, namely Mp*UVR8.1* and Mp*UVR8.2*, resulting in two different proteins
117 whereby residues 414 to 426 present in MpUVR8.1 are absent in MpUVR8.2 (Supplementary Fig.
118 S1) (Soriano et al., 2018). Whether MpUVR8 forms homodimers *in vivo* or is primarily monomeric
119 with a divergent inactivation mechanism is unclear (Soriano et al., 2018). We thus first tested if
120 MpUVR8.1 and MpUVR8.2 form dimers using a luciferase complementation imaging (LCI) assay
121 in transiently transformed *Nicotiana benthamiana* leaves (Zhou et al., 2018). Resulting LCI signals
122 showed interactions of MpUVR8.1 and MpUVR8.2 both with and between themselves, indicating
123 that MpUVR8 forms homodimers *in vivo* (Fig. 1A to C). In AtUVR8, the aspartate-96 (D96) and

124 aspartate-107 (D107) residues are key to homodimer formation and mutating each to asparagine
125 impairs UVR8^{D96N,D107N} dimer formation (Christie et al., 2012; Wu et al., 2012; Heilmann et al.,
126 2016; Podolec et al., 2021). Consistent with the conservation of these residues in MpUVR8
127 (Supplementary Fig. S1), no LCI signal was detected with the mutated MpUVR8.1^{D95N,D106N} and
128 MpUVR8.2^{D95N,D106N} variants (Fig. 1A and B), indicating that these residues are also key for
129 MpUVR8 homodimerization.

130 To further test if endogenous MpUVR8 forms homodimers, we crosslinked protein extracts
131 from Marchantia with dithiobis (succinimidyl propionate) (DSP), as described previously for
132 Arabidopsis (Rizzini et al., 2011; Podolec et al., 2021). Using a specific anti-MpUVR8 antibody,
133 we detected a band at the size of the predicted MpUVR8 dimer at about 100 kDa in the absence of
134 UV-B, and this band was strongly reduced in extracts from UV-B-treated plants (Fig. 1D). These
135 data indicate that UV-B exposure induces MpUVR8 monomerization. Of note, UV-B-activated
136 monomeric MpUVR8 was not well detected in crosslinked extracts, as in Arabidopsis (Rizzini et
137 al., 2011; Podolec et al., 2021). However, we detected MpUVR8 at its monomeric size of about 48
138 kDa (predicted sizes for MpUVR8.1 and MpUVR8.2 are 48.6 and 47.1 kDa, respectively) both
139 following the reversal of DSP crosslinking with the reducing agent β-mercaptoethanol (β-ME) and
140 in the absence of crosslinking (Fig. 1D). This indicates that MpUVR8 levels are not affected by
141 UV-B treatment or crosslinking.

142 To define MpUVR8 subcellular localization in Marchantia, we transformed wild-type Tak-
143 1 with the full genomic Mp*UVR8* locus containing an N-terminal green fluorescent protein (GFP)
144 tag and imaged the resulting fluorescence. GFP-MpUVR8 accumulated in the nucleus only when
145 plants were exposed to UV-B (Fig. 1E), similar to AtUVR8 (Kaiserli and Jenkins, 2007; Yin et al.,
146 2016) and the 35S promoter–driven expression of Citrine-MpUVR8 in Tak-1 (Kondou et al., 2019).
147 This contrasts with the apparent constitutive nuclear localization of GFP-MpUVR8.1 and GFP-
148 MpUVR8.2 when expressed with the 35S promoter in Arabidopsis and *N. benthamiana* (Soriano
149 et al., 2018).

150 Taken together, we conclude that endogenous MpUVR8.1 and MpUVR8.2 form
151 homodimers in Marchantia and possess conserved aspartate residues necessary for MpUVR8
152 homodimer formation. Moreover, upon UV-B exposure, MpUVR8 monomerizes and accumulates
153 in nuclei.
154

155 ## MpRUP facilitates MpUVR8 redimerization

156 We tested if MpUVR8 interacts with MpRUP, the putative ortholog of AtRUP1 and AtRUP2
157 (Gruber et al., 2010; Clayton et al., 2018). MpUVR8 and MpRUP exhibited interaction in yeast
158 two-hybrid (Fig. 2A and B), LCI assays in *N. benthamiana* (Fig. 2C and D), and MpRUP co-
159 purified with GFP-MpUVR8 in affinity purification coupled with mass spectrometry (AP-MS)
160 (Supplementary Fig. S2). Using immunoblotting of crosslinked protein extracts, we assayed if
161 MpRUP facilitates MpUVR8 redimerization in Marchantia. In wild-type Tak-1 plants, MpUVR8
162 dimer amount was strongly reduced upon exposure to UV-B, then reverted to initial levels within
163 approximately 1 h once under -UV-B conditions (Fig. 2E). However, in a Mp*rup* mutant generated
164 using CRISPR/Cas9 mutagenesis in the Tak-1 background (Supplementary Fig. S3), MpUVR8
165 dimer levels recovered slowly and did not reach "-UV" ground state levels even after 6 h (Fig. 2E).
166 We thus conclude that MpRUP facilitates MpUVR8 redimerization, indicating that there is a
167 conserved mechanism for negative feedback regulation of UVR8 activity.

168

169 ## MpUVR8 and MpRUP antagonistically regulate UV-B-dependent growth, pigment accumulation,
170 and acclimation

171 To explore the phenotypic consequences of MpUVR8 and MpRUP action, we established robust
172 UV-B conditions for phenotypic and molecular analysis. Under continuous white light, no striking
173 differences were detectable between Tak-1, Mp*uvr8*, and Mp*rup* (Fig. 3A, and Supplementary Fig.
174 S4A). However, when exposed to white light supplemented with narrowband UV-B (1.5 µmol m^{-}
175 ^{2} s^{-1}), Tak-1 exhibited a slight growth inhibition and slight accumulation of pigments (Fig. 3A, and
176 Supplementary Fig. S4A). These responses were reduced, if not absent, in Mp*uvr8* mutant and
177 Mp*RUP*^{OE} overexpression lines (Fig. 3A, and Supplementary Fig. S4A and F). By sharp contrast,
178 Mp*rup* mutants exhibited a striking UV-B-hyperresponsive photomorphogenic phenotype, with
179 extreme growth inhibition and strong pigmentation of the thallus specifically under UV-B (Fig. 3A,
180 and Supplementary Fig. S4A) (Clayton et al., 2018), similar to transgenic lines overexpressing
181 Mp*UVR8.1* or Mp*UVR8.2* photoreceptors (Supplementary Fig. S4A and E). We conclude that
182 MpRUP plays a major role in MpUVR8 inactivation through redimerization and that Mp*rup*
183 mutants show an extreme, UV-B-conditional growth phenotype.

184 To directly assess the effect of MpUVR8-mediated acclimation on photoprotection, we
185 measured F_v/F_m representing the maximum quantum yield of photosystem II (PSII) (Murchie and

186 Lawson, 2013). Tak-1, Mp*uvr8*, and Mp*rup* plants were grown for 7 days under white light
187 supplemented with narrowband UV-B (acclimated; +/-) or not (non-acclimated; -/-) (Fig. 3B).
188 Acclimated and non-acclimated plants were then exposed to 1 h of broadband UV stress (+/+ and
189 -/+, respectively). We measured F_v/F_m before and after UV stress in both acclimated and non-
190 acclimated plants (Fig. 3B). Non-stressed Tak-1, Mp*uvr8*, and Mp*rup* displayed an F_v/F_m value
191 close to 0.8 (Fig. 3C), which is characteristic of healthy Marchantia plants (Messant et al., 2023).
192 When exposed to UV stress, F_v/F_m decreased significantly and to the same extent in non-acclimated
193 plants of all genotypes (Fig. 3C), suggesting photoinhibition resulting from PSII damage. However,
194 applying the same UV stress treatment on acclimated plants revealed a UVR8-dependent
195 photoprotective effect: in Tak-1 and even more so in Mp*rup*, F_v/F_m following UV-B stress was
196 higher in acclimated compared to non-acclimated plants (Fig. 3C). This effect was MpUVR8-
197 dependent, as it was absent in Mp*uvr8* (Fig. 3C). Mp*UVR8.1*^{OE} and Mp*UVR8.2*^{OE} overexpression
198 lines (Supplementary Fig. S4E) and Mp*uvr8-1*/*Pro*$_{\text{MpUVR8}}$*:GFP*-Mp*UVR8* complementation lines
199 were similar to Mp*rup*, whereas Mp*RUP*^{OE} overexpression lines phenocopied Mp*uvr8*
200 (Supplementary Fig. S4B and F).

201 Next, we tested the survival rates of Tak-1, Mp*uvr8*, and Mp*rup* under UV-B stress. Plants
202 were acclimated or not under narrowband UV-B for 7 days, followed by a 7- or 9-h broadband UV-
203 B stress treatment, after which all plants were returned to white light for 7 days of recovery (Fig.
204 3D). Without acclimation, Tak-1, Mp*uvr8*, and Mp*rup* did not survive subsequent UV-B stress
205 (Fig. 3E). Acclimated wild-type plants did not survive the 9-h UV-B stress treatment but some
206 gemmalings resumed growth after 7 h of UV-B stress. Mp*rup* mutants recovered more than Tak-1
207 under both stress treatments (Fig. 3E, Supplementary Fig. S4C and D), indicating enhanced UV-B
208 protection. By contrast, the Mp*uvr8* mutant did not survive the UV-B stress treatment even with
209 prior UV-B acclimation, demonstrating that UV-B photoprotection was dependent on MpUVR8
210 (Fig. 3E). Complementing the Mp*uvr8-1* mutant with a *Pro*$_{\text{MpUVR8}}$*:*Mp*UVR8* construct restored
211 UV-B stress survival in acclimated plants (Supplementary Fig. S4C). By contrast, overexpression
212 of MpRUP driven by the strong Mp*EF1α* promoter (Tak-1/Mp*RUP*^{OE} and Mp*rup-2*/Mp*RUP*^{OE})
213 phenocopied the Mp*uvr8* mutant phenotype (Supplementary Fig. S4D).

214 We prepared methanolic extracts from gemmalings and measured the absorption spectra
215 between 280–400 nm to detect UV-absorbing compounds. There was a broad peak in UV-
216 absorbance at ~340 nm for UV-B-exposed Tak-1 plants, which was absent for the Mp*uvr8* mutant

217 (Fig. 3F), indicating Marchantia plants accumulate UV-absorbing compounds in a UV-B- and
218 UVR8-dependent manner. Consistent with their enhanced UV-B acclimatory response and
219 resulting UV-B tolerance, extracts from UV-B-exposed Mp*rup* mutants had an even greater peak
220 in UV absorption (Fig. 3F). Notably, the Mp*uvr8-1* Mp*rup-2* double mutant exhibited
221 photoprotection and UV-absorbing capacity comparable to the Mp*uvr8-1* single mutant
222 (Supplementary Fig. S5), demonstrating that the enhanced photoprotection and UV-B-absorbing
223 capacity of Mp*rup* is dependent on MpUVR8.
224 We conclude that MpUVR8 is key in mediating protection of the photosynthetic apparatus
225 and survival under UV-B stress, with MpRUP functioning as a key negative regulator of MpUVR8-
226 dependent responses. Moreover, enhanced photoprotection under UV-B is associated with the
227 accumulation of UV-absorbing compounds.
228

229 ## Mp*cop1* mutants exhibit constitutive photomorphogenesis and UV-B tolerance

230 Interaction of UVR8 with the COP1/SPA E3 ligase complex and its subsequent inactivation is a
231 key step in UV-B signal transduction (Favory et al., 2009; Yin et al., 2015; Lau et al., 2019).
232 MpCOP1 and MpSPA interacted in yeast two-hybrid assays, both in the absence and presence of
233 UV-B (Fig. 4A) (Zhang et al., 2021). By contrast, MpUVR8 interacted with MpCOP1 specifically
234 under UV-B in yeast two-hybrid (Fig. 4A), LCI (Fig. 4B), and AP-MS assays (Supplementary Fig.
235 S2).
236 Arabidopsis *cop1* null mutants have a seedling-lethal phenotype (McNellis et al., 1994) and
237 no Marchantia Mp*cop1* mutant has been recovered and described until now (Zhang et al., 2021).
238 We generated two viable Mp*cop1* null mutant alleles using CRISPR/Cas9 mutagenesis
239 (Supplementary Fig. S3). These mutants displayed stunted growth, delayed development, and
240 reduced gemmae production compared to that in wild-type Tak-1 when grown under standard
241 conditions (Fig. 5A). Whereas the Mp*cop1* mutants developed gemma cups and gemmae and thus
242 could complete their asexual life cycle,, they failed to complete their sexual life cycle because
243 antheridiophores did not develop when induced under continuous white light supplemented with
244 far-red light.
245 Mp*cop1* mutants exhibited constitutively enhanced photoprotection, as evidenced by their
246 elevated F_v/F_m ratios after UV-B stress (Fig. 5B). The strong constitutively photomorphogenic
247 phenotype and enhanced photoprotection of Mp*cop1* mutants agreed with how Mp*cop1* mutants

248 survived prolonged broadband UV-B stress exposure, both with or without acclimation (Fig. 5C;
249 note that the plants are viable as determined by non-stressed levels of F_v/F_m after recovery).
250 Absorption spectra of methanolic extracts also revealed constitutive hyperaccumulation of UV-
251 absorbing compounds in Mp*cop1* (Fig. 5D). Thus, MpCOP1 activity as key repressor of
252 photomorphogenesis is evident in Marchantia.
253
254 Mp*spa* mutants show only a minor constitutively photomorphogenic growth phenotype, but
255 strongly enhanced UV-B tolerance
256 To investigate the role of the single MpSPA protein, we generated two independent CRISPR/Cas9
257 knockout alleles (Supplementary Fig. S3). Surprisingly, both Mp*spa* alleles exhibited a phenotype
258 comparable to wild-type Tak-1 under both white light and white light supplemented with UV-B
259 (Fig. 5A). This was in stark contrast to the strong constitutively photomorphogenic phenotype
260 observed for the Mp*cop1* mutant (Fig. 5A) and Arabidopsis *spa* quadruple mutants (Ordonez-
261 Herrera et al., 2015).
262 Furthermore, we tested the UV-B acclimation response of Mp*spa* mutants. Mp*spa* showed
263 enhanced basal UV-B tolerance when compared to wild type ("-/+", Fig. 5B), as well as after UV-
264 B acclimation ("+/+", Fig. 5B). Mp*spa* mutants also showed an increased survival rate after
265 prolonged UV-B stress if plants were previously acclimated to low UV-B (Fig. 5C). In accordance
266 with their improved UV-B stress tolerance, Mp*spa* mutants constitutively accumulated more UV-
267 absorbing compounds which became further pronounced upon UV-B-mediated acclimation (Fig.
268 5D).
269 As enhanced UV-B-acclimation of Mp*spa* resembled Mp*rup* mutants, we investigated
270 whether MpSPA function was also associated with MpUVR8 redimerization. However, in contrast
271 to Mp*rup*, Mp*spa* showed efficient MpUVR8 redimerization (Supplementary Fig. S6A).
272 Additionally, overexpression of Mp*SPA* and Mp*COP1* reduced basal UV-B tolerance but did not
273 abolish UV-B-induced photoprotection, in contrast to Mp*RUP* overexpression (Supplementary Fig.
274 S6B to D). We conclude that MpCOP1 activity as a repressor of photomorphogenesis is not fully
275 dependent on MpSPA, and that the absence of MpSPA enhances UV-B tolerance.
276

MpUVR8 signaling components mediate transcriptional changes in response to UV-B

We analyzed the UVR8-mediated transcriptome in 7-day-old Marchantia gemmalings in response to 3 h of narrowband UV-B (Supplementary Tables S1 and S2). In Tak-1, we identified 480 and 114 genes up- and downregulated by UV-B, respectively ($|\log_2$ fold-change$|$ > 1; p-adj < 0.05), which all exhibited MpUVR8- and MpCOP1-dependent expression changes (Supplementary Tables S3A, B and S4), thus representing the transcriptional MpUVR8 signaling output.

In wild-type Tak-1, Mp*rup*, and Mp*spa*, we identified a combined total of 756 UV-B-induced genes and 298 UV-B-repressed genes ($|\log_2$ fold-change$|$ > 1; p-adj < 0.05), with substantial overlaps between the genotypes (Fig. 6A to C, Supplementary Tables S3A, B and S4). Interestingly, induction or repression of transcripts after 3 h of UV-B was enhanced in Mp*rup* and Mp*spa* compared to Tak-1 (Fig. 6C), consistent with their UV-B hyper-responsive phenotypes (Fig. 3 and Fig. 5). Consistent with this, over two-thirds of genes that were up- or downregulated ($|\log_2$ fold-change$|$ > 1) specifically in Mp*rup* and Mp*spa* ("unique Mp*rup*" and "unique Mp*spa*") were up- or downregulated in Tak-1 as well when considering a lower fold-change threshold ($|\log_2$ fold-change$|$ > 0 but <1; p-adj < 0.05) (Fig. 6A and B). Notably, whereas the transcriptomic profile of the Mp*cop1-1* mutant was unresponsive to UV-B, it resembled the profile of UV-B-responsive genotypes after UV-B exposure, with a large portion of genes constitutively up- or downregulated (Fig. 6C and D). These data support the role of MpCOP1 as a repressor of UV-B photomorphogenesis and COP1-inactivation by UVR8 as a key mechanism for UV-B-responsive gene expression changes.

Using hierarchical clustering, we defined seven major clusters of gene expression changes upon UV-B exposure (Fig. 6C and D, and Supplementary Table S4). Clusters 1 and 5 contain UV-B-downregulated genes, with gene expression in Mp*cop1* that is constitutively down- or upregulated, respectively. Cluster 7 consists of UV-B-downregulated genes that are more highly expressed in Mp*spa*. Clusters 4 and 6 contain genes that are induced after 3 h of UV-B in wild type, Mp*rup*, and Mp*spa*, but not in Mp*uvr8* and Mp*cop1*, and their constitutive expression in Mp*cop1* is either elevated or comparable in comparison to that in wild type, respectively. Clusters 2 and 3 contain genes induced after 3 h of UV-B exposure in wild type, with hyper-induced expression in Mp*spa* and Mp*rup*, respectively. We profiled the expression of components of the UVR8 pathway in the data: Mp*HY5*, Mp*RUP*, and Mp*COP1* (cluster 2) were upregulated upon UV-B in wild type (Supplementary Table S4), whereas Mp*UVR8* was constitutively expressed.

308

309 MpSPA plays a minor role in repressing visible light photomorphogenesis compared to MpCOP1

310 In Arabidopsis, *spa1234* (*spaQn*) quadruple mutants undergo constitutive photomorphogenesis
311 with a phenotype similar to strong *cop1* mutants (such as *cop1-1*) and stronger than the weak *cop1-*
312 *4* allele (Fig. 7A) (McNellis et al., 1994; Laubinger et al., 2004; Ordonez-Herrera et al., 2015).
313 However, Marchantia Mp*spa* mutants exhibited only a minor growth phenotype in white light
314 compared to the strongly affected Mp*cop1* mutants (Fig. 7A, Fig. 5A). Thus, we investigated the
315 transcriptome profile Mp*spa* and Mp*cop1* mutants in more detail.

316 By comparing white light–grown Mp*cop1* and Mp*spa* versus Tak-1, we found that in
317 Mp*cop1*, 1,256 and 1,898 genes were significantly up- or downregulated ($|\log_2$ fold-change$| > 1$;
318 p-adj < 0.05), respectively (Fig. 7B and C). By stark contrast, only 60 genes were upregulated and
319 15 genes were downregulated in Mp*spa* using the same threshold criteria (Fig. 7B and C, and
320 Supplementary Table S3C and D), which is significantly different from Arabidopsis, where over
321 7,000 differentially expressed genes (DEGs) were observed between the *spaQ* mutant and the wild
322 type (Pham et al., 2020). Of those genes dysregulated in Mp*spa*, 40 out of 60 and 12 out of 15
323 genes were also up- and downregulated, respectively, in Mp*cop1*. We further checked if genes
324 dysregulated in Mp*cop1* but not in Mp*spa* were in fact dysregulated in Mp*spa* but at a lower fold-
325 change threshold. Indeed, out of the 1,256 upregulated genes in Mp*cop1*, 486 were shared with
326 Mp*spa* when considering a looser threshold for genes upregulated in Mp*spa* ($|\log_2$ fold-change$| >$
327 0; p-adj < 0.05; Fig. 7B). Similarly, out of the 1,898 downregulated genes in Mp*cop1*, 349 were
328 also downregulated in Mp*spa* (Fig. 7C). This indicates a larger overlap between genes dysregulated
329 in Mp*cop1* and Mp*spa* mutants in comparison to wild type, but also identifies clear differences
330 between MpCOP1- and MpSPA-dependent genes at the genome-wide level.

331 A broader examination of gene expression levels across wild type, Mp*cop1*, and Mp*spa*
332 genotypes confirmed that, although the overall profile of Mp*spa* was similar to wild-type, many
333 transcripts had levels that were intermediate between Tak-1 and Mp*cop1* (Fig. 7D, Supplementary
334 Table S5). Using hierarchical clustering, we defined 11 main clusters of gene expression (Fig. 7E),
335 specifically four for Mp*cop1*-upregulated genes (clusters 1, 2, 7 and 10), six for Mp*cop1*-
336 downregulated genes (clusters 3, 4, 5, 6, 8 and 9), and a small cluster of genes specifically
337 upregulated in Mp*spa* (cluster 11). Interestingly, the cluster groups defined by Mp*cop1*-up- and

338 downregulated patterns of gene expression could be discriminated by the extent to which
339 expression in Mp*spa* aligned with the expression in Mp*cop1* (Fig. 7E).
340 Finally, since we observed that the regulation of many genes was dependent on MpCOP1
341 under white light, and we established that MpCOP1 has a conserved role as a repressor of
342 photomorphogenesis, we tested if genes dysregulated in Mp*cop1* were induced by UV-B in UV-
343 B-responsive genotypes. We observed that most genes upregulated under white light in Mp*cop1*
344 were induced by UV-B in Tak-1, Mp*rup*, or Mp*spa* (Fig. 7D), whereas many genes constitutively
345 downregulated in Mp*cop1* were repressed by UV-B. However, some of the Mp*cop1*-
346 downregulated genes were induced after 3 hours of UV-B, suggesting more complex dynamics
347 between induction under UV-B and steady-state levels in Mp*cop1*.
348 Overall, our analysis shows that MpCOP1 plays a major role in repressing the light-
349 inducible transcriptome of Marchantia, whereas MpSPA plays a minor yet detectable role, likely
350 as part of the repressive COP1-SPA complex (Zhang et al., 2021).
351
352 MpHY5 promotes MpUVR8 signaling
353 The induction of Mp*HY5* expression is UV-B- and MpUVR8-dependent, repressed by both
354 MpRUP and MpSPA, and Mp*HY5* is constitutively upregulated in the Mp*cop1-1* mutant
355 (Supplementary Table S4). To test the role of MpHY5 in Marchantia, we generated Mp*hy5*
356 knockout mutants by CRISPR/Cas9 (Supplementary Fig. S3). We further investigated the
357 photoprotection and UV-B-absorbing capacity of Mp*hy5* mutants. Mp*hy5* mutants showed slightly
358 reduced basal photoprotection, as determined by measuring the F_v/F_m ratio after UV-B stress
359 exposure (-/+; Fig. 8A). Interestingly, and in contrast to Arabidopsis *hy5 hyh* double mutants
360 (Leonardelli et al., 2024), Mp*hy5* mutants were able to acclimate to UV-B (+/+ versus -/+; Fig.
361 8A), but Mp*hy5* mutants nevertheless showed a significantly reduced capacity to protect their
362 photosynthetic machinery from subsequent UV-B-induced damage compared to UV-B-acclimated
363 wild type (+/+; Fig. 8A). In agreement, in contrast to wild type, UV-B-acclimated Mp*hy5* mutants
364 did not survive 7 h of UV-B stress (Fig. 8B). Finally, we measured the UV-B absorbance profiles
365 of methanolic extracts from different genotypes and found that, consistent with the reduced
366 photoprotection observed in UV-B-exposed Mp*hy5*, Mp*hy5* accumulated slightly less UV-B-
367 absorbing compounds compared to Tak-1 wild type (Fig. 8C).

368 To further understand how MpHY5 promotes MpUVR8 signaling, we performed another
369 RNA-seq experiment with 7-day-old Tak-1 and Mp*hy5-1* Marchantia gemmalings exposed or not
370 to 3 h of narrowband UV-B (Supplementary Tables S1, S2, S6 and S7). Using heatmap analysis
371 and hierarchical clustering, we examined the 501 genes regulated upon UV-B exposure in Tak-1
372 and/or Mp*hy5-1* ($|\log2 \text{ fold-change}| > 1$; p-adj < 0.05) (Supplementary Table S7). This analysis
373 revealed 10 major clusters of gene expression changes in response to UV-B exposure (Fig. 8D, and
374 Supplementary Fig. S7). Notably, few genes were entirely dependent on Mp*HY5*, though certain
375 trends were observed where some genes showed reduced or enhanced UV-B-induced expression
376 compared to the wild-type Tak-1. Mp*HY5-1* (one base deletion, see Supplementary Fig. S3) and
377 Mp*COP1* were hyperinduced in Mp*hy5-1* (cluster 3), while the induction of Mp*RUP* was
378 unaffected by the Mp*hy5-1* mutation (cluster 1). Most UV-B-induced genes were constitutively
379 upregulated in Mp*cop1-1* (Fig. 8D, and Supplementary Table S3), and we noticed that the most
380 MpHY5-dependent genes (clusters 2 and 7) were associated with the highest levels of constitutive
381 upregulation in Mp*cop1*, while the genes that showed the most hyperinduction in Mp*hy5* were
382 associated with the lowest constitutive expression levels in Mp*cop1* (Fig. 8D, Supplementary Fig.
383 S8 and Supplementary Table S6). This is in agreement with an evolutionary conservation of the
384 COP1-HY5 regulatory module in Marchantia photomorphogenesis. Taken together, our data
385 indicate that MpHY5 acts antagonistically to MpCOP1 and is involved in mediating UVR8-
386 responsive gene expression in Marchantia, although to a much lesser extent than that facilitated by
387 HY5 and HYH in Arabidopsis.
388

389 ## Aureusidin synthase MpAUS contributes to the synthesis of UV-absorbing pigments that support
390 Marchantia UV-B tolerance

391 Several genes involved in the phenylpropanoid biosynthetic pathway, including
392 *PHENYLALANINE AMMONIA LYASE 1* (Mp*PAL1*), *CHALCONE SYNTHASE 2* (Mp*CHS2*),
393 *CHALCONE ISOMERASE-LIKE* (Mp*CHIL2*), and *AUREUSIDIN SYNTHASE* (Mp*AUS*, also
394 named Mp*PPO* (Berland et al., 2019) and Mp*AS1* (Furudate et al., 2023)), were MpUVR8-
395 dependently induced upon UV-B exposure (Fig. 9A, Supplementary Fig. S9). Notably, the
396 transcript level of Mp*AUS*, encoding a key enzyme in biosynthesis of the auronidin flavonoid
397 pigments (Berland et al., 2019; Furudate et al., 2023), exhibited strong upregulation in response to
398 UV-B and was constitutively upregulated in Mp*cop1* (Fig. 9A). Additionally, RT-qPCR analysis

399 confirmed that the induction of Mp*AUS* following 3 h of UV-B exposure was absent or
400 significantly reduced in Mp*uvr8* and Mp*hy5* mutants, respectively, compared to that in Tak-1 wild
401 type (Fig. 9B). To test the role of Mp*AUS* in UV tolerance, we generated frameshift knockout
402 mutants of Mp*AUS* in Tak-1 using CRISPR/Cas9 mutagenesis (Supplementary Fig. S3). The F_v/F_m
403 ratio in UV-B-acclimated plants after UV-B stress was slightly reduced in Mp*aus-2* compared to
404 that in Tak-1, but not in Mp*rup* Mp*aus* and Mp*spa* Mp*aus* compared to that in Mp*rup* and Mp*spa*,
405 respectively (Fig. 9C, and Supplementary Fig. S10A). In addition, fewer UV-B-acclimated Mp*aus-*
406 *2* mutants survived subsequent UV-B stress compared to Tak-1 wild type (Fig. 9D and
407 Supplementary Fig. S10B). The Mp*aus* mutation decreased the survival rate of Mp*spa* Mp*aus*
408 double mutants (Supplementary Fig. S10B) but did not affect the survival rate of Mp*rup* Mp*aus*
409 double mutants (Fig. 9D). Altogether, this suggests that MpAUS plays a role in UV stress tolerance,
410 and compensatory effects can occur upon elevated UVR8 activity. Mutation of Mp*aus* affected
411 thallus growth slightly under UV-B in Tak-1 wild type but not in Mp*rup*; however, UV-B-grown
412 Mp*rup* Mp*aus* mutants failed to accumulate characteristic red pigments (Fig. 9E). The UV-B-
413 induced accumulation of UV-absorbing compounds was reduced by the Mp*aus* mutation in a wild-
414 type background, although to a variable extent (Fig. 9F, and Supplementary Fig. S10C). A similar
415 reduction of UV-absorbing compounds was detected in Mp*rup* Mp*aus* and Mp*spa* Mp*aus* versus
416 that in Mp*rup* and Mp*spa* single mutants, respectively (Fig. 9F, and Supplementary Fig. S10C).
417 However, the UV absorbance of Mp*rup* Mp*aus* extracts was much higher than that of wild-type
418 extracts, suggesting that the overaccumulation of UV-absorbing compounds in Mp*rup* occurs in
419 the absence of MpAUS. Next, we performed untargeted metabolomics of 9-day-old wild type Tak-
420 1, Mp*uvr8*, Mp*rup*, and Mp*aus* grown in white light for 7 days and exposed or not to supplemental
421 UV-B for 2 days, following which we detected a total of 609 metabolites that we annotated using
422 a workflow based on SIRIUS 6.2, including CSI:FingerID and CANOPUS, coupled with a
423 taxonomically informed reannotation using the Tima R package (Duhrkop et al., 2019; Rutz and
424 Allard, 2025) (Supplementary Table S8). Fifty-eight metabolites accumulated in response to UV-
425 B in wild-type Tak-1 that were not observed in Mp*uvr8* (Fig. 9G, Supplementary Fig. S11 and
426 Supplementary Table S9). Over half of these (30) were assigned to compounds from the shikimate-
427 phenylpropanoid biosynthetic pathway, whereas metabolites from that pathway represented only
428 about a quarter of all detected compounds (151/609) (Fig. 9H and Supplementary Table S9). This
429 indicates an overrepresentation of shikimate-phenylpropanoid compounds among those UVR8-

430 regulated metabolites. Similar to Arabidopsis, flavones and flavonol glycosides accumulated in an
431 MpUVR8-dependent manner upon UV-B exposure, which is consistent with previous reports
432 (Supplementary Fig. S11, and Supplementary Table S9, (Clayton et al., 2018)). However, unlike
433 in Arabidopsis whereby sinapate esters play a major role in UV-B photoprotection (Leonardelli et
434 al., 2024), no sinapate esters were detected in Marchantia (Supplementary Fig. S11A, B).
435 Notwithstanding this, 30 of the 58 compounds that accumulated in response to UV-B in wild-type
436 Tak-1 also accumulated in Mp*rup* (Fig. 9G). In addition, 59 compounds were specifically induced
437 under UV-B in Mp*rup*, including auronidin-4-neohesperidoside, a known product of MpAUS
438 (Berland et al., 2019). However, we did not detect the aglycon form of auronidin, possibly because
439 this compound may be present in the cell wall as an insoluble polymer (Jibran et al., 2024).
440 Importantly, we found that the Mp*aus* metabolome was almost non-responsive to UV-B in our
441 conditions (only a total of 17 metabolites accumulated, of which 6 overlapped with wild-type Tak-
442 1), suggesting that, in addition to impairing the synthesis of auronidins, Mp*aus* mutation also
443 affects the accumulation of many other flavonoids.
444 Taken together, our data suggest that MpAUS contributes to UV-B acclimation in wild type
445 through its direct or indirect effect on the synthesis of diverse phenylpropanoids. However, Mp*rup*
446 and Mp*rup* Mp*aus* absorption spectra reveal the potential contribution of further unidentified,
447 MpAUS-independent UV-absorbing compounds that function in UV-B acclimation in Marchantia.
448

449 ## DISCUSSION

450 UV-B exposure elicits UVR8-dependent transcriptional changes underlying UV-B acclimation
451 phenotypes in plants (Kliebenstein et al., 2002; Brown et al., 2005; Favory et al., 2009; Tilbrook
452 et al., 2016; Tavridou et al., 2020; Hu et al., 2024; Dannay et al., 2025). The present study provides
453 compelling evidence demonstrating that the core UVR8 photocycle is conserved among land plants,
454 defines the MpUVR8-mediated genome-wide transcriptional response, and provides physiological
455 evidence for how MpUVR8 regulates acclimation and UV-stress tolerance in Marchantia using a
456 broad panel of knock-out mutants in the UVR8 signaling pathway and its output.
457 In contrast to that in Arabidopsis and the moss *Physcomitrium patens* (hereafter
458 Physcomitrium), MpUVR8 has been reported to form weaker dimers and increased levels of
459 monomer *in vivo* in the absence of UV-B, which is observed when analyzing MpUVR8
460 dimer/monomer ratio by SDS-PAGE and immunoblotting using samples that are not heat-

461 denatured before electrophoresis (Soriano et al., 2018). Although this type of assay is accurate for
462 the dimer/monomer status of wild-type AtUVR8 (Rizzini et al., 2011; Heijde and Ulm, 2013;
463 Heilmann and Jenkins, 2013; Findlay and Jenkins, 2016; Moriconi et al., 2018), it can make weak
464 dimeric UVR8 mutant variants appear monomeric, whereas *in vitro* assays (Christie et al., 2012;
465 Wu et al., 2012; Heijde et al., 2013) as well as more stringent assays using protein-protein
466 crosslinking identify these variants as homodimeric *in vivo* (Rizzini et al., 2011; Podolec et al.,
467 2021). Thus, we employed crosslinking to show that MpUVR8 is indeed dimeric *in vivo* in the
468 absence of UV-B, consistent with the UV-B-dependent dimer-to-monomer transition being a
469 conserved feature of the UVR8 photocycle (Rizzini et al., 2011; Tilbrook et al., 2016; Podolec et
470 al., 2021). Furthermore, we provide evidence that negative feedback regulation through MpRUP-
471 facilitated redimerization of MpUVR8 is conserved in Marchantia (Heijde et al., 2013; Podolec et
472 al., 2021; Zhang et al., 2021). Consistent with this, the Mp*rup* mutant displayed a strong UV-B
473 photomorphogenic phenotype, characterized by both growth inhibition resulting in a small size and
474 a strong pigmentation of the thallus (this study and (Clayton et al., 2018)). Interestingly, this
475 conditional phenotype of Mp*rup* specifically under UV-B phenocopies the constitutive Mp*cop1*
476 phenotype, in agreement with active UVR8-mediated inactivation of COP1 underlying UV-B
477 signaling (Yin et al., 2015; Lau et al., 2019). We further show that GFP-MpUVR8 expressed under
478 its own promoter localizes mainly to the cytosol and displays UV-B-dependent nuclear
479 accumulation in Marchantia, confirming findings using a *Citrine*-Mp*UVR8* overexpression line
480 (Kondou et al., 2019). Thus, we conclude that the homodimeric ground state of UVR8, its UV-B
481 dependent monomerization, nuclear accumulation, and COP1 inactivation, as well as negative
482 feedback regulation of UVR8 through RUP-facilitated redimerization are well-conserved in
483 Marchantia.

484 In flowering plants, COP1 forms an E3 ligase complex together with SPA proteins, which
485 together function as suppressors of photomorphogenesis; i.e. COP1 requires SPA proteins to
486 function (Hoecker, 2017; Podolec and Ulm, 2018). Since non-plant COP1 orthologs are not
487 regulated by light, it is hypothesized that the evolution of SPA proteins was a crucial step in
488 enabling photoreceptor-mediated regulation of COP1/SPA complex activity (Ranjan et al., 2014;
489 Balcerowicz et al., 2017; Podolec and Ulm, 2018). Active phytochrome and cryptochrome
490 photoreceptors directly interact with SPA proteins, which represses the E3 ligase activity of the
491 COP1/SPA complex (Hoecker, 2017; Podolec and Ulm, 2018). In agreement, Arabidopsis

492 quadruple *spa* mutants exhibit strong constitutive photomorphogenesis (Ordonez-Herrera et al.,
493 2015). However, it is of note that *spa* quadruple null mutants can complete their life cycle whereas
494 *cop1* null mutants cannot (McNellis et al., 1994; Ordonez-Herrera et al., 2015), suggesting that
495 COP1 can function partially in a SPA-independent manner. COP1, but not SPA proteins, are also
496 necessary for transient gene expression changes upon exposure to UV-B (Favory et al., 2009).
497 Recently, the role of COP1/SPA has started to be explored in more phylogenetically distant land
498 plant lineages such as bryophytes, including Physcomitrium (Kreiss et al., 2023). A Physcomitrium
499 Pp*cop1_9x* mutant lacking all nine PpCOP1(a-i) orthologs was viable and displayed a rather minor
500 growth phenotype, certainly much less severe than the Arabidopsis *cop1* mutant phenotypes
501 (Kreiss et al., 2023). In this study, we analyzed mutants of the single Mp*COP1* gene in light-grown
502 Marchantia plants and found that, although they completed their asexual life cycle, they exhibited
503 profound transcriptome changes and a severe constitutively photomorphogenic phenotype.
504 Additionally, consistent with the described role of COP1 in UV-B signaling in Arabidopsis and
505 Chlamydomonas (Oravecz et al., 2006; Favory et al., 2009; Allorent et al., 2016; Tilbrook et al.,
506 2016), transient gene expression changes upon exposure to UV-B were dependent on MpCOP1.
507 The Marchantia genome contains a single gene encoding MpSPA that interacts with MpCOP1 and
508 MpCRY (Zhang et al., 2021). Surprisingly, Mp*spa* null mutants exhibited at most a mild
509 constitutively photomorphogenic phenotype in white light, unlike Mp*cop1*. Interestingly, in
510 Physcomitrium, a Pp*spa_ab* double mutant displayed an intermediate phenotype between that of
511 the wild type and Pp*cop1_9x*. This suggests that SPA proteins indeed play a lesser role in repressing
512 light signaling in bryophytes compared to in angiosperms (Huang et al., 2013; Ordonez-Herrera et
513 al., 2015; Artz et al., 2019; Kreiss et al., 2023) and that high dependence of COP1 on the accessory
514 SPA proteins evolved later, meaning that SPA protein evolution is separate to the evolution of
515 COP1 activity regulation by light. This is further supported by the discovery of the UVR8- and
516 cryptochrome photoreceptor–mediated COP1 inactivation mechanism of high-affinity competitive
517 binding and displacement of COP1 substrates (Lau et al., 2019; Ponnu et al., 2019; Trimborn et al.,
518 2025). Moreover, complementation of corresponding Arabidopsis mutant phenotypes was possible
519 with a Physcomitrium COP1 ortholog but not a SPA ortholog (Ranjan et al., 2014), further
520 indicating the divergence of SPA function between evolutionary lineages.

521 Enhanced UV-B-induced changes in gene expression, increased accumulation of UV-
522 absorbing compounds, and enhanced UV-B acclimation and photoprotection against UV stress in

523 Mp*spa* mutants compared to that in wild type revealed a repressor role for SPA in the UV-B
524 signaling pathway of Marchantia. This is similar to Mp*rup* mutants, although long-term growth
525 under UV-B was not as strongly inhibited in Mp*spa*. MpSPA also did not facilitate MpUVR8
526 redimerization like observed for MpRUP. Several hypotheses can be proposed to explain the
527 Mp*spa* phenotype. It has been reported that MpSPA can promote the ubiquitination of MpHY5 by
528 MpCOP1 (Zhang et al., 2021). Consequently, the lack of MpSPA could result in reduced
529 ubiquitination of MpHY5 by MpCOP1, leading to higher activation of downstream genes. Also,
530 UV-B-activated MpUVR8 may inactivate MpCOP1 more strongly in the absence of MpSPA,
531 leading to an enhanced UV-B response. MpSPA might function by "shielding" the MpCOP1/SPA
532 complex from being inhibited by MpUVR8 under UV-B by providing an additional UVR8-
533 irrepressible activity. Moreover, it has been suggested that SPA proteins promote the
534 phosphorylation of several proteins involved in light signaling in Arabidopsis, including UVR8
535 and HY5 (Wang et al., 2021; Liu et al., 2024). Therefore, in the event such activity is conserved,
536 the absence of MpSPA may affect the phosphorylation status and activity of light signaling
537 components, enabling the Mp*spa* mutant to respond more strongly to UV-B and to produce more
538 "sunscreen" metabolites. Future work is required to elucidate the precise mechanism by which
539 MpSPA exerts its repressive effect on UV-B signaling in Marchantia, and to determine if a similar
540 SPA protein function exists in Arabidopsis or whether this represents a species-specific UV-B
541 response regulatory mechanism. Overall, genetic analysis of COP1/SPA function suggests that,
542 whereas the role of COP1 is widely conserved within the green lineage, the importance of SPA
543 proteins in regulating COP1 activity and repressing photomorphogenesis increased during plant
544 evolution.

545 It is of note that the role and importance of the transcriptional regulators HY5/HYH in
546 UVR8-signaling has also changed during plant evolution. HY5 is a major player in UVR8-
547 signaling in Arabidopsis (Ulm et al., 2004; Brown et al., 2005; Oravecz et al., 2006; Binkert et al.,
548 2014), whereas the closest Chlamydomonas homolog of HY5, CrBLZ3, plays only a minor role in
549 the algal UV-B response (Dannay et al., 2025). Instead, the B-box family transcription factor and
550 CrCOP1 substrate CrCONSTANS is the main player in the CrUVR8 signaling pathway (Gabilly
551 et al., 2019; Tokutsu et al., 2019; Dannay et al., 2025). In Marchantia, MpHY5 controls a subset
552 of MpUVR8-induced genes but has a less prominent role than its counterpart in Arabidopsis. Other
553 transcription factor(s) mediating MpUVR8 signaling remain to be identified.

554 In land plants, UVR8 activates the phenylpropanoid pathway, increasing the accumulation
555 of visible anthocyanins and colorless, UV-absorbing phenylpropanoids, such as flavonoids and
556 hydroxycinnamic acids, which overall contribute to photoprotection. Sinapate esters play a major
557 UV-sunscreen role in Arabidopsis (Stracke et al., 2010; Ferreyra et al., 2021; Leonardelli et al.,
558 2024), but are not present in Marchantia. Anthocyanins are also absent in Marchantia, but a red
559 pigment derived from chalcones, auronidin, is strongly accumulated upon different stresses (Albert
560 et al., 2018; Berland et al., 2019). Auronidin biosynthesis is catalyzed by MpAUS, a polyphenol
561 oxidase (PPO) enzyme found exclusively in liverworts and angiosperms, but not in hornworts and
562 mosses (Fig. 9A) (Davies et al., 2022; Furudate et al., 2023). Expression of Mp*AUS* is strongly
563 upregulated by UV-B in a UVR8-dependent manner. As Mp*AUS* overaccumulation following
564 Mp*MYB14* overexpression was associated with increased UV-B tolerance (Clayton et al., 2018),
565 we further characterized the role of MpAUS in UV-B photoprotection. A combination of genetics,
566 physiological analysis, and metabolomics revealed that MpAUS contributes to photoprotection
567 against UV-B. However, this contribution may not solely be attributed to the synthesis of auronidin,
568 as the accumulation of many other UV-B absorbing compounds was affected in the Mp*aus* mutant.
569 This indicates that MpAUS has specificity for more than just auronidin biosynthesis as previously
570 proposed (Berland et al., 2019) and may accept different substrates (Furudate et al., 2023). Future
571 experiments will be necessary to more precisely characterize how different classes of
572 phenylpropanoids contribute to photoprotection, and to investigate other types of photoprotective
573 mechanisms in Marchantia.
574 In conclusion, our study provides a comprehensive understanding of the UV-B perception
575 and signaling mechanisms in the liverwort model organism Marchantia. Our findings further
576 confirm and strengthen the notion that the UVR8 photoreceptor and its associated signaling
577 components are conserved in Marchantia, highlighting the evolutionary importance of this pathway
578 in mediating UV-B responses across land plants. Our analysis of the COP1/SPA E3 ligase complex
579 and its HY5 substrate in Marchantia also revealed divergences in the functions of this
580 photomorphogenesis-repressing complex. Overall, our work further validates Marchantia as a
581 useful system to investigate light signaling and its evolution in plants.
582

583 # MATERIALS AND METHODS

584 ## Plant materials

585 The *Marchantia polymorpha* accessions Takaragaike-1 (Tak-1) and Takaragaike-2 (Tak-2) were
586 used as male and female wild type, respectively (Ishizaki et al., 2008). The Mp*uvr8-1* mutant was
587 described previously (Kondou et al., 2019), whereas the following mutants were generated using
588 CRISPR–Cas9-mediated mutagenesis (Sugano et al., 2018; Sauret-Güeto et al., 2020): Mp*rup-2,*
589 Mp*rup-3,* Mp*cop1-1,* Mp*cop1-2,* Mp*spa-9,* Mp*spa-10,* Mp*hy5-1,* Mp*hy5-3,* Mp*hy5-7,* Mp*aus-2*,
590 and Mp*aus-3*. Two different gene-specific guide RNAs (gRNAs, see Supplemental Table S10)
591 were selected using the CRISPRdirect (https://crispr.dbcls.jp/) or CasFinder
592 (https://marchantia.info/tools/casfinder/) tools (Aach et al., 2014). Corresponding complementary
593 DNA oligos were annealed and ligated into the BsaI sites of pMpGE_En03, then subcloned to the
594 binary vector pMpGE010 (Sugano et al., 2018) using Gateway LR Clonase II (Thermo Fisher
595 Scientific). To generate the Mp*hy5* and Mp*aus* mutants, complementary oligos were inserted into
596 BbsI sites of the L1_lacZgRNA-Ck2 and L1_lacZgRNA-Ck3 vectors, respectively, after which
597 these were recombined by SapI restriction enzymes with the L1_HyR-Ck1 and L1_Cas9-Ck4
598 vector into the pCsA acceptor plasmid using Golden Gate Loop Assembly (Sauret-Güeto et al.,
599 2020). Following transformation, frame-shift and early stop codon mutants were identified using
600 PCR genotyping and Sanger sequencing (Supplemental Table S10, and Supplemental Fig. S3 with
601 actual mutations).

602 To generate *Pro*$_{\text{Mp}UVR8}$:*GFP*-Mp*UVR8* reporter lines, we modified the previously described
603 pMpGWB301-MpUVR8 genomic construct (Kondou et al., 2019). The vector was digested with
604 MluI and HpaI restriction enzymes and the GFP coding sequence was ligated immediately
605 upstream of the Mp*UVR8* start codon. To create Pro$_{\text{Mp}CHS2}$:*LUC* reporter lines, the predicted
606 Mp*CHS2* promoter including 5′UTR sequence (3,000 bp region upstream of the Mp*CHS2* start
607 codon) was amplified from Tak-1 genomic DNA and the PCR product was inserted into
608 pDONR207 via Gateway BP reaction. The *Pro*$_{\text{Mp}CHS2}$ sequence was then transferred into the
609 pMpGWB331 vector by LR reaction, followed by transformation into the Tak-1 wild-type
610 background. To create *Pro*$_{\text{Mp}CHS2}$*:LUC* lines in the Mp*uvr8-1* and Mp*rup-1* backgrounds, Tak-
611 1/*Pro*$_{\text{Mp}CHS2}$*:LUC* was first crossed with Tak-2 to obtain Tak-2/*Pro*$_{\text{Mp}CHS2}$*:LUC* in female
612 background, and then the male Mp*uvr8-1* or Mp*rup-2* mutants were crossed with the female Tak-
613 2/*Pro*$_{\text{Mp}CHS2}$*:LUC* line. To generate overexpression lines in Tak-1, the coding sequences including

614 stop codons of Mp*UVR8.1*, Mp*UVR8.2*, Mp*RUP*, Mp*COP1*, and Mp*SPA* were first cloned into the
615 pDONR207 entry vector via BP reaction, then transferred via LR reaction into the pMpGWB336
616 destination vector containing the *ELONGATION FACTOR 1α* (Mp*EF1α*, Mp3g23400) promoter
617 and an N-terminal Red Fluorescent Protein (RFP) tag. Agrobacterium-mediated Marchantia thallus
618 transformation was performed as previously described (Kubota et al., 2013). Marchantia spore
619 transformation was used to generate Mp*hy5* and Mp*aus* mutants as previously described (Chiyoda
620 et al., 2008).

621 Mp*rup-2* Mp*aus-2*, Mp*spa-10* Mp*aus-2*, and Mp*uvr8-1* Mp*rup-2* Cas9-free double mutants
622 were generated by crossing: first Mp*aus-2* (male) and Mp*rup-2* (male) were crossed with Tak-2 to
623 select for female lines, followed by crossing Mp*rup-2* (male) or Mp*spa-10* (male) with Mp*aus-2*
624 (female), and Mp*uvr8-1* (male) with Mp*rup-2* (female), as previously described (Mulvey and
625 Dolan, 2023). The inheritance of the parental Mp*rup-2* Mp*aus-2* and Mp*spa-10* Mp*aus-2* alleles
626 was evaluated by Sanger sequencing for hygromycin-sensitive T1 plants. For those plants where
627 the inheritance of the parental alleles was confirmed, replica plating on plates with and without
628 hygromycin was repeated to further verify the absence of the Cas9 transgene.
629

630 **Growth conditions and light treatments**

631 For maintenance, Marchantia plants were cultured aseptically on half-strength Gamborg's B5
632 medium with 1.2% (w/v) agar at 22°C under continuous white light (50 µmol m^{-2} s^{-1}) in a CLF
633 GroBank growth chamber. For UV-B acclimation experiments, continuous white light was
634 supplemented with narrowband UV-B tubes (Philips TL20W/01RS, 1.5 µmol m^{-2} s^{-1}). For UV-B
635 stress treatments, plates were irradiated under broadband UV-B tubes (Philips TL20W/12RS; 25
636 µmol m^{-2} s^{-1}).
637

638 **Crosslinking and immunoblotting**

639 Crosslinking of proteins and immunoblot analysis of 7-day-old Marchantia gemmalings was
640 performed following a modified version of a previously described method (Rizzini et al., 2011),
641 except that the extraction buffer did not contain leupeptine, dichloroisocumarin, MG115, and PSI.
642 Polyclonal rabbit anti-MpUVR8$^{(3-17)}$ antibodies raised and purified against a synthetic peptide
643 (amino acids C + 3–17: CDSKMSSNERPRRRVL) were used as the primary antibodies
644 (Eurogentec), with horseradish peroxidase (HRP)-conjugated anti-rabbit immunoglobulins (Dako

645 A/S) as secondary antibodies. The signal was revealed using ECL Select Western Blotting
646 Detection Reagent (GE Healthcare) and analyzed using an Amersham Imager 680 camera system
647 (GE Healthcare).
648

649 **Quantitative reverse transcription PCR (RT-qPCR) analysis**

650 RNA was isolated with the RNeasy Plant Mini kit (Qiagen) according to the manufacturer's
651 instructions and was treated on-column with the RQ1 RNase-Free DNase (Promega), before
652 serving as template for cDNA synthesis using the TaqMan Reverse Transcription Reagents kit
653 (Thermo Fisher Scientific) with a 1:1 mix of oligo-dT and random hexamer primers. RT-qPCR
654 was performed using the PowerUp SYBR Green Master Mix (Thermo Fisher Scientific) on a
655 QuantStudio™ 5 Real-Time PCR System (Thermo Fisher Scientific). Mp*EF1α* was used as
656 reference gene for normalization (Saint-Marcoux et al., 2015), and expression values were
657 calculated using the $2^{(-\Delta\Delta Ct)}$ method (Livak and Schmittgen, 2001). Gene-specific primers are listed
658 in Supplemental Table S10. Every experiment was performed using three biological replicates, and
659 all expression values were normalized against the average of untreated wild type, which was set to
660 1.
661

662 **Yeast two-hybrid**

663 Yeast two-hybrid assays were performed as described previously (Rizzini et al., 2011). Gateway-
664 based cloning was used to insert the Mp*UVR8.1*, Mp*UVR8.2*, Mp*RUP*, Mp*COP1*, and Mp*SPA*
665 coding sequences downstream of the LexA DNA binding domain (BD) in pBTM116-D9 (Stelzl et
666 al., 2005) or GAL4 activation domain (AD) in pGADT7-GW (Marrocco et al., 2006). The empty
667 vectors were used as negative controls. All the constructs were transformed into the yeast strain
668 L40 using the lithium-acetate protocol (Gietz et al., 2014). For the interaction assays, serial
669 dilutions of transformed yeast colonies were grown under narrowband UV-B (1.5 µmol m^{-2} s^{-1}) at
670 30°C for three days either under a WG305 (+UV-B) or a WG368 (-UV-B control) cut-off filter
671 (Schott Glaswerke). For quantification, transformed yeast colonies were grown under +UV-B or -
672 UV-B control conditions for 16 h. Ten colonies were then combined and resuspended in YPD
673 media, OD_{600} was measured, and cells were spun down and washed. The quantitative interaction
674 assay was carried out with chlorophenol red-β-D-galactopyranoside (CPRG; Roche Applied
675 Science) as substrate, according to the Yeast Protocols Handbook (Clontech, Version PR973283).

676

677 **Affinity purification – mass spectrometry (AP–MS)**

678 AP–MS was performed using a Marchantia transgenic line expressing *Pro*$_{\mathrm{Mp}UVR8}$*:GFP*-Mp*UVR8*,
679 with wild-type Tak-1 and a *Pro*$_{\mathrm{Mp}UBQ2}$*:mVenus* line as negative controls. Plants were grown for 7
680 days under continuous white light (50 µmol m^{-2} s^{-1}) without UV-B, or under continuous white light
681 (50 µmol m^{-2} s^{-1}) supplemented with narrowband UV-B (1.5 µmol m^{-2} s^{-1}) followed by a 20 min
682 broadband UV-B exposure (25 µmol m^{-2} s^{-1}) immediately prior to harvest. Total protein was
683 extracted and GFP-Trap agarose beads (Chromotek) were used for affinity purifications. Eluted
684 proteins were subjected to LC-MS/MS analysis.

685 Sample preparation and LC-MS/MS data acquisition: enriched proteins were submitted to
686 an on-bead digestion using trypsin. In brief, dry beads were re-dissolved in 25 µL digestion buffer
687 1 (50 mM Tris, pH 7.5, 2M urea, 1mM DTT, 5 ng/µL trypsin) and incubated for 30 min at 30 °C
688 in a Thermomixer with 400 rpm. Next, beads were pelleted and the supernatant was transferred to
689 a fresh tube. Digestion buffer 2 (50 mM Tris, pH 7.5, 2M urea, 5 mM CAA) was added to the
690 beads, after mixing the beads were pelleted, the supernatant was collected and combined with the
691 previous one. The combined supernatants were then incubated o/n at 32°C in a Thermomixer with
692 400 rpm; samples were protected from light during incubation. The digestion was stopped by
693 adding 1 µL TFA and desalted with C18 Empore disk membranes according to the StageTip
694 protocol (Rappsilber et al., 2003).

695 Dried peptides were re-dissolved in 2% ACN, 0.1% TFA (10 µL) for analysis. Samples
696 were analyzed using an EASY-nLC 1200 (Thermo Fisher) coupled to a Q Exactive Plus mass
697 spectrometer (Thermo Fisher). Peptides were separated on 16 cm frit-less silica emitters (New
698 Objective, 75 µm inner diameter), packed in-house with reversed-phase ReproSil-Pur C18 AQ 1.9
699 µm resin (Dr. Maisch). Peptides were loaded on the column and eluted for 115 min using a
700 segmented linear gradient of 5% to 95% solvent B (0 min : 5%B; 0-5 min -> 5%B; 5-65 min ->
701 20%B; 65-90 min ->35%B; 90-100 min -> 55%; 100-105 min ->95%, 105-115 min ->95%)
702 (solvent A 0% ACN, 0.1% FA; solvent B 80% ACN, 0.1%FA) at a flow rate of 300 nL/min. Mass
703 spectra were acquired in data-dependent acquisition mode with a TOP15 method. MS spectra were
704 acquired in the Orbitrap analyzer with a mass range of 300–1750 m/z at a resolution of 70,000
705 FWHM and a target value of 3×10^6 ions. Precursors were selected with an isolation window of 1.3
706 m/z (Q Exactive Plus). HCD fragmentation was performed at a normalized collision energy of 25.

707 MS/MS spectra were acquired with a target value of 10^5 ions at a resolution of 17,500 FWHM, a
708 maximum injection time (max.) of 55 ms and a fixed first mass of m/z 100. Peptides with a charge
709 of +1, greater than 6, or with unassigned charge state were excluded from fragmentation for MS^2,
710 dynamic exclusion for 30s prevented repeated selection of precursors.

711 Data analysis: raw data were processed using MaxQuant software (version 1.6.3.4,
712 http://www.maxquant.org/) (Cox and Mann, 2008) with label-free quantification (LFQ) and iBAQ
713 enabled (Tyanova et al., 2016).

714 MS/MS spectra were searched by the Andromeda search engine against a combined
715 database containing the sequences from *M. polymorpha* (MpTak_v6.1r2.protein.fasta;
716 https://marchantia.info/download/MpTak_v6.1r2/) and sequences of 248 common contaminant
717 proteins and decoy sequences. Trypsin specificity was required and a maximum of two missed
718 cleavages allowed. Minimal peptide length was set to seven amino acids. Carbamidomethylation
719 of cysteine residues was set as fixed, oxidation of methionine and protein N-terminal acetylation
720 as variable modifications. The match between runs option was enabled. Peptide-spectrum-matches
721 and proteins were retained if they were below a false discovery rate of 1% in both cases. The MS
722 data have been deposited in the ProteomeXchange Consortium via the PRIDE partner repository
723 with the dataset identifier PXD065691.

724 Statistical analysis of the MaxLFQ values was carried out using Perseus (version 1.5.8.5,
725 http://www.maxquant.org/). Quantified proteins were filtered for reverse hits and hits "identified
726 by site" and MaxLFQ values were log2 transformed. After grouping samples by condition only
727 those proteins were retained for the subsequent analysis that had three valid values in one of the
728 conditions. Missing values were imputed from a normal distribution (1.8 downshift, separately for
729 each column). Significantly enriched proteins were identified using a p-value cutoff of < 0.01 and
730 a log10 fold change threshold of ±1.0 (Supplementary Table S11).

731

732 **F_v/F_m measurements**

733 A PSI (Photon Systems Instruments) FluorCam 800 MF was used to measure the maximum
734 quantum efficiency of PSII (F_v/F_m). Plates containing 15 gemmalings per genotype were incubated
735 in darkness for at least 5 minutes, which was sufficient to ensure a steady state under the plant
736 growth conditions. Maximum fluorescence in the dark (F_m) was measured using saturating pulses
737 of 2000 µmol m^{-2} s^{-1} white light (400–720 nm) for 960 ms, followed by detection pulses of orange-

738 red light (620 nm) lasting 10 µs. The F_v/F_m ratio was calculated using the formula $F_v/F_m = (F_m -$
739 $F_o) / F_m$, where Fm represents the maximal fluorescence, and F_o represents the minimal
740 fluorescence in the dark-adapted state.
741

742 **Luciferase complementation imaging (LCI) and reporter assays**

743 The split-luciferase assays were performed as previously described (Zhou et al., 2018). Site-
744 directed mutagenesis was performed as described previously (Sawano and Miyawaki, 2000) to
745 generate MpUVR8.1^{D95N,D106N} and MpUVR8.2^{D95N,D106N}. The pCambia1300–nLUC vector was
746 first digested with BamHI and SalI, while the pCambia1300–cLUC vector was digested with KpnI
747 and SalI. Subsequently, the cDNA fragments of Mp*UVR8.1*, Mp*UVR8.2*, Mp*UVR8.1*^{D95N,D106N},
748 Mp*UVR8.2*^{D95N,D106N}, Mp*RUP*, and Mp*COP1* were cloned into the two digested vectors using
749 Gibson assembly. *Agrobacterium tumefaciens* strain GV3101 harboring the indicated
750 combinations of constructs expressing nLUC and cLUC fusion proteins were mixed in a 1:1 ratio
751 and infiltrated into *N. benthamiana* leaves. The plants were kept in the growth chamber for 2 days
752 before being incubated with 1 mM luciferin (D-luciferin sodium salt, Yeasen Biotechnology) for
753 10 min (in darkness). Luciferase activity was detected using a NightSHADE LB985 In Vivo Plant
754 Imaging System (Berthold).

755 For *Pro*$_{MpCHS2}$*:LUC* luciferase reporter assays, gemmae were transferred into 96-well plates
756 containing ½-strength Gamborg's B5 medium with 1.2% (w/v) agar and grown under at 22°C
757 continuous white light (50 µmol m^{-2} s^{-1}) in a CLF GroBank growth chamber for two days. Four-
758 µL of 1 mM luciferin (Yeasen Biotechnology) were added to each well and the following day plants
759 were exposed to UV-B for 20 min and luminescence was recorded using a Centro XS LB 960
760 luminometer.
761

762 **Extraction of phenolic compounds, measurements of absorption spectra, and high-**
763 **performance thin-layer chromatography (HPTLC)**

764 Phenolic compounds were extracted in 100 µL of 80% (v/v) methanol from 50 mg of fresh plant
765 material homogenized using a Silamat S6 (Ivodar Vivadent). Extracts were incubated for 10 min
766 at 70°C on a shaker and centrifuged for 10 min at 12,000 *g* at room temperature (RT). A 40-µL
767 aliquot of clear supernatant from each extract was transferred to a transparent 96-well plate and
768 absorption spectra (200–1000 nm wavelengths) were measured using a TECAN Spark 10M

769 Multimode Microplate Reader. In case absorbance values exceeded the linear range, aliquots were
770 uniformly diluted with extraction buffer.
771 HPTLC was used to analyze the phenolic compound profile using silica-60 HPTLC glass
772 plates (Sigma-Aldrich), as described previously (Stracke et al., 2010; Leonardelli et al., 2024).
773

774 **Microscopy**

775 *Pro*Mp*UVR8*:*GFP*-Mp*UVR8* transgenic gemmalings were grown for 7 days under
776 50 µmol $m^{-2}s^{-1}$ white light and irradiated for 20 min with 25 µmol m^{-2} s^{-1} broadband UV-B.
777 Imaging was performed using a Leica Thunder Widefield microscope in both GFP and bright-field
778 modes. Z-stack images were acquired at 2-µm intervals. Image processing and Z-projection were
779 conducted using ImageJ software.
780

781 **Transcriptome analysis**

782 Gemmalings were grown for 7 days in 50 µmol m^{-2} s^{-1} white light and exposed or not to
783 supplemental UV-B (1.5 µmol m^{-2} s^{-1}) for 3 h. Total RNA was extracted using the RNeasy Plant
784 Mini kit (Qiagen) and Illumina Tru-Seq libraries were generated from cDNA and sequenced using
785 Illumina NovaSeq 100-bp single-end at the iGE3 genomics platform of the University of Geneva
786 (Supplementary Table S1). Raw reads were trimmed for quality using Trim Galore (v0.6.7;
787 github.com/FelixKrueger/TrimGalore) with "-q 25 --stringency 5" as parameters. Trimmed reads
788 were mapped to the MpTak.v7.1 genome reference using STAR (v2.7.4; (Dobin et al., 2013),
789 followed by read quantification using featureCounts (Subread v2.0.1; (Liao et al., 2019). The raw
790 counts were normalized and differential expression analysis was performed using DESeq2 (Love
791 et al., 2014). Genes with a $\log_2$ fold change greater than 1 and a p-adj value of less than 0.05 were
792 considered as significantly differentially expressed. Genes with lower log2 fold change values and
793 p-adj < 0.05 were considered when comparing different genotypes in which gene expression
794 changes may occur at varying magnitude (Supplementary Table S2). Euler plots were generated
795 using the eulerr package in R. Heatmaps were generated using the heatmap.2 function in the gplots
796 package in R. The raw RNA-sequencing data has been deposited in the NCBI Gene Expression
797 Omnibus (www.ncbi.nlm.nih.gov/geo) and is accessible through GEO Series accession number
798 GSE296364.
799

800 ## Untargeted metabolomics

801 7-day-old Marchantia gemmalings were ground in liquid nitrogen using a mortar and pestle. 50 mg
802 of tissue powder were transferred into a 1.5-mL tube and compounds were extracted with 5
803 volumes of 80% (v/v) methanol containing 0.1% (v/v) formic acid. After centrifugation, the
804 supernatant was transferred to an HPLC glass vial fitted with a conical insert. A 0.75-µL injection
805 of the extract was performed into ultrahigh performance liquid chromatography coupled to high-
806 resolution mass spectrometry (UHPLC-HRMS) equipped with an electrospray ionization (ESI)
807 source operating in negative (ESI-) ionization mode. Specifically, the system used was an Acquity
808 UPLC I-Class (Waters) interfaced with a Synapt XS QTOF (Waters). The parameters used for
809 untargeted metabolomics were based on (Defossez et al., 2023) with minor adjustments. Briefly,
810 chromatography was done on a Waters Acquity UPLC™ HSS T3 column (100 × 2.1 mm, 1.8 µm)
811 with mobile phases consisting of H2O + 0.05% (v/v) formic acid (solvent A) and acetonitrile + 0.05%
812 (v/v) formic acid (solvent B). A linear gradient from 0 to 100% B in 10.0 min at a flow rate of 0.5
813 mL/min was applied. MS detection was performed in negative electrospray ionisation using data-
814 dependent acquisition (DDA). The mass range for both MS and MS/MS was 50–1200 Da. Scan
815 times for MS and MS/MS were 0.1 and 0.05 s, respectively. The top 7 precursor ions were selected
816 for MS/MS with an intensity threshold of 15,000 counts per second. An exclusion list of the 150
817 most intense background ions was generated from a blank sample run just before the plant samples,
818 and a dynamic exclusion of 1.5 s was applied after each MS/MS acquisition. For MS/MS
819 acquisition, a ramped collision energy of 5–40 V (at *m/z* 50) and 20–70 V (at *m/z* 1200) was set.
820 The entire system and method were controlled by MassLynx 4.2 (Waters). Raw profile data were
821 first centroided in MassLynx and further converted to MzML using MSConvert (ProteoWizard).
822 We used MZmine 4.5 for feature detection, deconvolution, and alignment of DDA (data-dependent
823 acquisition) data, with noise thresholds set to 2000 for MS1 and 50 for MS2 (Schmid et al., 2023).
824 The resulting peak table and MS/MS spectral data were exported and annotated using SIRIUS 6.2
825 (Duhrkop et al., 2019), including CSI:FingerID for structural identification and CANOPUS for the
826 prediction of compound classes, superclasses, and biosynthetic pathways. Taxonomically informed
827 reannotation of molecular features was performed using the Tima R package (Rutz and Allard,
828 2025).
829

830 ## Statistical analyses

831 Statistical analyses were performed using GraphPad Software Prism 10 software (San Diego,
832 California). Statistical significance of the differences between means was determined using one-
833 or two-way analysis of variance (ANOVAs) followed by Tukey's post hoc honestly significant
834 difference (HSD) test for multiple comparisons. For metabolomics, adjusted p-values were
835 calculated and corrected using the Benjamini-Hochberg in R.

836

837 ## Accession numbers

838 Mp2g11590 (Mp*UVR8*), Mp2g18040 (Mp*RUP*), Mp5g12010 (Mp*COP1*), Mp3g25460 (Mp*SPA*),
839 Mp1g16800 (Mp*HY5*), Mp2g05850 (Mp*AUS*), Mp2g07060 (Mp*CHS2*), Mp1g10150 (Mp*PAL1*),
840 Mp6g00020 (Mp*C4H1*), Mp8g05070 (Mp*C4H2*), Mp8g05080 (Mp*C4H3*), Mp1g27780
841 (Mp*4CL1*), Mp1g05060 (Mp*4CL2*), Mp2g22700 (Mp*CHS6*), Mp5g01410 (Mp*CHIL2*),
842 Mp6g05290 (Mp*CHI*), Mp1g26540 (Mp*F3H*), Mp3g23400 (Mp*EF1α*).

843

844 ## Supplementary data

845 **Supplementary Figure S1.** Alignment of Marchantia MpUVR8.1 and MpUVR8.2 with
846 Arabidopsis AtUVR8.

847 **Supplementary Figure S2.** Volcano plot of GFP-MpUVR8 AP-MS under +UV versus -UV
848 conditions.

849 **Supplementary Figure S3.** Gene structure and indication of the mutated sites in the corresponding
850 mutants generated by CRISPR/Cas9.

851 **Supplementary Figure S4.** UV-B photomorphogenesis and photoprotection in MpUVR8 and
852 MpRUP transgenic lines.

853 **Supplementary Figure S5.** Enhanced photoprotection and UV-B-absorbing capacity of Mp*rup*
854 depends on MpUVR8.

855 **Supplementary Figure S6.** MpSPA does not affect MpUVR8 redimerization, but MpCOP1 and
856 MpSPA overexpression reduce basal UV-B tolerance.

857 **Supplementary Figure S7.** MpHY5 plays a minor role in the regulation of UV-B-induced gene
858 expression changes.

859 **Supplementary Figure S8.** MpHY5 and MpCOP1 regulate UV-B-induced gene expression in an
860 antagonist manner.

861 **Supplementary Figure S9.** LUC activity of a *Pro*$_{MpCHS2}$*:LUC* reporter in Tak-1, Mp*uvr8-1* and
862 Mp*rup-2* backgrounds upon UV-B exposure.
863 **Supplementary Figure S10.** MpAUS contributes to protection against UV-B stress.
864 **Supplementary Figure S11.** MpUVR8- and MpAUS-dependent regulation of metabolite
865 accumulation upon UV-B exposure.
866 **Supplementary Table S1.** List of RNA-seq libraries.
867 **Supplementary Table S2.** Raw read counts, normalized read counts and differential expression
868 analysis from RNA-seq experiments.
869 **Supplementary Table S3.** Overlaps between UV-B regulated genes in Tak-1, Mp*rup* and Mp*spa*
870 (lists corresponding to Figure 6A,B) and overlaps between genes misregulated in Mp*cop1* and
871 Mp*spa* in white light (lists corresponding to Figure 7B,C).
872 **Supplementary Table S4.** Hierarchical clustering of UV-B-regulated gene expression.
873 **Supplementary Table S5.** Hierarchical clustering of MpCOP1/SPA-regulated gene expression.
874 **Supplementary Table S6.** Overlaps between genes misregulated in Mp*cop1* in white light and
875 genes regulated by MpHY5 after UV-B exposure (lists corresponding to Supplementary Figure S8).
876 **Supplementary Table S7.** Hierarchical clustering of UV-B-regulated gene expression in Tak-1
877 and Mp*hy5*.
878 **Supplementary Table S8.** Methanol-soluble metabolites of Marchantia in presence and absence
879 of UV-B.
880 **Supplementary Table S9.** Overlaps of methanol-soluble metabolites in response to UV-B
881 between Tak-1, Mp*uvr8*, Mp*rup* and Mp*aus*. Metabolite lists corresponding to Figure 9G.
882 **Supplementary Table S10.** Primer list.
883 **Supplementary Table S11.** AP-MS data.
884

885 ## ACKNOWLEDGEMENTS

886 We would like to thank Youichi Kondou (Kanto Gakuin University College of Science and
887 Engineering, Yokohama, Japan) for kindly providing the Mp*uvr8-1* mutant and the pMpGWB301-
888 MpUVR8 construct, Félix Rico-Reséndiz (University of Geneva) for sharing protocols and tips
889 regarding Marchantia cultivation and transformation, Yanfei Zhou (The New Zealand Institute for
890 Plant and Food Research Limited, Palmerston North, New Zealand) for precious suggestions, and
891 Anne Harzen (Max-Planck Institute for Plant Breeding Research) for MS sample preparation. The

892 RNA-seq experiments were performed at the iGE3 Genomics Platform of the University of Geneva
893 (https://ige3.genomics.unige.ch/). This work was supported by the University of Geneva, and, in
894 part, the Swiss National Science Foundation (grant 310030_207716 to R.U.).
895

896 AUTHOR CONTRIBUTIONS

897 Y.L., R.P., and R.U. conceived and designed the research; Y.L., R.P., and R.C. performed the
898 experiments; G.G. and E.Def. performed and contributed metabolomic data; S.C.S and H.N.
899 performed and analyzed LC-MS/MS data; J.R. and L.D. contributed Mp*hy5* mutants; Y.L., R.P.,
900 E.Dem., and R.U. analyzed the data and wrote the manuscript. All authors reviewed and approved
901 the submitted manuscript.

902 Competing interests: The authors have declared that no competing interests exist.

903

904 # REFERENCES

905 Aach J, Mali P, Church GM (2014) CasFinder: Flexible algorithm for identifying specific Cas9 targets in
906 genomes. bioRxiv: 005074
907 Albert NW, Thrimawithana AH, McGhie TK, Clayton WA, Deroles SC, Schwinn KE, Bowman JL, Jordan BR,
908 Davies KM (2018) Genetic analysis of the liverwort *Marchantia polymorpha* reveals that R2R3MYB
909 activation of flavonoid production in response to abiotic stress is an ancient character in land
910 plants. New Phytol 218: 554-566
911 Allorent G, Lefebvre-Legendre L, Chappuis R, Kuntz M, Truong TB, Niyogi KK, Ulm R, Goldschmidt-Clermont
912 M (2016) UV-B photoreceptor-mediated protection of the photosynthetic machinery in
913 *Chlamydomonas reinhardtii*. Proc Natl Acad Sci USA 113: 14864-14869
914 Artz O, Dickopf S, Ranjan A, Kreiss M, Abraham ET, Boll V, Rensing SA, Hoecker U (2019) Characterization
915 of spa mutants in the moss Physcomitrella provides evidence for functional divergence of SPA
916 genes during the evolution of land plants. New Phytol 224: 1613-1626
917 Balcerowicz M, Kerner K, Schenkel C, Hoecker U (2017) SPA proteins affect the subcellular localization of
918 COP1 in the COP1/SPA ubiquitin ligase complex during photomorphogenesis. Plant Physiol 174:
919 1314-1321
920 Berland H, Albert NW, Stavland A, Jordheim M, McGhie TK, Zhou Y, Zhang H, Deroles SC, Schwinn KE,
921 Jordan BR, Davies KM, Andersen OM (2019) Auronidins are a previously unreported class of
922 flavonoid pigments that challenges when anthocyanin biosynthesis evolved in plants. Proc Natl
923 Acad Sci USA 116: 20232-20239
924 Binkert M, Kozma-Bognar L, Terecskei K, De Veylder L, Nagy F, Ulm R (2014) UV-B-responsive association
925 of the Arabidopsis bZIP transcription factor ELONGATED HYPOCOTYL5 with target genes, including
926 its own promoter. Plant Cell 26: 4200-4213
927 Bowman JL, Kohchi T, Yamato KT, Jenkins J, Shu S, Ishizaki K, Yamaoka S, Nishihama R, Nakamura Y, Berger
928 F, Adam C, Aki SS, Althoff F, Araki T, Arteaga-Vazquez MA, Balasubrmanian S, Barry K, Bauer D,
929 Boehm CR, Briginshaw L, Caballero-Perez J, Catarino B, Chen F, Chiyoda S, Chovatia M, Davies KM,
930 Delmans M, Demura T, Dierschke T, Dolan L, Dorantes-Acosta AE, Eklund DM, Florent SN, Flores-
931 Sandoval E, Fujiyama A, Fukuzawa H, Galik B, Grimanelli D, Grimwood J, Grossniklaus U, Hamada

932 T, Haseloff J, Hetherington AJ, Higo A, Hirakawa Y, Hundley HN, Ikeda Y, Inoue K, Inoue SI, Ishida
933 S, Jia Q, Kakita M, Kanazawa T, Kawai Y, Kawashima T, Kennedy M, Kinose K, Kinoshita T, Kohara
934 Y, Koide E, Komatsu K, Kopischke S, Kubo M, Kyozuka J, Lagercrantz U, Lin SS, Lindquist E, Lipzen
935 AM, Lu CW, De Luna E, Martienssen RA, Minamino N, Mizutani M, Mizutani M, Mochizuki N,
936 Monte I, Mosher R, Nagasaki H, Nakagami H, Naramoto S, Nishitani K, Ohtani M, Okamoto T,
937 Okumura M, Phillips J, Pollak B, Reinders A, Rovekamp M, Sano R, Sawa S, Schmid MW, Shirakawa
938 M, Solano R, Spunde A, Suetsugu N, Sugano S, Sugiyama A, Sun R, Suzuki Y, Takenaka M, Takezawa
939 D, Tomogane H, Tsuzuki M, Ueda T, Umeda M, Ward JM, Watanabe Y, Yazaki K, Yokoyama R,
940 Yoshitake Y, Yotsui I, Zachgo S, Schmutz J (2017) Insights into land plant evolution garnered from
941 the *Marchantia polymorpha* genome. Cell 171: 287-304 e215
942 Brown BA, Cloix C, Jiang GH, Kaiserli E, Herzyk P, Kliebenstein DJ, Jenkins GI (2005) A UV-B-specific signaling
943 component orchestrates plant UV protection. Proc Natl Acad Sci USA 102: 18225-18230
944 Chen H, Huang X, Gusmaroli G, Terzaghi W, Lau OS, Yanagawa Y, Zhang Y, Li J, Lee JH, Zhu D, Deng XW
945 (2010) Arabidopsis CULLIN4-damaged DNA binding protein 1 interacts with CONSTITUTIVELY
946 PHOTOMORPHOGENIC1-SUPPRESSOR OF PHYA complexes to regulate photomorphogenesis and
947 flowering time. Plant Cell 22: 108-123
948 Chiyoda S, Ishizaki K, Kataoka H, Yamato KT, Kohchi T (2008) Direct transformation of the liverwort
949 *Marchantia polymorpha* L. by particle bombardment using immature thalli developing from spores.
950 Plant Cell Rep 27: 1467-1473
951 Christie JM, Arvai AS, Baxter KJ, Heilmann M, Pratt AJ, O'Hara A, Kelly SM, Hothorn M, Smith BO, Hitomi K,
952 Jenkins GI, Getzoff ED (2012) Plant UVR8 photoreceptor senses UV-B by tryptophan-mediated
953 disruption of cross-dimer salt bridges. Science 335: 1492-1496
954 Clayton WA, Albert NW, Thrimawithana AH, McGhie TK, Deroles SC, Schwinn KE, Warren BA, McLachlan
955 ARG, Bowman JL, Jordan BR, Davies KM (2018) UVR8-mediated induction of flavonoid biosynthesis
956 for UVB tolerance is conserved between the liverwort *Marchantia polymorpha* and flowering
957 plants. Plant J 96: 503-517
958 Cox J, Mann M (2008) MaxQuant enables high peptide identification rates, individualized p.p.b.-range
959 mass accuracies and proteome-wide protein quantification. Nat Biotechnol 26: 1367-1372
960 Dannay M, Bertin C, Cavallari E, Albanese P, Tolleter D, Giustini C, Menneteau M, Brugiere S, Coute Y,
961 Finazzi G, Demarsy E, Ulm R, Allorent G (2025) Photoreceptor-induced LHL4 protects the
962 photosystem II monomer in *Chlamydomonas reinhardtii*. Proc Natl Acad Sci USA 122:
963 e2418687122
964 Davies KM, Landi M, van Klink JW, Schwinn KE, Brummell DA, Albert NW, Chagne D, Jibran R, Kulshrestha
965 S, Zhou Y, Bowman JL (2022) Evolution and function of red pigmentation in land plants. Ann Bot
966 130: 613-636
967 Defossez E, Bourquin J, von Reuss S, Rasmann S, Glauser G (2023) Eight key rules for successful data-
968 dependent acquisition in mass spectrometry-based metabolomics. Mass Spectrom Rev 42: 131-
969 143
970 Demarsy E, Goldschmidt-Clermont M, Ulm R (2018) Coping with 'dark sides of the sun' through
971 photoreceptor signaling. Trends Plant Sci 23: 260-271
972 Dobin A, Davis CA, Schlesinger F, Drenkow J, Zaleski C, Jha S, Batut P, Chaisson M, Gingeras TR (2013) STAR:
973 ultrafast universal RNA-seq aligner. Bioinformatics 29: 15-21
974 Duhrkop K, Fleischauer M, Ludwig M, Aksenov AA, Melnik AV, Meusel M, Dorrestein PC, Rousu J, Bocker S
975 (2019) SIRIUS 4: a rapid tool for turning tandem mass spectra into metabolite structure
976 information. Nat Methods 16: 299-302
977 Fang F, Lin L, Zhang Q, Lu M, Skvortsova MY, Podolec R, Zhang Q, Pi J, Zhang C, Ulm R, Yin R (2022)
978 Mechanisms of UV-B light-induced photoreceptor UVR8 nuclear localization dynamics. New Phytol
979 236: 1824-1837

980 Favory JJ, Stec A, Gruber H, Rizzini L, Oravecz A, Funk M, Albert A, Cloix C, Jenkins GI, Oakeley EJ, Seidlitz
981 HK, Nagy F, Ulm R (2009) Interaction of COP1 and UVR8 regulates UV-B-induced
982 photomorphogenesis and stress acclimation in Arabidopsis. EMBO J 28: 591-601
983 Ferreyra MLF, Serra P, Casati P (2021) Recent advances on the roles of flavonoids as plant protective
984 molecules after UV and high light exposure. Physiol Plant 173: 736-749
985 Findlay KM, Jenkins GI (2016) Regulation of UVR8 photoreceptor dimer/monomer photo-equilibrium in
986 Arabidopsis plants grown under photoperiodic conditions. Plant Cell Environ 39: 1706-1714
987 Frangedakis E, Yelina NE, Billakurthi K, Hua L, Schreier T, Dickinson PJ, Tomaselli M, Haseloff J, Hibberd JM
988 (2024) MYB-related transcription factors control chloroplast biogenesis. Cell 187: 4859-4876
989 e4822
990 Furudate H, Manabe M, Oshikiri H, Matsushita A, Watanabe B, Waki T, Nakayama T, Kubo H, Takanashi K
991 (2023) A polyphenol oxidase catalyzes aurone synthesis in *Marchantia polymorpha*. Plant Cell
992 Physiol 64: 637-645
993 Gabilly ST, Baker CR, Wakao S, Crisanto T, Guan K, Bi K, Guiet E, Guadagno CR, Niyogi KK (2019) Regulation
994 of photoprotection gene expression in Chlamydomonas by a putative E3 ubiquitin ligase complex
995 and a homolog of CONSTANS. Proc Natl Acad Sci USA 116: 17556-17562
996 Gietz R, Smith J, Burke D (2014) Yeast genetics: methods and protocols.
997 Gruber H, Heijde M, Heller W, Albert A, Seidlitz HK, Ulm R (2010) Negative feedback regulation of UV-B-
998 induced photomorphogenesis and stress acclimation in Arabidopsis. Proc Natl Acad Sci USA 107:
999 20132-20137
1000 Heijde M, Binkert M, Yin R, Ares-Orpel F, Rizzini L, Van De Slijke E, Persiau G, Nolf J, Gevaert K, De Jaeger
1001 G, Ulm R (2013) Constitutively active UVR8 photoreceptor variant in Arabidopsis. Proc Natl Acad
1002 Sci USA 110: 20326-20331
1003 Heijde M, Ulm R (2013) Reversion of the Arabidopsis UV-B photoreceptor UVR8 to the homodimeric
1004 ground state. Proc Natl Acad Sci USA 110: 1113-1118
1005 Heilmann M, Jenkins GI (2013) Rapid reversion from monomer to dimer regenerates the ultraviolet-B
1006 photoreceptor UV RESISTANCE LOCUS8 in intact Arabidopsis plants. Plant Physiol 161: 547-555
1007 Heilmann M, Velanis CN, Cloix C, Smith BO, Christie JM, Jenkins GI (2016) Dimer/monomer status and in
1008 vivo function of salt-bridge mutants of the plant UV-B photoreceptor UVR8. Plant J 88: 71-81
1009 Hoecker U (2017) The activities of the E3 ubiquitin ligase COP1/SPA, a key repressor in light signaling. Curr
1010 Opin Plant Biol 37: 63-69
1011 Holm M, Ma LG, Qu LJ, Deng XW (2002) Two interacting bZIP proteins are direct targets of COP1-mediated
1012 control of light-dependent gene expression in Arabidopsis. Genes Dev 16: 1247-1259
1013 Hu S, Chen Y, Qian C, Ren H, Liang X, Tao W, Chen Y, Wang J, Dong Y, Han J, Ouyang X, Huang X (2024)
1014 Nuclear accumulation of rice UV-B photoreceptors is UV-B- and OsCOP1-independent for UV-B
1015 responses. Nat Commun 15: 6396
1016 Huang X, Ouyang X, Yang P, Lau OS, Chen L, Wei N, Deng XW (2013) Conversion from CUL4-based COP1-
1017 SPA E3 apparatus to UVR8-COP1-SPA complexes underlies a distinct biochemical function of COP1
1018 under UV-B. Proc Natl Acad Sci USA 110: 16669-16674
1019 Ishizaki K, Chiyoda S, Yamato KT, Kohchi T (2008) Agrobacterium-mediated transformation of the haploid
1020 liverwort *Marchantia polymorpha* L., an emerging model for plant biology. Plant Cell Physiol 49:
1021 1084-1091
1022 Jibran R, Hill SJ, Lampugnani ER, Hao P, Doblin MS, Bacic A, Vaidya AA, O'Donoghue EM, McGhie TK, Albert
1023 NW, Zhou Y, Raymond LG, Schwinn KE, Jordan BR, Bowman JL, Davies KM, Brummell DA (2024)
1024 The auronidin flavonoid pigments of the liverwort *Marchantia polymorpha* form polymers that
1025 modify cell wall properties. Plant J 120: 1159-1175
1026 Kaiserli E, Jenkins GI (2007) UV-B promotes rapid nuclear translocation of the Arabidopsis UV-B specific
1027 signaling component UVR8 and activates its function in the nucleus. Plant Cell 19: 2662-2673

1028 Kliebenstein DJ, Lim JE, Landry LG, Last RL (2002) Arabidopsis UVR8 regulates ultraviolet-B signal
1029 transduction and tolerance and contains sequence similarity to human regulator of chromatin
1030 condensation 1. Plant Physiol 130: 234-243
1031 Kondou Y, Miyagi Y, Morito T, Fujihira K, Miyauchi W, Moriyama A, Terasawa T, Ishida S, Iwabuchi K, Kubo
1032 H, Nishihama R, Ishizaki K, Kohchi T (2019) Physiological function of photoreceptor UVR8 in UV-B
1033 tolerance in the liverwort *Marchantia polymorpha*. Planta 249: 1349-1364
1034 Kreiss M, Haas FB, Hansen M, Rensing SA, Hoecker U (2023) Co-action of COP1, SPA and cryptochrome in
1035 light signal transduction and photomorphogenesis of the moss *Physcomitrium patens*. Plant J 114:
1036 159-175
1037 Kubota A, Ishizaki K, Hosaka M, Kohchi T (2013) Efficient Agrobacterium-mediated transformation of the
1038 liverwort *Marchantia polymorpha* using regenerating thalli. Biosci Biotechnol Biochem 77: 167-
1039 172
1040 Lau K, Podolec R, Chappuis R, Ulm R, Hothorn M (2019) Plant photoreceptors and their signaling
1041 components compete for COP1 binding via VP peptide motifs. EMBO J 38: e102140
1042 Laubinger S, Fittinghoff K, Hoecker U (2004) The SPA quartet: a family of WD-repeat proteins with a central
1043 role in suppression of photomorphogenesis in arabidopsis. Plant Cell 16: 2293-2306
1044 Leonardelli M, Tissot N, Podolec R, Ares-Orpel F, Glauser G, Ulm R, Demarsy E (2024) Photoreceptor-
1045 induced sinapate synthesis contributes to photoprotection in Arabidopsis. Plant Physiol 196: 1518-
1046 1533
1047 Li H, Li Y, Deng H, Sun X, Wang A, Tang X, Gao Y, Zhang N, Wang L, Yang S, Liu Y, Wang S (2018) Tomato
1048 UV-B receptor SlUVR8 mediates plant acclimation to UV-B radiation and enhances fruit chloroplast
1049 development via regulating SlGLK2. Sci Rep 8: 6097
1050 Li X, Ren H, Kundu M, Liu Z, Zhong FW, Wang L, Gao J, Zhong D (2020) A leap in quantum efficiency through
1051 light harvesting in photoreceptor UVR8. Nat Commun 11: 4316
1052 Liang Y, Heyman J, Xiang Y, Vandendriessche W, Canher B, Goeminne G, De Veylder L (2022) The wound-
1053 activated ERF15 transcription factor drives *Marchantia polymorpha* regeneration by activating an
1054 oxylipin biosynthesis feedback loop. Sci Adv 8: eabo7737
1055 Liao Y, Smyth GK, Shi W (2019) The R package Rsubread is easier, faster, cheaper and better for alignment
1056 and quantification of RNA sequencing reads. Nucleic Acids Res 47: e47
1057 Liu W, Giuriani G, Havlikova A, Li D, Lamont DJ, Neugart S, Velanis CN, Petersen J, Hoecker U, Christie JM,
1058 Jenkins GI (2024) Phosphorylation of Arabidopsis UVR8 photoreceptor modulates protein
1059 interactions and responses to UV-B radiation. Nat Commun 15: 1221
1060 Livak KJ, Schmittgen TD (2001) Analysis of relative gene expression data using real-time quantitative PCR
1061 and the 2(-Delta Delta C(T)) Method. Methods 25: 402-408
1062 Love MI, Huber W, Anders S (2014) Moderated estimation of fold change and dispersion for RNA-seq data
1063 with DESeq2. Genome Biol 15: 550
1064 Marrocco K, Zhou Y, Bury E, Dieterle M, Funk M, Genschik P, Krenz M, Stolpe T, Kretsch T (2006) Functional
1065 analysis of EID1, an F-box protein involved in phytochrome A-dependent light signal transduction.
1066 Plant J 45: 423-438
1067 McNellis TW, von Arnim AG, Araki T, Komeda Y, Misera S, Deng XW (1994) Genetic and molecular analysis
1068 of an allelic series of *cop1* mutants suggests functional roles for the multiple protein domains.
1069 Plant Cell 6: 487-500
1070 Messant M, Hani U, Hennebelle T, Guerard F, Gakiere B, Gall A, Thomine S, Krieger-Liszkay A (2023)
1071 Manganese concentration affects chloroplast structure and the photosynthetic apparatus in
1072 *Marchantia polymorpha*. Plant Physiol 192: 356-369
1073 Moriconi V, Binkert M, Costigliolo C, Sellaro R, Ulm R, Casal JJ (2018) Perception of sunflecks by the UV-B
1074 photoreceptor UV RESISTANCE LOCUS8. Plant Physiol 177: 75-81

1075 Mulvey H, Dolan L (2023) RHO GTPase of plants regulates polarized cell growth and cell division orientation
1076 during morphogenesis. Curr Biol 33: 2897-2911 e2896
1077 Murchie EH, Lawson T (2013) Chlorophyll fluorescence analysis: a guide to good practice and
1078 understanding some new applications. J Exp Bot 64: 3983-3998
1079 Oravecz A, Baumann A, Mate Z, Brzezinska A, Molinier J, Oakeley EJ, Adam E, Schafer E, Nagy F, Ulm R
1080 (2006) CONSTITUTIVELY PHOTOMORPHOGENIC1 is required for the UV-B response in Arabidopsis.
1081 Plant Cell 18: 1975-1990
1082 Ordonez-Herrera N, Fackendahl P, Yu X, Schaefer S, Koncz C, Hoecker U (2015) A *cop1 spa* mutant deficient
1083 in COP1 and SPA proteins reveals partial co-action of COP1 and SPA during Arabidopsis post-
1084 embryonic development and photomorphogenesis. Mol Plant 8: 479-481
1085 Pham VN, Paik I, Hoecker U, Huq E (2020) Genomic evidence reveals SPA-regulated developmental and
1086 metabolic pathways in dark-grown Arabidopsis seedlings. Physiol Plant 169: 380-396
1087 Podolec R, Demarsy E, Ulm R (2021) Perception and signaling of ultraviolet-B radiation in plants. Annu Rev
1088 Plant Biol 72: 793-822
1089 Podolec R, Lau K, Wagnon TB, Hothorn M, Ulm R (2021) A constitutively monomeric UVR8 photoreceptor
1090 confers enhanced UV-B photomorphogenesis. Proc Natl Acad Sci USA 118: e2017284118
1091 Podolec R, Ulm R (2018) Photoreceptor-mediated regulation of the COP1/SPA E3 ubiquitin ligase. Curr
1092 Opin Plant Biol 45: 18-25
1093 Ponnu J, Hoecker U (2021) Illuminating the COP1/SPA ubiquitin ligase: fresh insights into its structure and
1094 functions during plant photomorphogenesis. Front Plant Sci 12: 662793
1095 Ponnu J, Riedel T, Penner E, Schrader A, Hoecker U (2019) Cryptochrome 2 competes with COP1 substrates
1096 to repress COP1 ubiquitin ligase activity during Arabidopsis photomorphogenesis. Proc Natl Acad
1097 Sci USA 116: 27133-27141
1098 Qian C, Chen Z, Liu Q, Mao W, Chen Y, Tian W, Liu Y, Han J, Ouyang X, Huang X (2020) Coordinated
1099 transcriptional regulation by the UV-B photoreceptor and multiple transcription factors for plant
1100 UV-B responses. Mol Plant 13: 777-792
1101 Rai N, Neugart S, Yan Y, Wang F, Siipola SM, Lindfors AV, Winkler JB, Albert A, Brosche M, Lehto T, Morales
1102 LO, Aphalo PJ (2019) How do cryptochromes and UVR8 interact in natural and simulated sunlight?
1103 J Exp Bot 70: 4975-4990
1104 Ranjan A, Dickopf S, Ullrich KK, Rensing SA, Hoecker U (2014) Functional analysis of COP1 and SPA
1105 orthologs from Physcomitrella and rice during photomorphogenesis of transgenic Arabidopsis
1106 reveals distinct evolutionary conservation. BMC Plant Biol 14: 178
1107 Rappsilber J, Ishihama Y, Mann M (2003) Stop and go extraction tips for matrix-assisted laser
1108 desorption/ionization, nanoelectrospray, and LC/MS sample pretreatment in proteomics. Anal
1109 Chem 75: 663-670
1110 Rizzini L, Favory JJ, Cloix C, Faggionato D, O'Hara A, Kaiserli E, Baumeister R, Schafer E, Nagy F, Jenkins GI,
1111 Ulm R (2011) Perception of UV-B by the Arabidopsis UVR8 protein. Science 332: 103-106
1112 Rutz A, Allard P (2025) tima: taxonomically informed metabolite annotation (2.11.0) [R package]. Zenodo:
1113 https://doi.org/10.5281/zenodo.5797920
1114 Saint-Marcoux D, Proust H, Dolan L, Langdale JA (2015) Identification of reference genes for real-time
1115 quantitative PCR experiments in the liverwort *Marchantia polymorpha*. PLoS One 10: e0118678
1116 Sauret-Güeto S, Frangedakis E, Silvestri L, Rebmann M, Tomaselli M, Markel K, Delmans M, West A, Patron
1117 NJ, Haseloff J (2020) Systematic tools for reprogramming plant gene expression in a simple model,
1118 *Marchantia polymorpha*. ACS Synth Biol 9: 864-882
1119 Sawano A, Miyawaki A (2000) Directed evolution of green fluorescent protein by a new versatile PCR
1120 strategy for site-directed and semi-random mutagenesis. Nucleic Acids Res 28: E78
1121 Schmid R, Heuckeroth S, Korf A, Smirnov A, Myers O, Dyrlund TS, Bushuiev R, Murray KJ, Hoffmann N, Lu
1122 M, Sarvepalli A, Zhang Z, Fleischauer M, Duhrkop K, Wesner M, Hoogstra SJ, Rudt E, Mokshyna O,

1123 Brungs C, Ponomarov K, Mutabdzija L, Damiani T, Pudney CJ, Earll M, Helmer PO, Fallon TR, Schulze
1124 T, Rivas-Ubach A, Bilbao A, Richter H, Nothias LF, Wang M, Oresic M, Weng JK, Bocker S, Jeibmann
1125 A, Hayen H, Karst U, Dorrestein PC, Petras D, Du X, Pluskal T (2023) Integrative analysis of
1126 multimodal mass spectrometry data in MZmine 3. Nat Biotechnol 41: 447-449
1127 Soriano G, Cloix C, Heilmann M, Nunez-Olivera E, Martinez-Abaigar J, Jenkins GI (2018) Evolutionary
1128 conservation of structure and function of the UVR8 photoreceptor from the liverwort *Marchantia*
1129 *polymorpha* and the moss *Physcomitrella patens*. New Phytol 217: 151-162
1130 Stelzl U, Worm U, Lalowski M, Haenig C, Brembeck FH, Goehler H, Stroedicke M, Zenkner M, Schoenherr
1131 A, Koeppen S, Timm J, Mintzlaff S, Abraham C, Bock N, Kietzmann S, Goedde A, Toksoz E, Droege
1132 A, Krobitsch S, Korn B, Birchmeier W, Lehrach H, Wanker EE (2005) A human protein-protein
1133 interaction network: a resource for annotating the proteome. Cell 122: 957-968
1134 Stockenhuber R, Akiyama R, Tissot N, Milosavljevic S, Yamazaki M, Wyler M, Arongaus AB, Podolec R, Sato
1135 Y, Widmer A, Ulm R, Shimizu KK (2024) UV RESISTANCE LOCUS 8-mediated UV-B response is
1136 required alongside CRYPTOCHROME 1 for plant survival in sunlight under field conditions. Plant
1137 Cell Physiol 65: 35-48
1138 Stracke R, Favory JJ, Gruber H, Bartelniewoehner L, Bartels S, Binkert M, Funk M, Weisshaar B, Ulm R (2010)
1139 The Arabidopsis bZIP transcription factor HY5 regulates expression of the *PFG1*/*MYB12* gene in
1140 response to light and ultraviolet-B radiation. Plant Cell Environ 33: 88-103
1141 Sugano SS, Nishihama R, Shirakawa M, Takagi J, Matsuda Y, Ishida S, Shimada T, Hara-Nishimura I, Osakabe
1142 K, Kohchi T (2018) Efficient CRISPR/Cas9-based genome editing and its application to conditional
1143 genetic analysis in *Marchantia polymorpha*. PLoS One 13: e0205117
1144 Tavridou E, Pireyre M, Ulm R (2020) Degradation of the transcription factors PIF4 and PIF5 under UV-B
1145 promotes UVR8-mediated inhibition of hypocotyl growth in Arabidopsis. Plant J 101: 507-517
1146 Tavridou E, Schmid-Siegert E, Fankhauser C, Ulm R (2020) UVR8-mediated inhibition of shade avoidance
1147 involves HFR1 stabilization in Arabidopsis. PLoS Genet 16: e1008797
1148 Tilbrook K, Dubois M, Crocco CD, Yin R, Chappuis R, Allorent G, Schmid-Siegert E, Goldschmidt-Clermont
1149 M, Ulm R (2016) UV-B perception and acclimation in *Chlamydomonas reinhardtii*. Plant Cell 28:
1150 966-983
1151 Tokutsu R, Fujimura-Kamada K, Matsuo T, Yamasaki T, Minagawa J (2019) The CONSTANS flowering
1152 complex controls the protective response of photosynthesis in the green alga Chlamydomonas.
1153 Nat Commun 10: 4099
1154 Trimborn L, Kuttig F, Ponnu J, Yu P, Korsching KR, Lederer P, Urquiza-Garcia U, Zurbriggen MD, Hoecker U
1155 (2025) Cryptochrome 1 promotes photomorphogenesis in Arabidopsis by displacing substrates
1156 from the COP1 ubiquitin ligase. Plant J 121: e70071
1157 Tyanova S, Temu T, Cox J (2016) The MaxQuant computational platform for mass spectrometry-based
1158 shotgun proteomics. Nat Protoc 11: 2301-2319
1159 Ulm R, Baumann A, Oravecz A, Mate Z, Adam E, Oakeley EJ, Schafer E, Nagy F (2004) Genome-wide analysis
1160 of gene expression reveals function of the bZIP transcription factor HY5 in the UV-B response of
1161 Arabidopsis. Proc Natl Acad Sci USA 101: 1397-1402
1162 Wang L, Wang Y, Chang H, Ren H, Wu X, Wen J, Guan Z, Ma L, Qiu L, Yan J, Zhang D, Huang X, Yin P (2023)
1163 RUP2 facilitates UVR8 redimerization via two interfaces. Plant Commun 4: 100428
1164 Wang W, Paik I, Kim J, Hou X, Sung S, Huq E (2021) Direct phosphorylation of HY5 by SPA kinases to regulate
1165 photomorphogenesis in Arabidopsis. New Phytol 230: 2311-2326
1166 Wang Y, Wang L, Guan Z, Chang H, Ma L, Shen C, Qiu L, Yan J, Zhang D, Li J, Deng XW, Yin P (2022) Structural
1167 insight into UV-B-activated UVR8 bound to COP1. Sci Adv 8: eabn3337
1168 Wu D, Hu Q, Yan Z, Chen W, Yan C, Huang X, Zhang J, Yang P, Deng H, Wang J, Deng X, Shi Y (2012) Structural
1169 basis of ultraviolet-B perception by UVR8. Nature 484: 214-219

1170 Yelina NE, Frangedakis E, Wang Z, Schreier TB, Rever J, Tomaselli M, Forestier ECF, Billakurthi K, Ren S, Bai
1171 Y, Stewart-Wood J, Haseloff J, Zhong S, Hibberd JM (2024) Streamlined regulation of chloroplast
1172 development in the liverwort *Marchantia polymorpha*. Cell Rep 43: 114696
1173 Yin R, Arongaus AB, Binkert M, Ulm R (2015) Two distinct domains of the UVR8 photoreceptor interact
1174 with COP1 to initiate UV-B signaling in Arabidopsis. Plant Cell 27: 202-213
1175 Yin R, Skvortsova MY, Loubery S, Ulm R (2016) COP1 is required for UV-B-induced nuclear accumulation of
1176 the UVR8 photoreceptor. Proc Natl Acad Sci USA 113: E4415-4422
1177 Zhang C, Zhang Q, Guo H, Yu X, Liang W, Chen Y, Yin R, Lin L (2021) Tomato SlRUP is a negative regulator
1178 of UV-B photomorphogenesis. Mol Hortic 1: 8
1179 Zhang L, Li T, Su S, Peng H, Li S, Li K, Ji L, Xing Y, Zhang J, Du X, Bian M, Liao Y, Yang Z, Zuo Z (2021) Functions
1180 of COP1/SPA E3 ubiquitin ligase mediated by MpCRY in the liverwort *Marchantia polymorpha*
1181 under blue light. Int J Mol Sci 23: 158
1182 Zhou Z, Bi G, Zhou JM (2018) Luciferase complementation assay for protein-protein interactions in plants.
1183 Curr Protoc Plant Biol 3: 42-50

1184

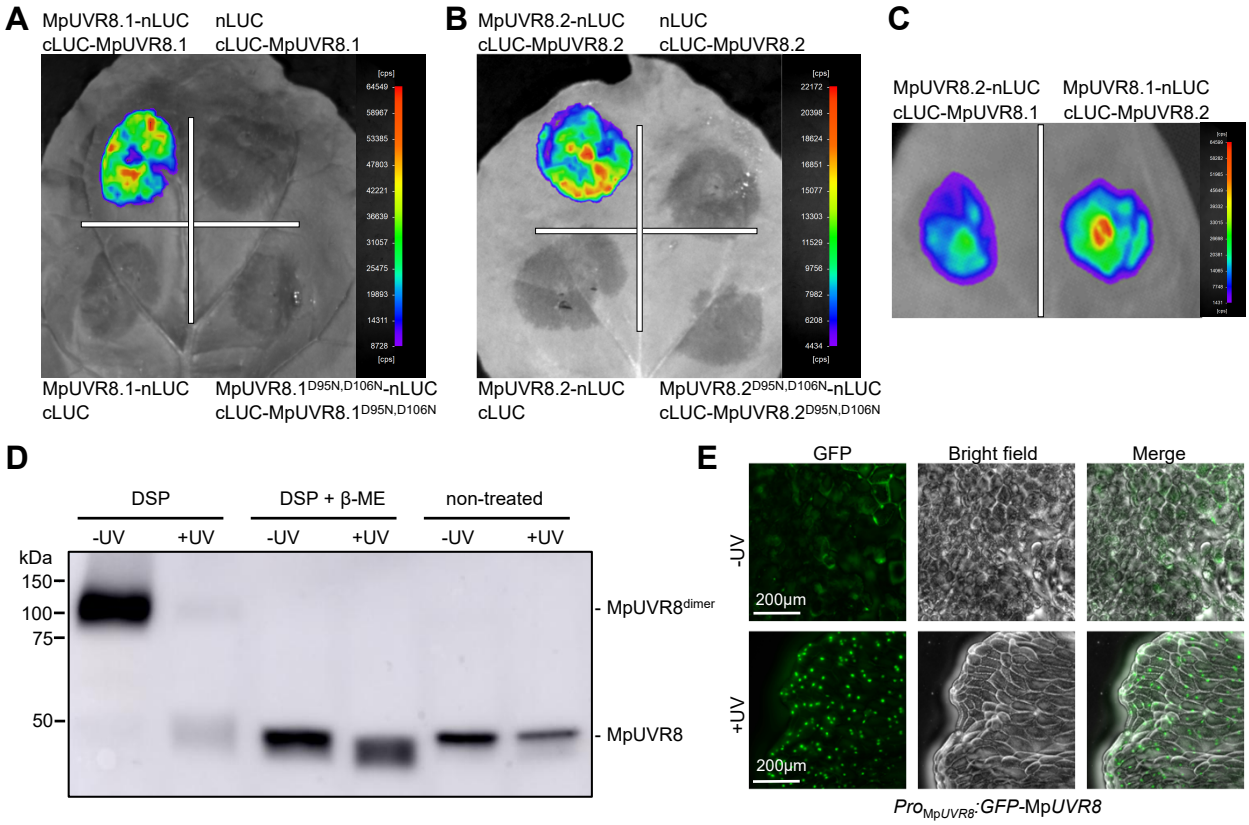

Figure 1. MpUVR8.1 and MpUVR8.2 form dimers in their ground state, monomerize upon UV-B exposure, and accumulate in the nucleus.

(A-C) Luciferase complementation imaging (LCI) assays assessing monomer interaction for MpUVR8.1 (A) and MpUVR8.2 (B), as well as their D95N,D106N variants, and MpUVR8.1 and MpUVR8.2 (C). MpUVR8 versions were fused to N-terminal (nLUC) or C-terminal (cLUC) fragments of luciferase, expressed in *N. benthamiana* leaves and imaged 2 days after infiltration. An image of a representative leaf is shown. Cps, counts per second.

(D) Immunoblot analysis of MpUVR8 dimer/monomer levels in 7-day-old wild type (Tak-1) gemmalings irradiated (+UV) or not (-UV) for 20 min with broadband UV-B. Protein extracts were either crosslinked with DSP, DSP crosslinked then reversed with the reducing agent β-mercaptoethanol (DSP + β-ME), or non-treated.

(E) Subcellular localization of GFP-MpUVR8 in 7-day-old gemmalings of a Tak-1/*Pro*$_{\text{Mp}UVR8}$*:GFP*-Mp*UVR8* line, grown in white light and irradiated or not for 20 min with 25 µmol m^{-2} s^{-1} broadband UV-B (+UV and -UV, respectively). Bars = 200 µm.

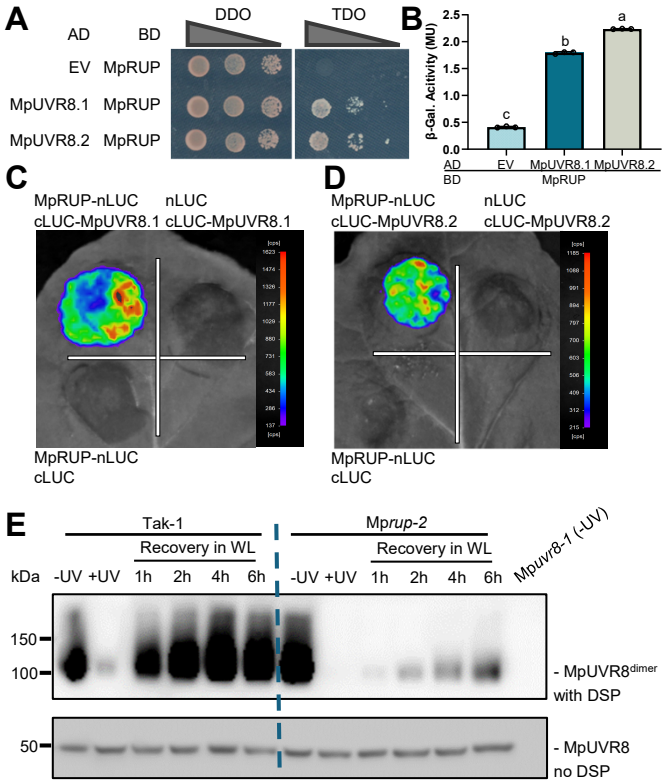

Figure 2. MpRUP facilitates MpUVR8 redimerization.

(A) Yeast two-hybrid assays of MpUVR8.1 and MpUVR8.2 interactions with MpRUP. Representative images of serial dilutions spotted on non-selective SD/-Trp/-Leu double dropout (DDO) and selective SD/-Trp/-Leu/-His triple dropout (TDO) media are shown. AD, transcriptional activation domain; BD, DNA-binding domain; EV, empty vector.

(B) Quantitative yeast two-hybrid assays of MpUVR8.1 and MpUVR8.2 interactions with MpRUP. Individual data points of biological replicates and means ± SD are shown (n = 3). Different letters indicate statistically significant differences between the means ($P < 0.01$) as determined by one-way ANOVA followed by Tukey's post hoc honestly significant difference (HSD) test. β-Gal., β-galactosidase; MU, Miller units.

(C,D) LCI assays of MpRUP interactions with MpUVR8.1 (C) and MpUVR8.2 (D) fused to N-terminal (nLUC) or C-terminal (cLUC) luciferase fragments, expressed in *N. benthamiana* leaves and imaged 2 days after infiltration. Images of representative leaves are shown. Cps, counts per second.

(E) Immunoblot analysis of MpUVR8 levels in 7-day-old wild type (Tak-1) and Mp*rup-2* gemmalings irradiated for 20 min with broadband UV-B (+UV) before recovery in white light (WL) for the indicated times (1–6 h). Non-irradiated samples (-UV) are included as MpUVR8 ground state controls alongside a negative control -UV Mp*uvr8-1* sample. Top: MpUVR8 dimer levels in DSP-crosslinked protein extracts; bottom: total MpUVR8 levels in non-crosslinked extracts.

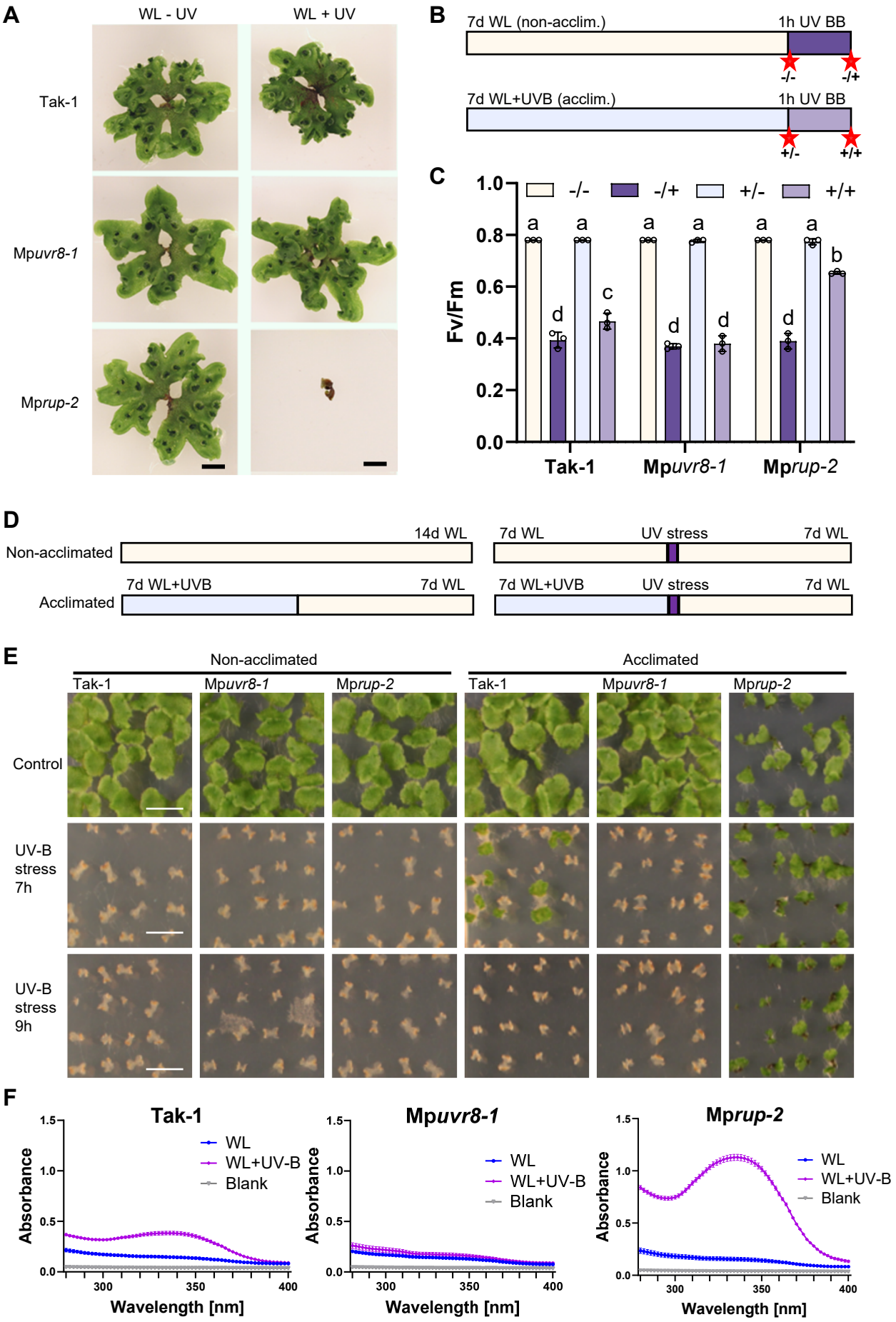

Figure 3. UV-B acclimation and survival is impaired in Mp*uvr8* and enhanced in Mp*rup*.

Figure 3. UV-B acclimation and survival is impaired in Mp*uvr8* and enhanced in Mp*rup*.

(A) Growth phenotype of 4-week-old wild-type (Tak-1), Mp*uvr8-1*, and Mp*rup-2* grown in white light supplemented (WL+UV) or not (WL-UV) with UV-B (1.5 µmol m^{-2} s^{-1}). Bars = 1 cm.

(B) Scheme for UV-B treatment and sampling for F_v/F_m measurements. Light yellow bar: white light (WL, 50 µmol m^{-2} s^{-1}), non-acclimated condition; light blue bar: white light supplemented with narrowband UV-B (WL+UVB, 1.5 µmol m^{-2} s^{-1}), acclimated condition; light/dark purple bars: broadband UV stress (UV BB, 25 µmol m^{-2} s^{-1}). Red stars indicate timepoints of measurements: -/-, non-acclimated, non-stressed; -/+, non-acclimated, stressed; +/-, acclimated, non-stressed; +/+, acclimated, stressed.

(C) F_v/F_m in 7-day-old wild-type (Tak-1), Mp*uvr8-1*, and Mp*rup-2* gemmalings grown and sampled as indicated in (B). Individual data points of biological replicates and means ± SD are shown (*n* = 3). Different letters indicate statistically significant differences between the means ($P < 0.01$) as determined by two-way ANOVA followed by Tukey's post hoc honestly significant difference (HSD) test.

(D) Scheme for UV-B stress survival experiments. Plants were grown in WL or WL+UVB for 7 days, then exposed to 7 or 9 h of broadband UV-B stress, followed by recovery for 7 days in WL, after which they were imaged.

(E) UV-B stress survival in Tak-1, Mp*uvr8-1*, and Mp*rup-2* gemmalings grown as indicated in (D). Representative images are shown; bars = 1 cm.

(F) Absorbance spectra (280–400 nm) of methanolic extracts from 9-day-old Tak-1, Mp*uvr8-1*, and Mp*rup-2* gemmalings grown for 7 days in white light and exposed (WL+UV-B, purple lines) or not (WL, blue lines) to supplemental UV-B (1.5 µmol m^{-2} s^{-1}) for 2 days. The gray line shows the absorbance of the buffer (blank). Values of independent measurements and means ± SEM are shown (*n* = 3).

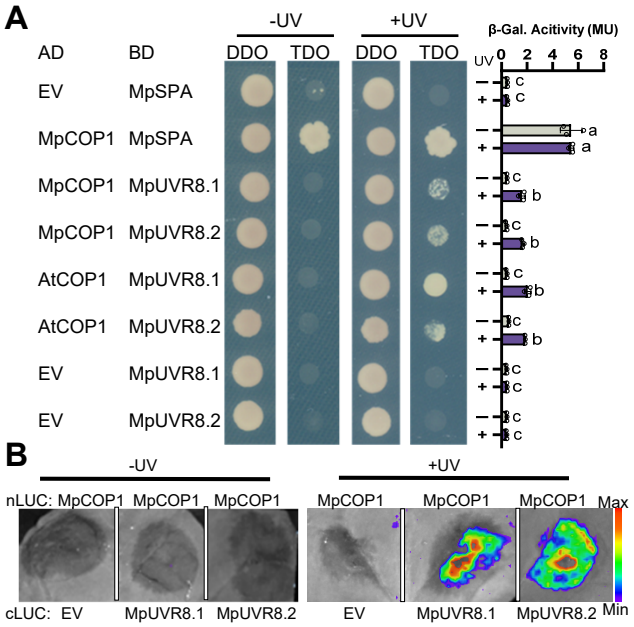

Figure 4. MpUVR8 and MpCOP1 interact in a UV-B-dependent manner.
(**A**) Yeast two-hybrid assay of the interactions of MpCOP1 with MpSPA and MpUVR8, as well as AtCOP1 with MpUVR8, in the presence (+UV) or absence (-UV) of UV-B. Left, growth assay; right, quantitative assay. Yeasts were grown on non-selective SD/-Trp/-Leu (DDO) or selective SD /-Trp/-Leu/-His (TDO) media. Individual data points of biological replicates and means ± SD are shown (n = 3). Different letters indicate statistically significant differences between the means ($P < 0.01$) as determined by one-way ANOVA followed by Tukey's post hoc honestly significant difference (HSD) test. AD, Gal4 activation domain; BD, LexA DNA-binding domain; β-Gal., β-galactosidase; MU, Miller units; EV, empty vector.
(**B**) LCI assays of MpCOP1 with MpUVR8.1 and MpUVR8.2. N-terminal (nLUC) or C-terminal (cLUC) luciferase fusion proteins were expressed in *N. benthamiana* leaves and imaged 2 days after infiltration, with (+UV) or without (-UV) exposure to 20 min of broadband UV-B. An image of a representative leaf is shown.

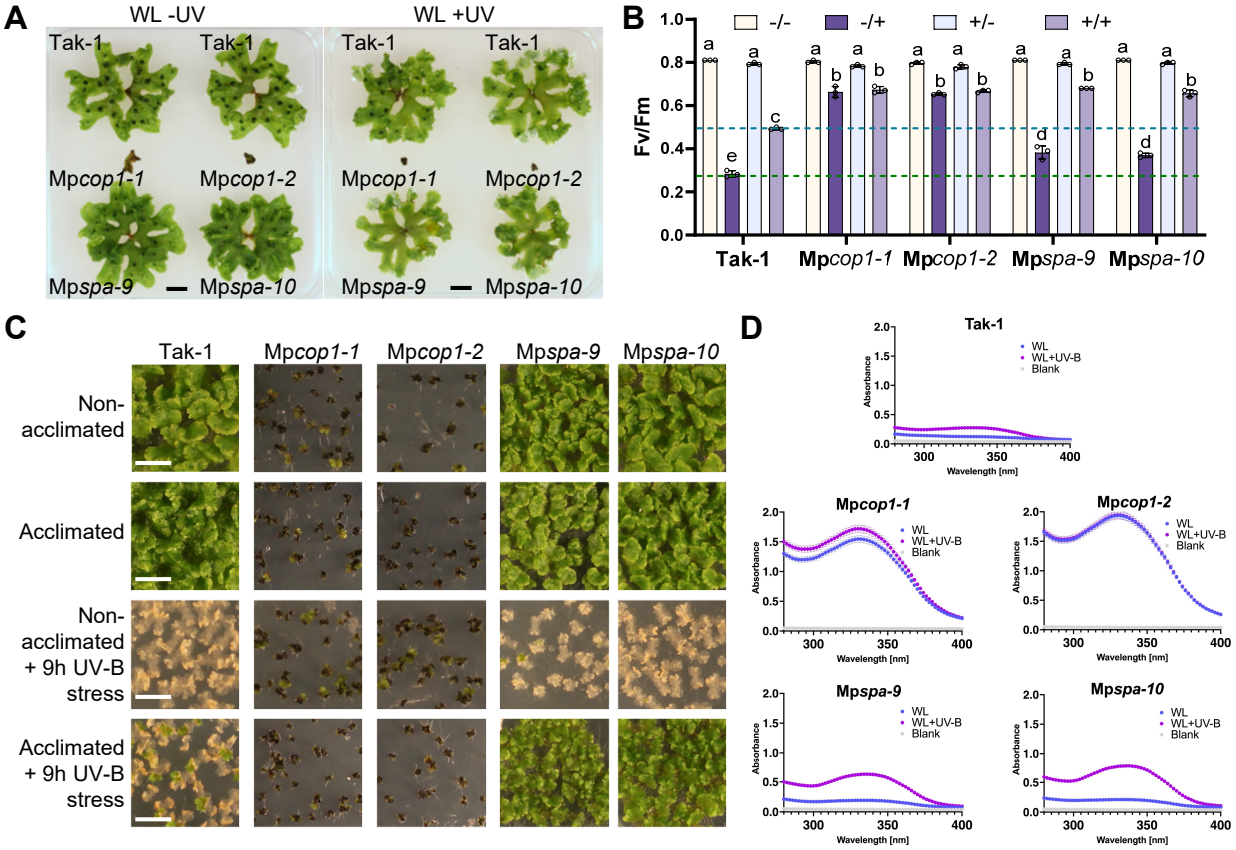

Figure 5. Mp*cop1* shows constitutive photomorphogenesis and UV-B tolerance, whereas Mp*spa* shows enhanced UV-B-induced UV-B tolerance.

(**A**) Growth phenotype of 4-week-old wild-type (Tak-1), Mp*cop1-1*, Mp*cop1-2*, Mp*spa-9*, and Mp*spa-10* plants grown in white light supplemented (WL +UV) or not (WL -UV) with UV-B. Scale bars = 1 cm.

(**B**) F_v/F_m measurements in 7-day-old wild-type (Tak-1), Mp*cop1-1*, *Mpcop1-2*, Mp*spa-9*, and Mp*spa-10* gemmalings grown in white light (non-acclimated) or white light supplemented with UV-B (acclimated), without (non-stressed) or with (stressed) additional exposure to broadband UV-B stress for 60 min. -/-, non-acclimated, non-stressed; -/+, non-acclimated, stressed; +/-, acclimated, non-stressed; +/+, acclimated, stressed. Individual data points of biological replicates and means ± SD are shown (n = 3). Different letters indicate statistically significant differences between the means ($P < 0.01$) as determined by two-way ANOVA followed by Tukey's post hoc honestly significant difference (HSD) test.

(**C**) UV-B stress survival in wild-type (Tak-1), Mp*cop1-1*, Mp*cop1-2*, Mp*spa-9*, and Mp*spa-10* plants grown for 7 days in white light supplemented (acclimated) or not (non-acclimated) with UV-B, then exposed or not to 9 h of broadband UV-B stress. Pictures were taken after a further 7-day recovery period in white light.

(**D**) Absorbance spectra (280–400 nm) of methanolic extracts from 9-day-old wild-type (Tak-1), Mp*cop1-1,* Mp*cop1-2*, Mp*spa-9*, and Mp*spa-10* gemmalings grown for 7 days in white light supplemented (WL+UV-B, purple lines) or not (WL, blue lines) with UV-B. The gray line shows the absorbance of the buffer (blank). Values of independent measurements and means ± SEM are shown (n = 3).

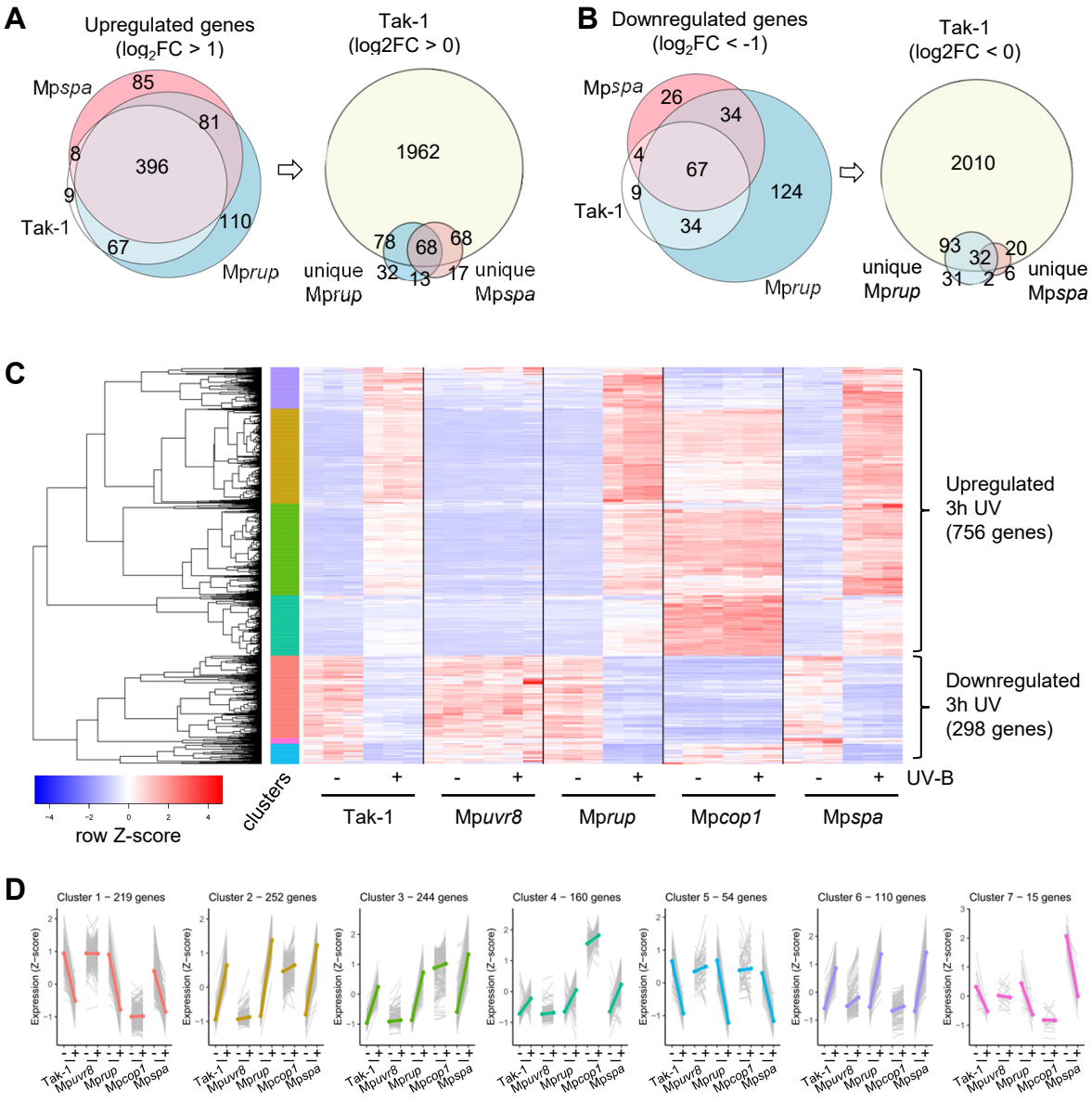

Figure 6. Transcriptome analysis reveals MpUVR8- and MpCOP1-dependent, UV-B-responsive gene regulation that is repressed by MpRUP and MpSPA

(A) Euler plots showing overlaps between upregulated differentially expressed genes (DEGs) (p-adj < 0.05) upon exposure to 3 h UV-B in 7-day-old wild-type (Tak-1), Mp*rup*, and Mp*spa* gemmalings. Left: overlap between genes upregulated at least two-fold ($\log_2$FC > 1) in either Tak-1, Mp*rup*, or Mp*spa*. Right: overlap between upregulated ($\log_2$FC > 1) genes that are unique to Mp*rup* and/or Mp*spa*, and Tak-1 upregulated genes without a fold-change threshold ($\log_2$FC > 0). Corresponding gene lists: Supplementary Table S3a.

(B) Euler plots showing overlaps between downregulated DEGs (p-adj < 0.05) upon exposure to 3 h UV-B in 7-day-old Tak-1, Mp*rup*, and Mp*spa* gemmalings. Left: overlap between genes downregulated at least two-fold ($\log_2$FC < -1) in either Tak-1, Mp*rup*, or Mp*spa*. Right: overlap between downregulated ($\log_2$FC < -1) genes that are unique to Mp*rup* and/or Mp*spa*, and Tak-1 downregulated genes without a fold-change threshold ($\log_2$FC < 0). Corresponding gene lists: Supplementary Table S3b.

(**C**) Hierarchical clustering and heatmap of UV-B-regulated gene expression in Tak-1, Mp*uvr8-1,* Mp*rup-2,* Mp*cop1-1*, and Mp*spa-9* plants grown for 7 days under white light and exposed or not to supplemental UV-B for 3 h. All genes with a greater than two-fold change in expression in response to UV-B and a p-adj < 0.05 in at least one genotype are shown (total = 1005 genes). Red and blue colors indicate normalized read count Z-scores. The color bar on the left side indicates 7 major profiles (clusters) of gene expression.

(**D**) Gene expression profiles in clusters identified by hierarchical clustering. Z-scores for normalized read count values for each gene (gray lines) and for the cluster average (colored line) are shown.

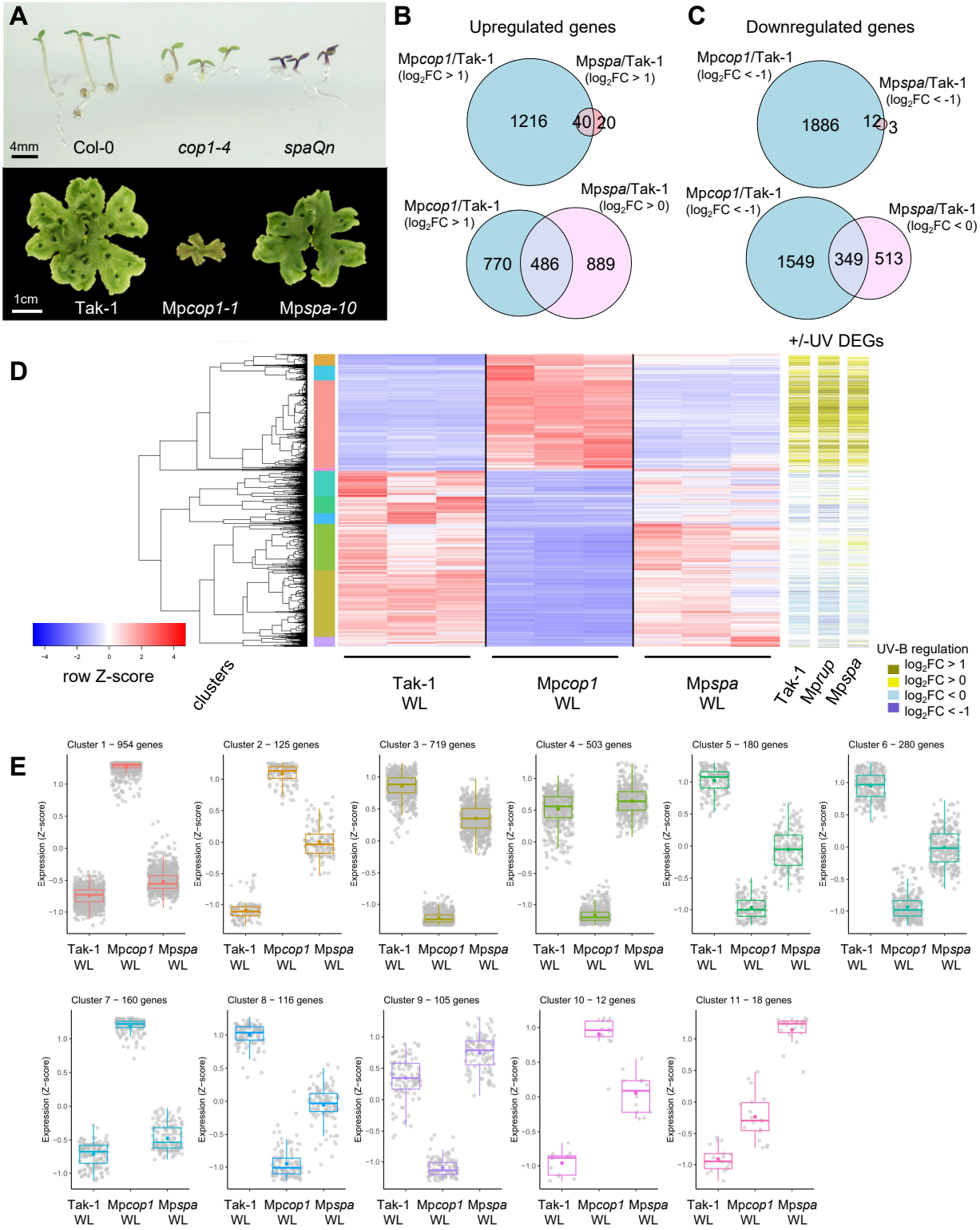

Figure 7. MpSPA plays a minor role in repressing Marchantia photomorphogenesis under visible light.
(**A**) Representative images of 4-day-old Arabidopsis seedlings of wild-type (Col-0), *cop1-4*, and *spaQn* mutants, and 28-day-old Marchantia thalli of wild-type (Tak-1), Mp*cop1-1*, and Mp*spa-10* grown in white light. Scale bars: 4 mm or 1 cm, as indicated.
(B) Euler plots showing overlaps between upregulated DEGs (p-adj < 0.05) in Mp*cop1* and Mp*spa* mutants compared to Tak-1 wild type. Gemmalings were grown for 7 days in white light. Top: overlap between genes upregulated at least two-fold ($log_2FC > 1$) in either Mp*cop1*/Tak-1 or Mp*spa*/Tak-1. Bottom: overlap between genes upregulated at least two-fold ($log_2FC > 1$) in Mp*cop1*/Tak-1 and genes upregulated without a fold-change threshold ($log_2FC > 0$) in Mp*spa*/Tak-1. Corresponding gene lists: Supplementary Table S3c.
(C) Euler plots showing overlaps between downregulated DEGs (p-adj < 0.05) in Mp*cop1* and Mp*spa* mutants compared to Tak-1 wild type. Gemmalings were grown for 7 days in white light. Top: overlap between genes downregulated at least two-fold ($log_2FC < -1$) in either Mp*cop1*/Tak-1 or Mp*spa*/Tak-1. Bottom: overlap between genes downregulated at least two-fold ($log_2FC < -1$) in Mp*cop1*/Tak-1 and genes downregulated without a fold-change threshold ($log_2FC < 0$) in Mp*spa*/Tak-1. Corresponding gene lists: Supplementary Table S3d.
(**D**) Hierarchical clustering and heatmap of gene expression in Tak-1, Mp*cop1-1*, and Mp*spa-9* plants grown for 7 days in white light. All genes with a greater than two-fold change in expression between mutants and wild type and a p-adj < 0.05 in at least one comparison are shown (total = 2975 genes). Red and blue colors indicate normalized read count Z-scores. The color bar on the left side indicates 11 major profiles (clusters) of gene expression. The color bars on the right indicate if genes are significantly regulated after UV-B exposure in Tak-1, Mp*rup*, and Mp*spa*.
(**E**) Gene expression profiles in clusters identified by hierarchical clustering. Z-scores for normalized read count values for each gene are shown as gray points; their distribution is represented as a colored box plot.

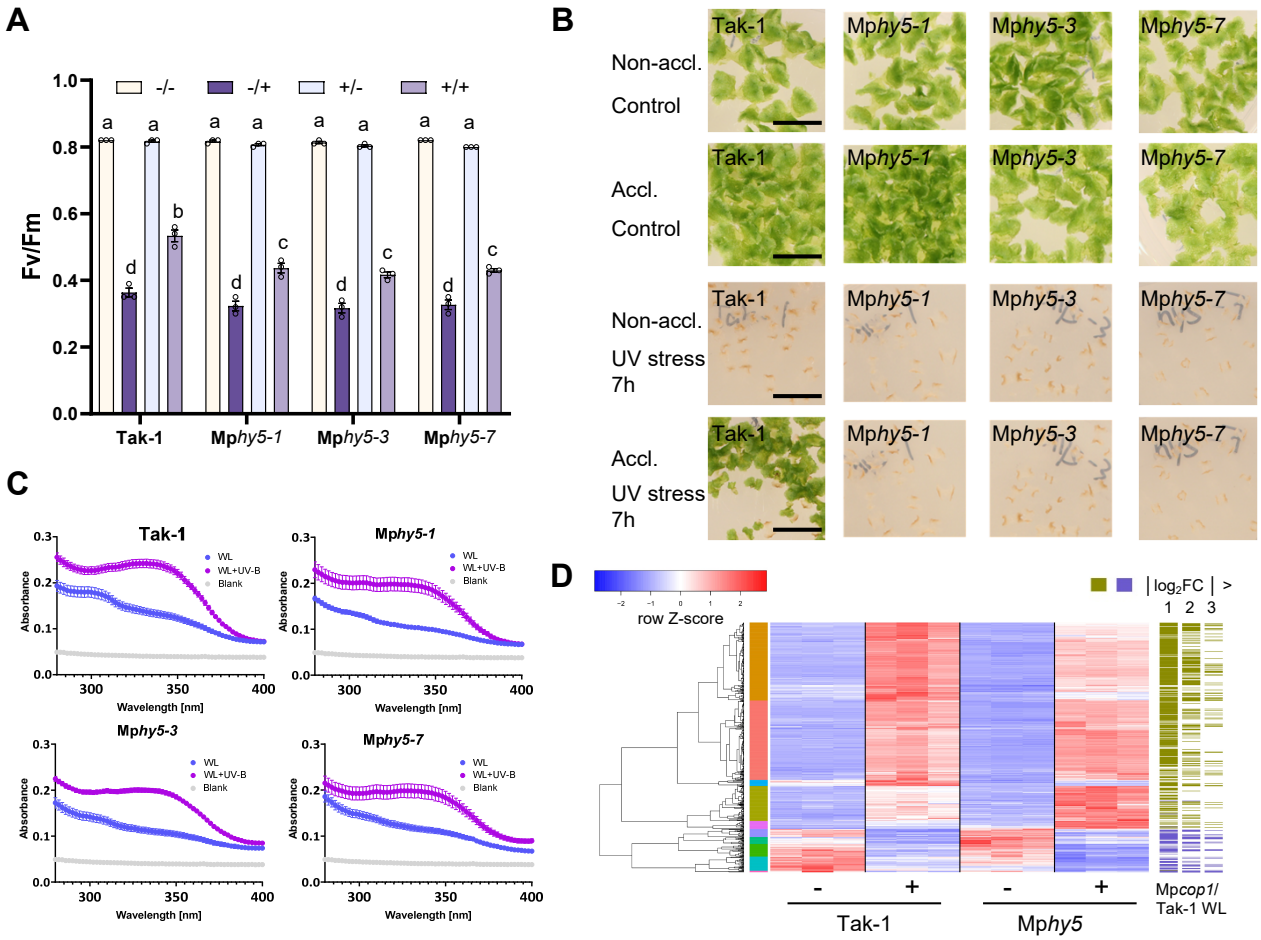

Figure 8. MpHY5 is involved in UV-B and visible light photomorphogenesis.
(**A**) F_v/F_m measurements in wild-type (Tak-1), Mp*hy5-1*, Mp*hy5-3*, and Mp*hy5-7* plants grown for 7 days in white light (non-acclimated) or white light supplemented with UV-B (acclimated), without (not stressed) or with (stressed) additional exposure to broadband UV-B stress for 60 min. -/-, not acclimated, not stressed; -/+, not acclimated, stressed; +/-, acclimated, not stressed; +/+, acclimated, stressed. Individual data points of biological replicates and means ± SD are shown (*n* = 3). Letters indicate statistically significant differences between the means (P < 0.01) as determined by two-way ANOVA followed by Tukey's post hoc honestly significant difference (HSD) test.
(**B**) UV-B stress survival of Tak-1, Mp*hy5-1*, Mp*hy5-3*, and Mp*hy5-7* plants grown for 7 days in white light supplemented (Accl.) or not (Non-accl.) with UV-B, then exposed to 7 h of broadband UV-B stress (UV stress 7 h) or not (Control). Pictures were taken after recovery for another 7 days in white light. Bars = 1 cm.
(**C**) Absorbance spectra (280–400 nm) of methanolic extracts from 9-day-old Tak-1, Mp*hy5-1*, Mp*hy5-3*, and Mp*hy5-7* gemmalings grown for 7 days in white light and exposed (WL+UV-B, purple lines) or not (WL, blue lines) to supplemental UV-B (1.5 µmol m^{-2} s^{-1}) for 2 days. The gray lines show absorbance of the buffer (blank). Values of independent measurements and means ± SEM are shown (*n* = 3).
(**D**) Hierarchical clustering and heatmap of UV-B-regulated gene expression in Tak-1 and Mp*hy5-1* plants grown for 7 days and exposed, or not, to supplemental UV-B for 3h. All genes with a greater than two-fold change in expression under UV-B and a p-adj < 0.05 in at least one genotype are shown (total = 501 genes). Red and blue colors indicate normalized read count Z-scores. The color bar on the left side indicates 10 major profiles (clusters) of gene expression. The color bars on the right indicate if genes are significantly misregulated in white light in Mp*cop1* compared to Tak-1, at varying fold-change thresholds.

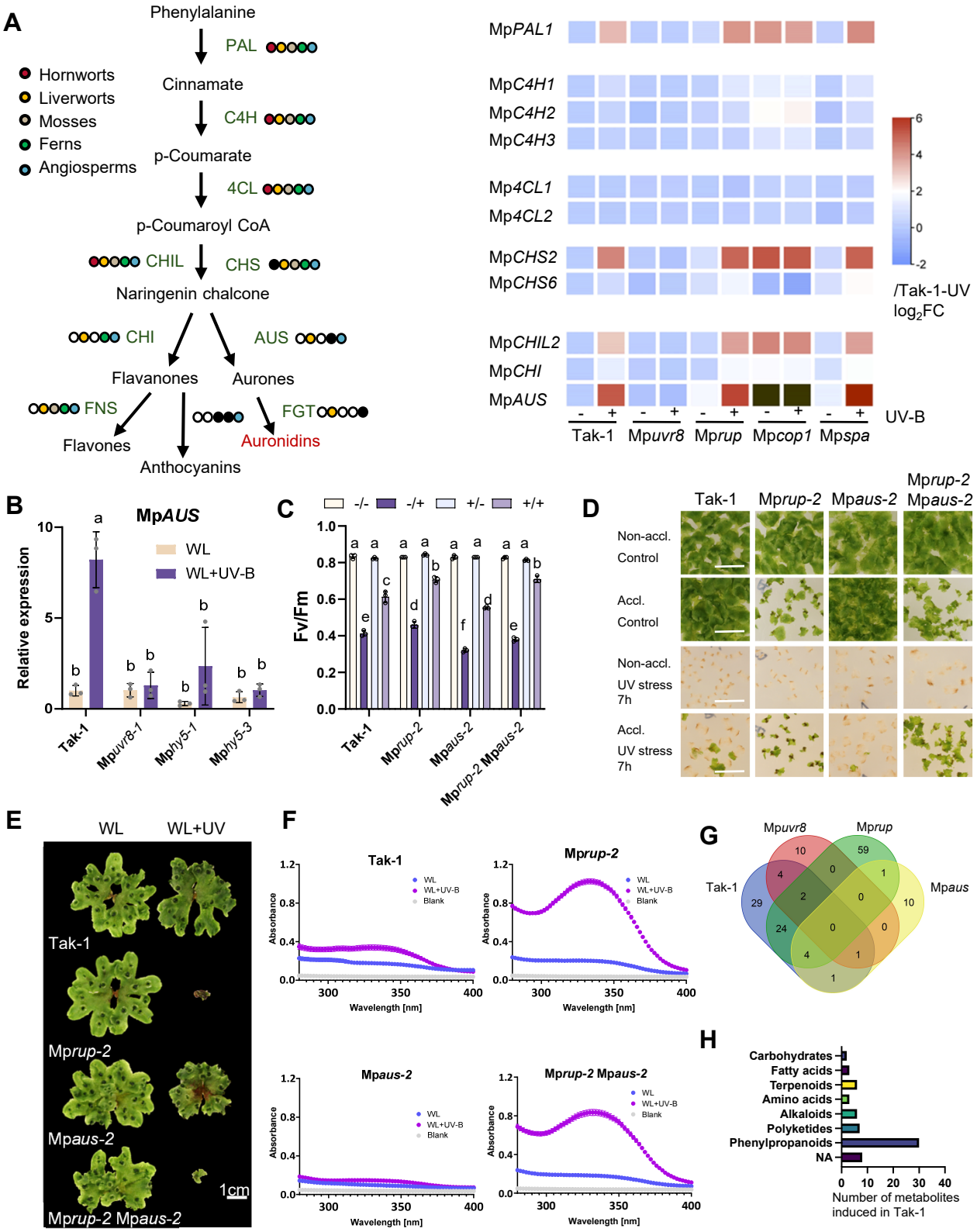

Figure 9. Auronidins and related flavonoid pigments may play an important role in protecting Marchantia from UV-B stress.

Figure 9. Auronidins and related flavonoid pigments may play an important role in protecting Marchantia from UV-B stress.

(**A**) Left: Schematic of the phenylpropanoid pathway leading to flavonoid pigments and the occurrence of biosynthetic enzymes in different land plant lineages (according to Davies et al., 2022). A colored circle next to an enzyme step indicates that the activity is present in the corresponding plant lineage, as indicated by the color key. An empty white circle indicates its absence in that lineage. A black circle indicates that there is some support for the presence of the enzyme, provided from either sequence analysis or presence of the biosynthetic product, but that definitive evidence is lacking. Right: Heat map showing gene expression levels as determined by RNA-seq of phenylpropanoid biosynthetic enzymes in Tak-1, Mp*uvr8-1,* Mp*rup-2,* Mp*cop1-1*, and Mp*spa-10* plants grown for 7 days in white light exposed (+) or not (-) to supplemental UV-B for 3 h. The $\log_2$ fold change of normalized read counts relative to Tak-1 without UV-B exposure (/Tak-1-UV $\log_2$FC) was calculated. Enzyme abbreviations: PAL, PHENYLALANINE AMMONIA LYASE; C4H, CINNAMATE 4-HYDROXYLASE; 4CL, COUMAROYL CoA LIGASE; CHS, CHALCONE SYNTHASE; CHI, CHALCONE ISOMERASE; CHIL, CHALCONE ISOMERASE-LIKE; AUS, AUREUSIDIN SYNTHASE; FGT, FLAVONOID O-GLYCOSYLTRANSFERASES; FNS, FLAVONE SYNTHASE.

(**B**) RT-qPCR analysis of Mp*AUS* in 7-day-old Tak-1, Mp*uvr8-1*, Mp*hy5-1*, and Mp*hy5-3* plants grown for 7 days in white light and exposed to supplemental UV-B for 3 h (WL+UV-B) or not (WL). Individual data points of biological replicates and means ± SD are shown (*n* = 3). Letters indicate statistically significant differences between the means (P < 0.01) as determined by two-way ANOVA followed by Tukey's post hoc honestly significant difference (HSD) test.

(**C**) F_v/F_m measurements in Tak-1, Mp*rup-2*, Mp*aus-2*, and Mp*rup-2* Mp*aus-2* gemmalings grown for 7 days in white light (non-acclimated) or white light supplemented with UV-B (acclimated), without (not stressed) or with (stressed) additional exposure to broadband UV-B stress for 60 min. -/-, not acclimated, not stressed; -/+, not acclimated, stressed; +/-, acclimated, not stressed; +/+, acclimated, stressed. Individual data points of biological replicates and means ± SD are shown (*n* = 3). Letters indicate statistically significant differences between the means (P < 0.01) as determined by two-way ANOVA followed by Tukey's post hoc honestly significant difference (HSD) test.

(**D**) UV-B stress survival of Tak-1, Mp*rup-2*, Mp*aus-2*, and Mp*rup-2* Mp*aus-2* plants grown for 7 days in white light supplemented (Accl.) or not (Non-accl.) with UV-B, then exposed to 7 h of broadband UV-B (UV stress 7 h) or not (Control). Pictures were taken after recovery for another 7 days in white light. Bars = 1 cm.

(**E**) Growth phenotype of 4-week-old wild-type (Tak-1), Mp*rup-2*, Mp*aus-2*, and Mp*rup-2* Mp*aus-2* plants grown in white light supplemented with UV-B (WL +UV) or not (WL). Bar = 1 cm.

(**F**) Absorbance spectra (280–400 nm) of methanolic extracts from 9-day-old Tak-1, Mp*rup-2*, Mp*aus-2*, and Mp*rup-2* Mp*aus-2* gemmalings grown for 7 days in white light and exposed (WL+UV-B, purple lines) or not (WL, blue lines) to supplemental UV-B for 2 days. The gray lines show absorbance of the buffer (blank). Values of independent measurements and means ± SEM are shown (*n* = 3).

(**G**) and **(H)** Metabolomic analysis of 9-day-old plants of Tak-1, Mp*uvr8-1*, Mp*rup-2*, and Mp*aus-2* grown for 7 days in white light and exposed (+) or not (-) to supplemental UV-B (1.5 µmol m^{-2} s^{-1}) for 2 days (*n* = 5, 12 plants per replicate). (G) Venn diagram showing overlaps between upregulated metabolites (FC> or =1.5, p-adj < or =0.05) upon exposure to 2 days UV-B in 9-day-old wild-type (Tak-1), Mp*uvr8-1* (Mp*uvr8*), Mp*rup-2* (Mp*rup*), and Mp*aus-2 (*Mp*aus)* gemmalings. (H) Distribution of the number of compounds induced under UV-B in wild type (FC> or =1.5, p-adj < or =0.05), according to their chemical classes. Corresponding metabolite lists: Supplementary Table S9.

```
AtUVR8      1 MAEDMAADEVTAPPRKVLIISAGASHSVALLSGDIVCSWGRGEDGQLGHGDAEDRPSPTQ  60
MpUVR8.1    1 -MEDSKMSSNERPRRRVLFVSAGASHSVALLTGDSVCSWGRGEDGQLGHGDADERHLPTI  59
MpUVR8.2    1 -MEDSKMSSNERPRRRVLFVSAGASHSVALLTGDSVCSWGRGEDGQLGHGDADERHLPTI  59
                                                        *

AtUVR8     61 LSALDGHQIVSVTCGADHTVAYSQSGMEVYSWGWGDFGRLGHGNSSDLFTPLPIKALHGI 120
MpUVR8.1   60 ISTLGECEISAITCGADHTTAYADSTRTVYSWGWGDFGRLGHGNSSDLFIPHPIKALRGI 119
MpUVR8.2   60 ISTLGECEISAITCGADHTTAYADSTRTVYSWGWGDFGRLGHGNSSDLFIPHPIKALRGI 119
                                                 *  *  *            *

AtUVR8    121 RIKQIACGDSHCLAVTMEGEVQSWGRNQNGQLGLGDTEDSLVPQKIQAFEGIRIKMVAAG 180
MpUVR8.1  120 EISQIACGDSHCLAITTQGDVHSWGRNQNGQLGLGHNEDSLVPKKVVAFEGIAVKMLAAG 179
MpUVR8.2  120 EISQIACGDSHCLAITTQGDVHSWGRNQNGQLGLGHNEDSLVPKKVVAFEGIAVKMLAAG 179
                                     *

AtUVR8    181 AEHTAAVTEDGDLYGWGWGRYGNLGLGDRTDRLVPERVTSTGGEKMSMVACGWRHTISVS 240
MpUVR8.1  180 AEHTAAVTESGKLYGWGWGRYGNLGLGDRNDRLVPAEVAGVNNEKFTLVACGWRHTIAVA 239
MpUVR8.2  180 AEHTAAVTESGKLYGWGWGRYGNLGLGDRNDRLVPAEVAGVNNEKFTLVACGWRHTIAVA 239
                            *  *                                       *

AtUVR8    241 YSGALYTYGWSKYGQLGHGDLEDHLIPHKLEALSNSFISQISGGWRHTMALTSDGKLYGW 300
MpUVR8.1  240 ESGNLYTFGWSKYGQLGHGDYLDHLVPHQVAALKNNPIVQISGGWRHTVALDSSGRLYGW 299
MpUVR8.2  240 ESGNLYTFGWSKYGQLGHGDYLDHLVPHQVAALKNNPIVQISGGWRHTVALDSSGRLYGW 299
                        *                                   *                *

AtUVR8    301 GWNKFGQVGVGNNLDQCSPVQVRFPDDQKVVQVSCGWRHTLAVTERNNVFAWGRGTNGQL 360
MpUVR8.1  300 GWNKFGQVGVGNTDDQTSPQLVKNLAEEKVKQVSCGWRHTVCITERGNVFSWGRGTSGQL 359
MpUVR8.2  300 GWNKFGQVGVGNTDDQTSPQLVKNLAEEKVKQVSCGWRHTVCITERGNVFSWGRGTSGQL 359
                 *                                   *                *

AtUVR8    361 GIGESVDRNFPKIIEALSVDGASGQHIESSNIDPSSGKSWVSPAERYAVVPDET------ 414
MpUVR8.1  360 GHGDAVDRSLPKRIEALSADGLACQELESSRTTTSTGSHWISPSERYAVVPVETVRSLSR 419
MpUVR8.2  360 GHGDAVDRSLPKRIEALSADGLACQELESSRTTTSTGSHWISPSERYAVVPVET------ 413
                                                        *

AtUVR8    415 ----GLTDGSSKGNGGDISVPQTDVKRVRI--                              440
MpUVR8.1  420 NMHQNANVGDNEVPSSDASVPDTDVKRLRTGF                              451
MpUVR8.2  414 -------VGDNEVPSSDASVPDTDVKRLRTGF                              438
```

Supplementary Figure S1. Alignment of Marchantia MpUVR8.1 and MpUVR8.2 with Arabidopsis AtUVR8.
Red asterisks (*) highlight conserved tryptophan (W) amino acid residues, including the AtUVR8 key triad tryptophans W233 (W232 in MpUVR8), W285 (W284 in MpUVR8), and W337 (W336 in MpUVR8), within their conserved GWRHT sequence motif. Green asterisks (*) highlight AtUVR8 aspartates D96 (D95 in MpUVR8) and D107 (D106 in MpUVR8).

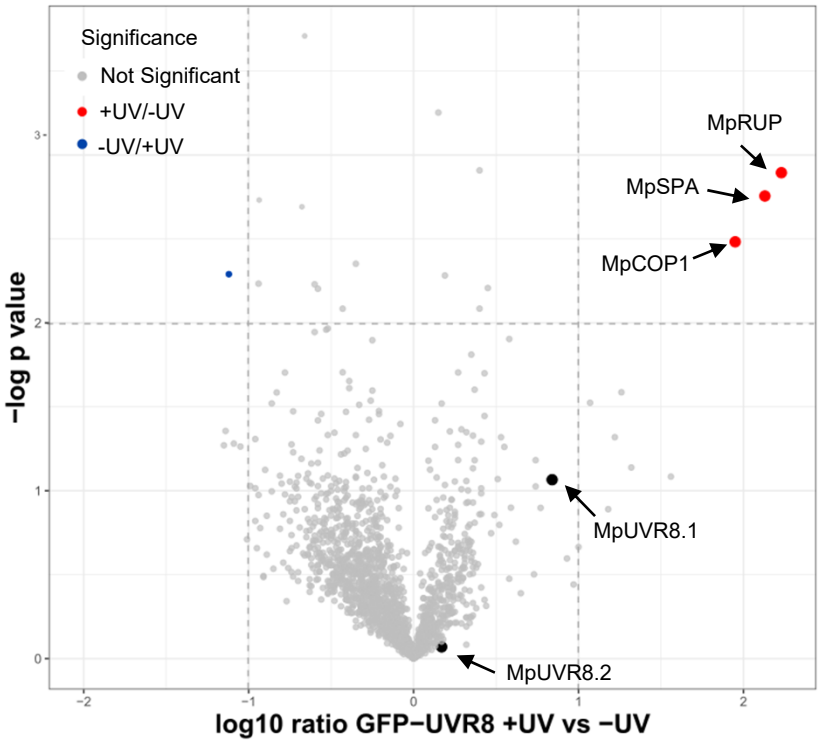

Supplementary Figure S2. Volcano plot of GFP-MpUVR8 AP-MS under +UV versus -UV conditions.
AP–MS was performed using a Marchantia *Pro*$_{MpUVR8}$:*GFP*-Mp*UVR8* (genomic) transgenic line grown for 7 days under continuous white light (50 µmol m^{-2} s^{-1}) without UV-B, or under continuous white light supplemented with narrowband UV-B (1.5 µmol m^{-2} s^{-1}) followed by a 20 min broadband UV-B exposure (25 µmol m^{-2} s^{-2}). Significantly different proteins were identified using a p-value cutoff of < 0.01 and a log10 fold change threshold of ±1.0. Grey dots represent non-significant proteins; red dots indicate proteins significantly enriched in +UV compared to –UV; blue dots indicate proteins significantly enriched in –UV compared to +UV. Arrows highlight proteins of interest.

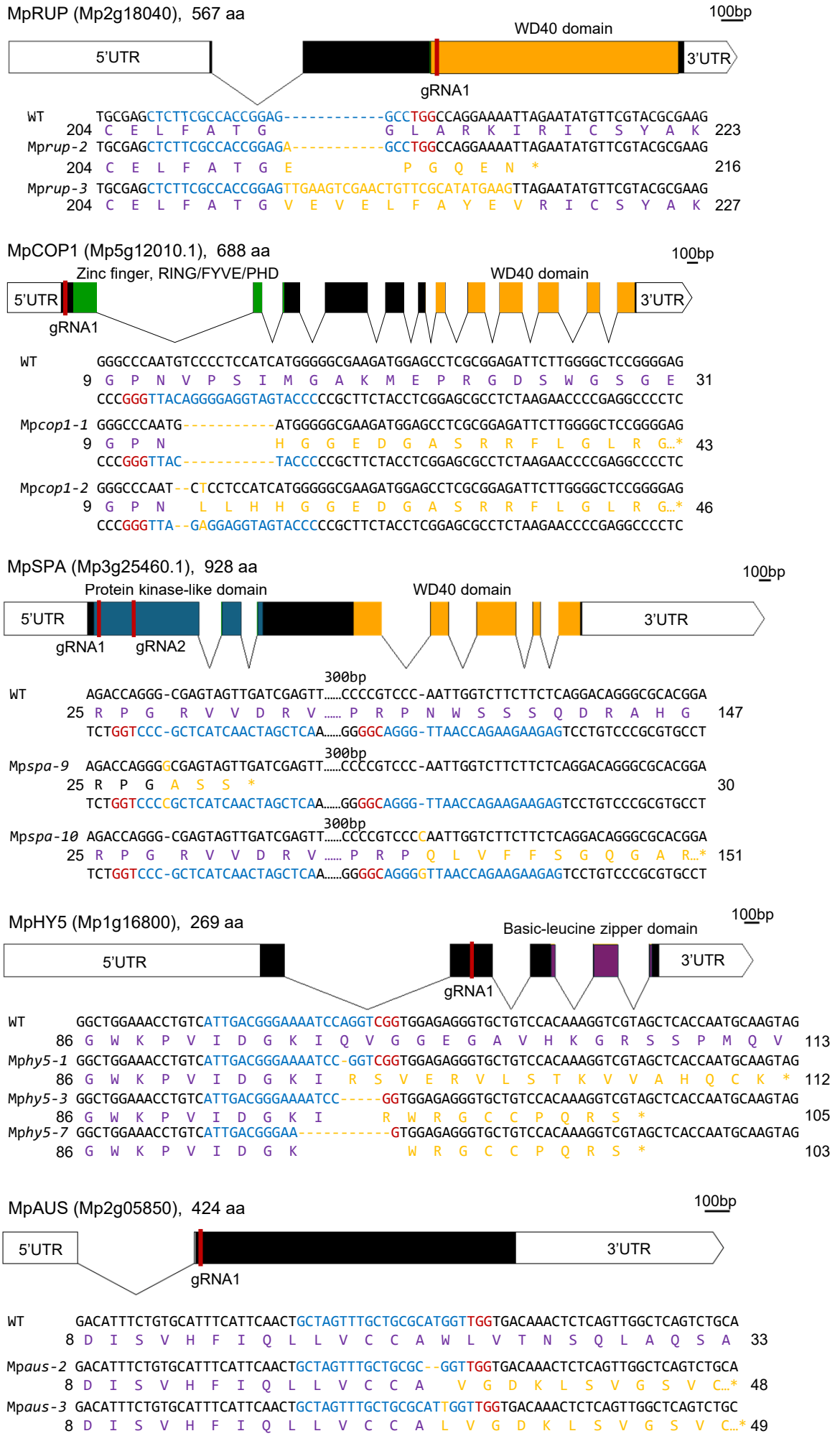

Supplementary Figure S3. Gene structure and indication of the mutated sites in the corresponding mutants generated by CRISPR/Cas9.

Supplementary Figure S3. Gene structure and indication of the mutated sites in the corresponding mutants generated by CRISPR/Cas9.

Untranslated (5' and 3' UTRs) and coding sequences are highlighted as white and colored boxes, respectively, with specific domains indicated. Introns are represented by lines connecting exons. The positions of the guide RNA (gRNA) (red bar, sequence in blue), protospacer adjacent motif (PAM) sequences (sequence in red), different mutations including resulting amino acid changes (in yellow), translated amino acids of wild-type (in purple) and the number of translated amino acids are also highlighted. The Mp*rup-2* mutant exhibits an insertion of one adenine (A) nucleotide, while Mp*rup-3* displays 27-bp insertion with a 15-bp deletion of endogenous sequence. Mp*cop1-1* and Mp*cop1-2* mutants show an 11-bp deletion and a 2-bp deletion with one cytosine (C) nucleotide substituted by thymine (T), respectively. Mp*spa-9* has an insertion of one guanine (G) nucleotide for gRNA1, whereas Mp*spa-10* exhibits an insertion of one cytosine (C) nucleotide for gRNA2. The Mp*hy5-1* mutant displays a deletion of one adenine (A) nucleotide, whereas Mp*hy5-3* and Mp*hy5-7* mutants show a 5-bp deletion and 11-bp deletion, respectively. Mp*aus-2* shows a 2-bp deletion and Mp*aus-3* shows an insertion of one thymine (T) nucleotide. All these mutations, except for Mp*rup-3*, result in a frameshift and early STOP codon in the coding sequence.

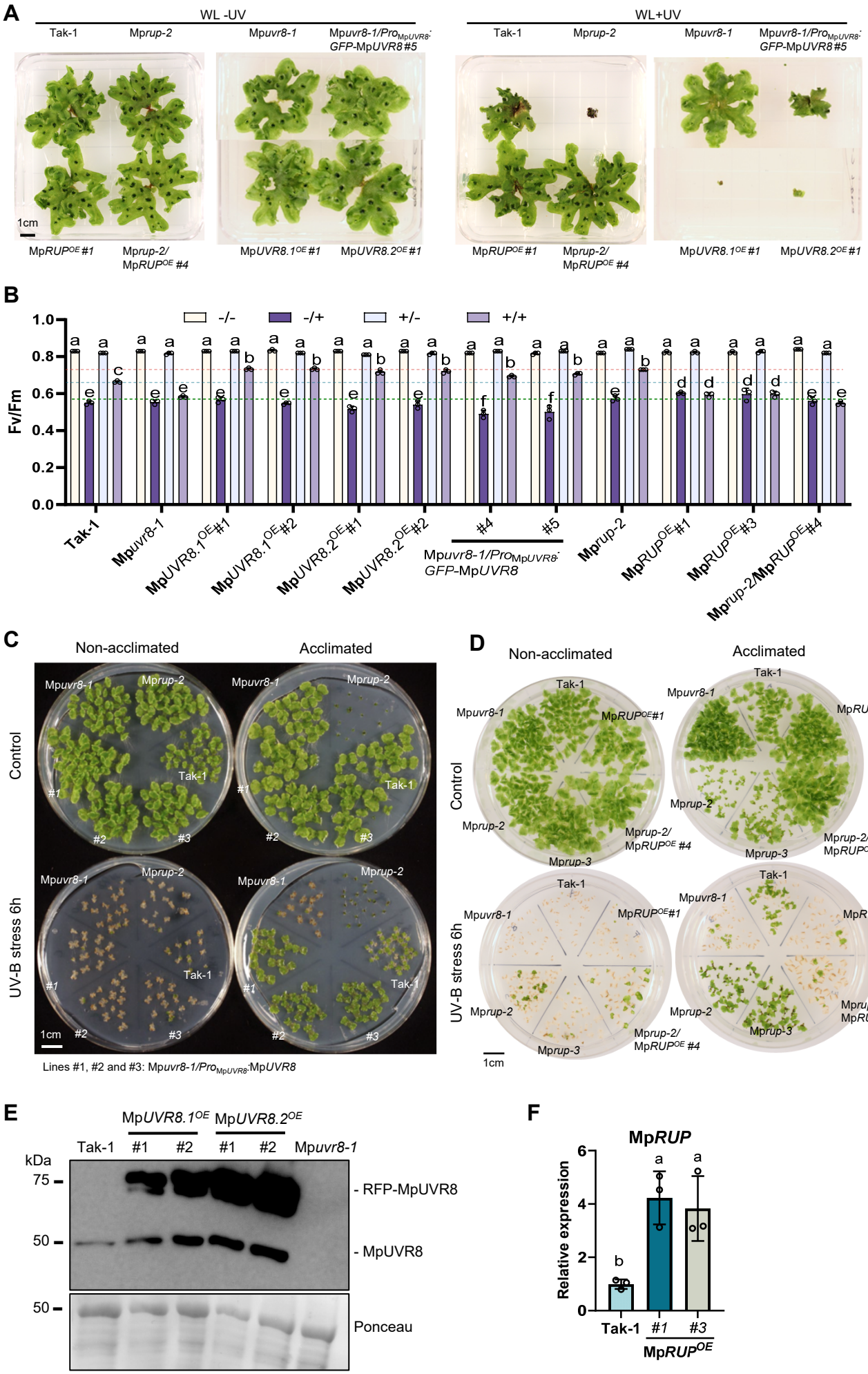

Supplementary Figure S4. UV-B photomorphogenesis and photoprotection in MpUVR8 and MpRUP transgenic lines.

Supplementary Figure S4. UV-B photomorphogenesis and photoprotection in MpUVR8 and MpRUP transgenic lines.

(**A**) Growth phenotype of 4-week-old wild-type (Tak-1), Mp*rup-2*, Mp*uvr8-1*, Mp*uvr8-1/Pro*$_{MpUVR8}$*:GFP*-Mp*UVR8* line *#5,* Mp*RUP*^{OE} *#1*, Mp*rup-2/*Mp*RUP*^{OE} *#4*, Mp*UVR8.1*^{OE} *#1*, and Mp*UVR8.2*^{OE} *#1* plants grown in white light supplemented (WL +UV) or not (WL -UV) with UV-B. Bar = 1 cm.

(**B**) F_v/F_m measurements in wild-type (Tak-1), Mp*uvr8-1*, Mp*UVR8.1*^{OE} lines *#1* and *#2*, Mp*UVR8.2*^{OE} *#1* and *#2*, Mp*uvr8-1/Pro*$_{MpUVR8}$*:GFP-*Mp*UVR8 #4* and *#5,* Mp*rup-2*, Mp*RUP*^{OE} *#1* and *#3*, and Mp*rup-2/*Mp*RUP*^{OE} *#4* grown for 7 days in white light (non-acclimated) or white light supplemented with UV-B (acclimated), without (non-stressed) or with (stressed) additional exposure to broadband UV-B stress for 60 min. -/-, non-acclimated, non-stressed; -/+, non-acclimated, stressed; +/-, acclimated, non-stressed; +/+, acclimated, stressed. Individual data points of biological replicates and means ± SD are shown (n = 3). Dashed horizontal lines indicate levels corresponding to acclimated and stressed Tak-1 (blue), Mp*uvr8-1* (green), and Mp*rup-2* (orange) plants. Different letters indicate statistically significant differences between the means ($P < 0.01$) as determined by two-way ANOVA followed by Tukey's post hoc honestly significant difference (HSD) test.

(**C,D**) UV-B stress tolerance of indicated plant genotypes grown for 7 days in white light supplemented (acclimated) or not (non-acclimated) with UV-B, then exposed or not to 6 hours of broadband UV-B. Pictures were taken after recovery for another 7 days in white light. Bar = 1 cm. (C) #1, #2 and #3: three independent Mp*uvr8-1/Pro*$_{MpUVR8}$:Mp*UVR8* lines.

(**E**) Immunoblot analysis of MpUVR8 and RFP-MpUVR8 levels in 14-day-old Tak-1, Mp*UVR8.1*^{OE}*#1*, Mp*UVR8.1*^{OE}*#2*, Mp*UVR8.2*^{OE}*#1*, Mp*UVR8.2*^{OE}*#2*, and Mp*uvr8-1* thallus. Ponceau staining is shown as loading control. Mp*UVR8.1*^{OE} = Tak-1/*Pro*$_{MpEF1\alpha}$:RFP-UVR8.1; Mp*UVR8.2*^{OE} = Tak-1/*Pro*$_{MpEF1\alpha}$:RFP-UVR8.2.

(**F**) RT-qPCR analysis of Mp*RUP* expression level in 14-day-old Tak-1 and two Mp*RUP*^{OE} lines. Individual data points of biological replicates and means ± SD are shown (n = 3). Different letters indicate statistically significant differences between the means ($P < 0.05$) as determined by one-way ANOVA followed by Tukey's post hoc honestly significant difference (HSD) test.

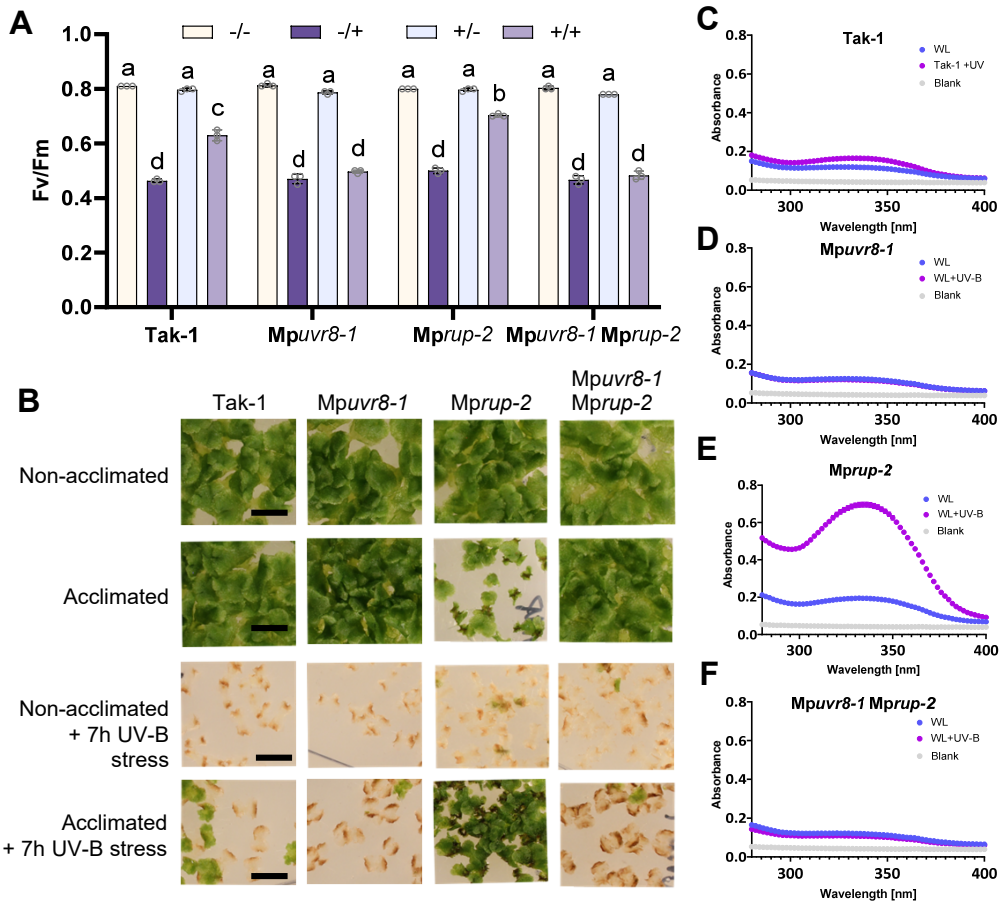

Supplementary Figure S5. Enhanced photoprotection and UV-B-absorbing capacity of Mp*rup* depends on MpUVR8.
(**A**) F_v/F_m measurements in wild-type (Tak-1), Mp*uvr8-1*, Mp*rup-2*, and Mp*uvr8-1* Mp*rup-2* grown for 7 days in white light (non-acclimated) or white light supplemented with UV-B (acclimated), without (non-stressed) or with (stressed) additional exposure to broadband UV-B stress for 60 min. -/-, non-acclimated, non-stressed; -/+, non-acclimated, stressed; +/-, acclimated, non-stressed; +/+, acclimated, stressed. Individual data points of biological replicates and means ± SD are shown (*n* = 3). Different letters indicate statistically significant differences between the means ($P < 0.01$) as determined by two-way ANOVA followed by Tukey's post hoc honestly significant difference (HSD) test.
(**B**) UV-B stress resistance in Tak-1, Mp*uvr8-1*, Mp*rup-2*, and Mp*uvr8-1* Mp*rup-2* plants grown for 7 days in white light supplemented (acclimated) or not (non-acclimated) with UV-B, then exposed or not to 7 hours of broadband UV-B. Pictures were taken after recovery for another 7 days in white light. Bars = 1 cm.
(**C-F**) Absorbance spectra (280–400 nm) of methanolic extracts from 9-day-old Tak-1 (A), Mp*uvr8-1* (B), Mp*rup-2* (C), and Mp*uvr8-1* Mp*rup-2* (D) gemmalings grown for 7 days in white light and exposed (WL+UV-B, purple lines) or not (WL, blue lines) to supplemental UV-B (1.5 µmol m^{-2} s^{-1}) for 2 days. The gray line shows the absorbance of the buffer (blank). Values of independent measurements and means ± SEM are shown (*n* = 3).

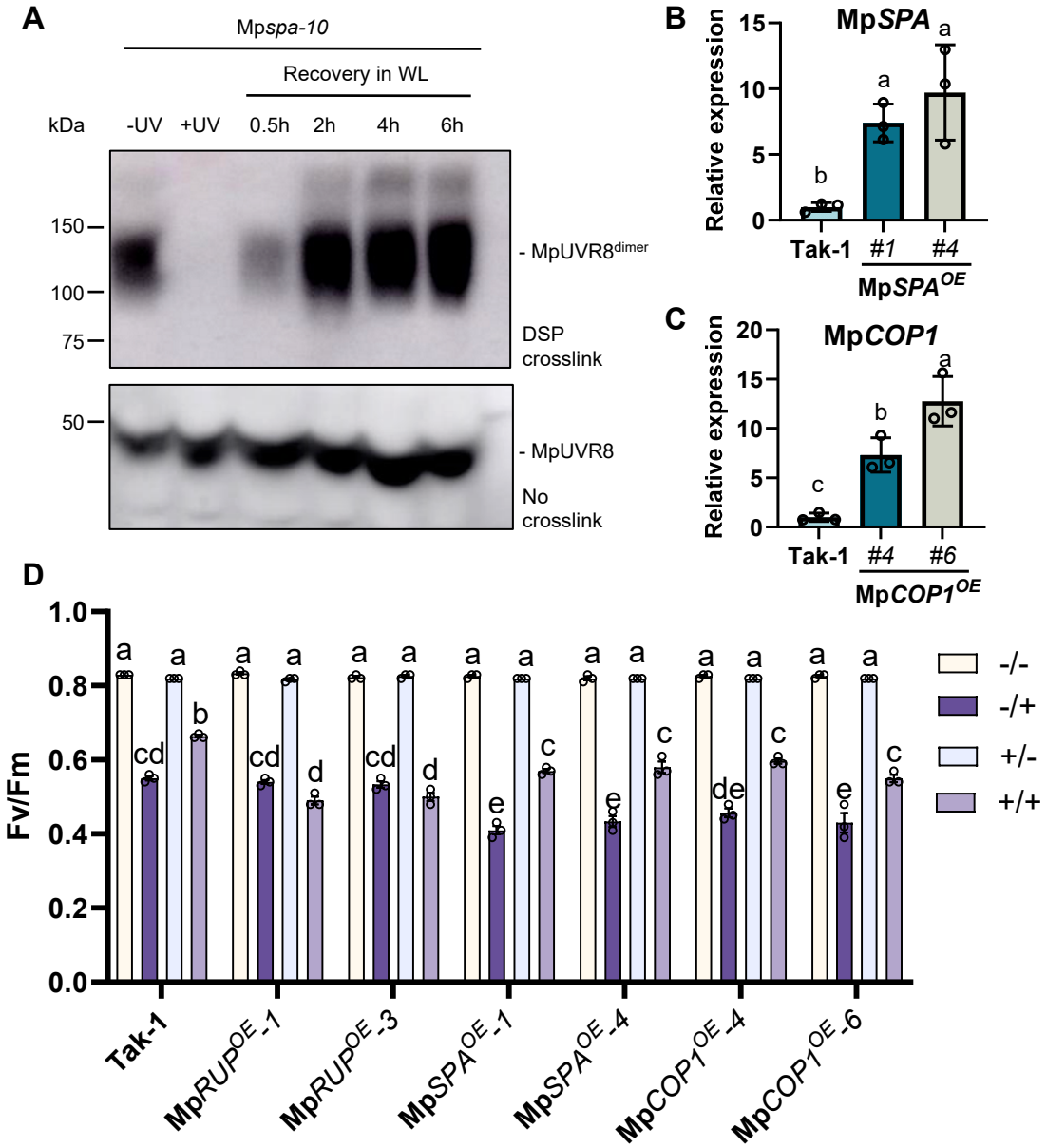

Supplementary Figure S6. MpSPA does not affect MpUVR8 redimerization, but MpCOP1 and MpSPA overexpression reduces basal UV-B tolerance.

(**A**) Immunoblot analysis of MpUVR8 levels in 7-day-old Mp*spa-10* gemmalings irradiated for 20 min with broadband UV-B before recovery in white light (WL) for the indicated times. Top: MpUVR8 dimer levels in DSP-crosslinked protein extracts. Bottom: total MpUVR8 levels in non-crosslinked extracts.

(**B**) RT-qPCR analysis of Mp*SPA* expression level in 14-day-old plants of Tak-1 and Mp*SPA*^{OE} lines *#1* and *#4*. Individual data points of biological replicates and means ± SD are shown (*n* = 3). Letters indicate statistically significant differences between the means (P < 0.05) as determined by one-way ANOVA followed by Tukey's post hoc honestly significant difference (HSD) test.

(**C**) RT-qPCR analysis of Mp*COP1* expression level in 14-day-old plants of Tak-1, Mp*COP1*^{OE} lines *#4* and *#6*. Individual data points of biological replicates and means ± SD are shown (*n* = 3). Letters indicate statistically significant differences between the means (P < 0.05) as determined by one-way ANOVA followed by Tukey's post hoc honestly significant difference (HSD) test.

(**D**) F_v/F_m measurements in wild-type (Tak-1), Mp*RUP*^{OE} lines *#1* and *#3*, Mp*SPA*^{OE} *#1* and *#4*, and Mp*COP1*^{OE} *#4* and *#6* grown for 7 days in white light (non-acclimated) or white light supplemented with UV-B (acclimated), without (not stressed) or with (stressed) additional exposure to broadband UV-B stress for 60 min. -/-, not acclimated, not stressed; -/+, not acclimated, stressed; +/-, acclimated, not stressed; +/+, acclimated, stressed. Individual data points of biological replicates and means ± SD are shown (*n* = 3). Letters indicate statistically significant differences between the means (P < 0.01) as determined by two-way ANOVA followed by Tukey's post hoc honestly significant difference (HSD) test.

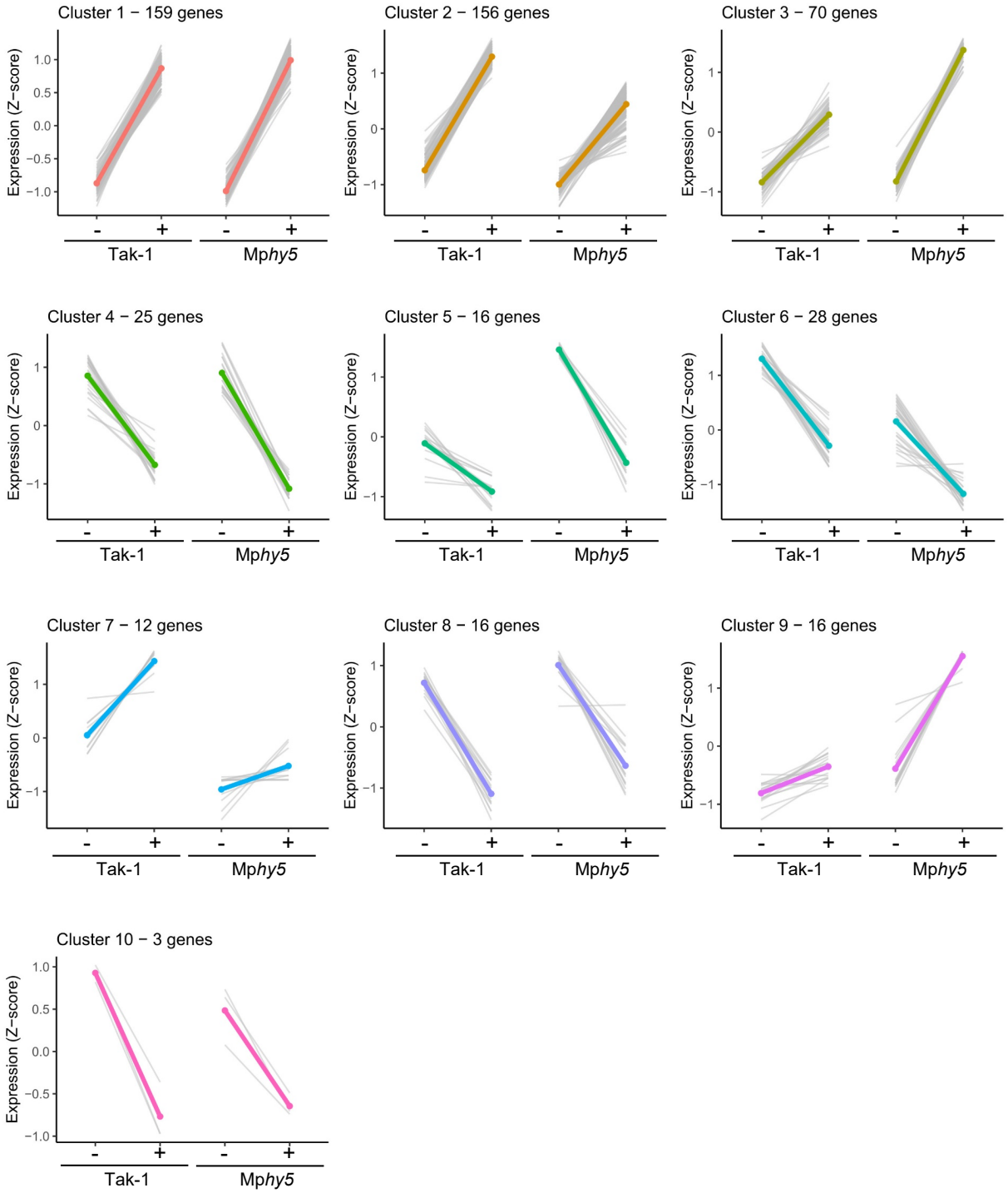

Supplementary Figure S7. MpHY5 plays a minor role in the regulation of UV-B-induced gene expression changes.
Gene expression profiles in clusters identified by hierarchical clustering. Z-scores for normalized read count values for each gene (gray lines) and for the cluster average (colored line) are shown.

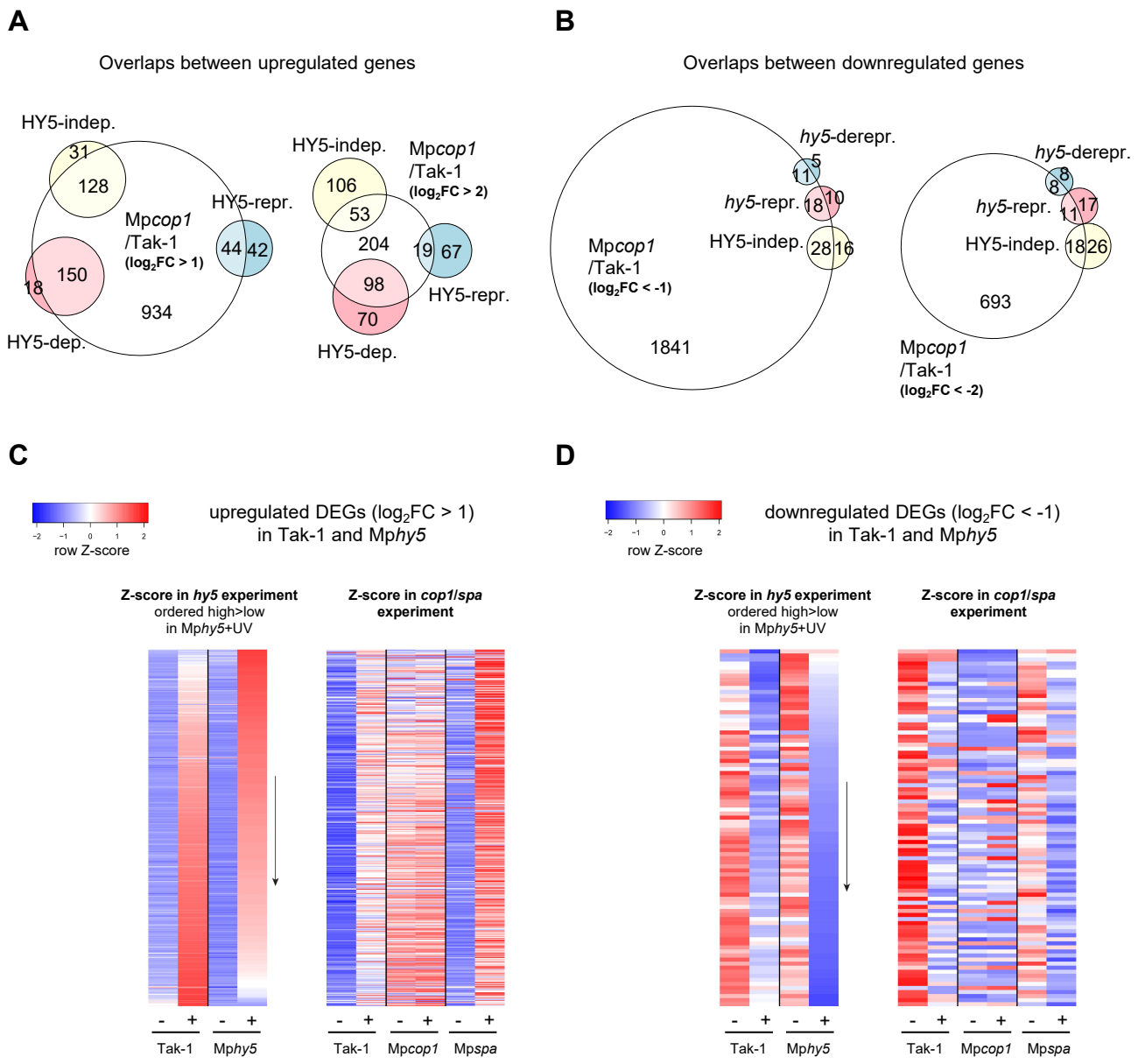

Supplementary Figure S8. MpHY5 and MpCOP1 regulate UV-B-induced gene expression in an antagonist manner.
(**A**) Euler plots showing overlaps between upregulated DEGs (p-adj < 0.05) in Mp*cop1*/Tak-1 in white light (left: $\log_2$FC > 1; right: $\log_2$FC > 2) and genes that are induced after 3h of UV-B. UV-B-upregulated genes are separated into 3 categories: genes that are induced in a MpHY5-independent manner ("HY5-indep.", Fig. S6 cluster 1), genes that are dependent on MpHY5 for their full induction or hypoinduced in Mp*hy5* ("HY5-dep.", Fig. S6 clusters 2 and 7) and genes that are hyperinduced in Mp*hy5* or whose induction is repressed by HY5 ("HY5-repr.", Fig. S6 clusters 3 and 9). Corresponding gene lists: Supplementary Table S6a.
(**B**) Euler plots showing overlaps between downregulated DEGs (p-adj < 0.05) in Mp*cop1*/Tak-1 in white light (left: $\log_2$FC < -1; right: $\log_2$FC < -2) and genes that are repressed after 3h of UV-B. UV-B-downregulated genes are separated into 3 categories: genes that are repressed in a MpHY5-independent manner ("HY5-indep.", Fig. S6 clusters 4, 8 and 10), genes that are somewhat constitutively repressed in Mp*hy5* ("*hy5*-repr.", Fig. S6 cluster 6) and genes that are derepressed in white light-grown Mp*hy5* ("*hy5*-derepr.", Fig. S6 cluster 5). Corresponding gene lists: Supplementary Table S6b.
(**C**) Heatmap of all genes upregulated ($\log_2$FC > 1 and p-adj < 0.05) by UV-B in Tak-1 and/or Mp*hy5*. Red and blue colors indicate normalized read count Z-scores in RNA-seq experiments including Tak-1 and Mp*hy5* (left) and Tak-1, Mp*cop1* and Mp*spa* (right). Z-scores were calculated separately for the two experiments and genes were ordered in a decreasing order according to the Z-score in Mp*hy5*+UV (arrow).
(**D**) Heatmap of all genes downregulated ($\log_2$FC < -1 and p-adj < 0.05) by UV-B in Tak-1 and/or Mp*hy5*. Red and blue colors indicate normalized read count Z-scores in RNA-seq experiments including Tak-1 and Mp*hy5* (left) and Tak-1, Mp*cop1* and Mp*spa* (right). Z-scores were calculated separately for the two experiments and genes were ordered in a decreasing order according to the Z-score in Mp*hy5*+UV (arrow).

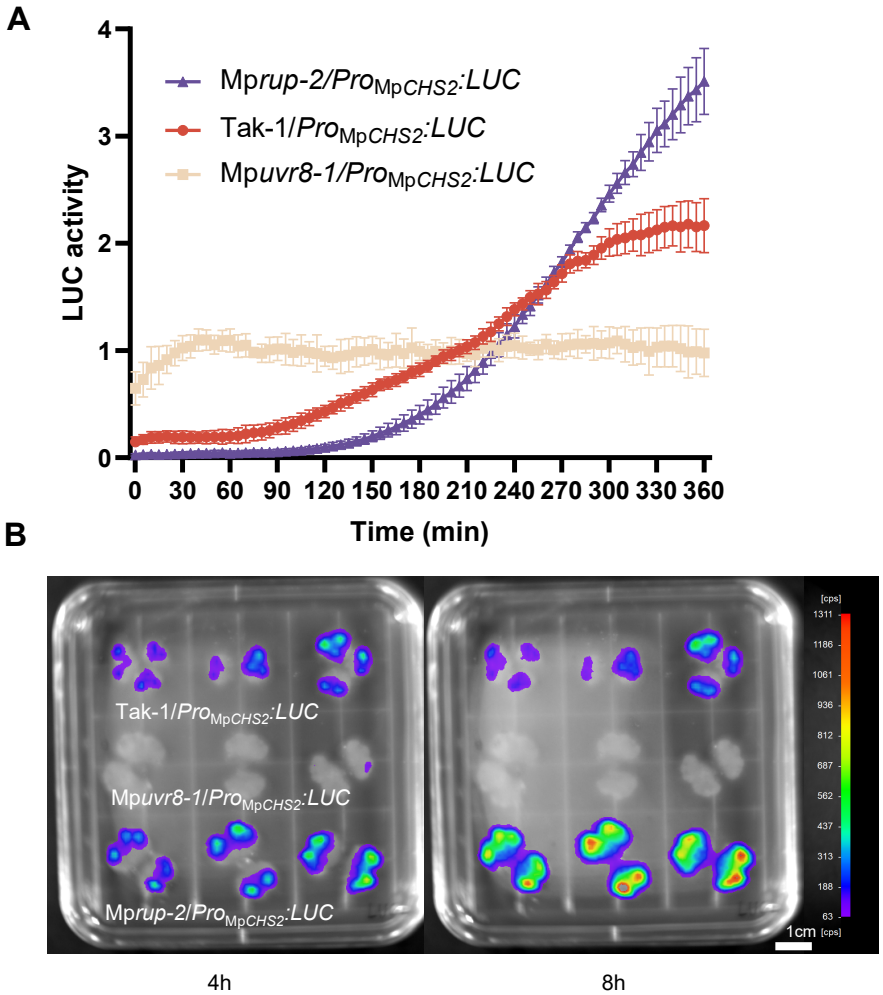

Supplementary Figure S9. LUC activity of a *Pro*$_{\mathbf{MpCHS2}}$*:LUC* reporter in Tak-1, Mp*uvr8-1*, and Mp*rup-2* backgrounds upon UV-B exposure.

(**A**) The counts per second (cps) of luciferase (LUC) activity were normalized to average expression level measured in 3-day-old gemmalings of the following lines: Tak-1/*Pro*$_{MpCHS2}$*:LUC*, Mp*uvr8-1*/*Pro*$_{MpCHS2}$*:LUC*, and Mp*rup-2*/*Pro*$_{MpCHS2}$*:LUC*. These gemmalings were grown in 96-well plates under white light, and pre-sprayed with luciferin 24 h before a 20-min exposure to broadband UV-B. The LUC activity was monitored for up to 360 min after the UV-B induction. Values of independent measurements and means ± SD are shown (n = 8).

(**B**) Analysis of LUC activity in 14-day-old thalli of Tak-1/*Pro*$_{MpCHS2}$*:LUC*, Mp*uvr8-1*/*Pro*$_{MpCHS2}$*:LUC*, and Mp*rup-2*/*Pro*$_{MpCHS2}$*:LUC* lines followed by 20 min of broadband UV-B exposure at 4 h (left) and 8 h (right).

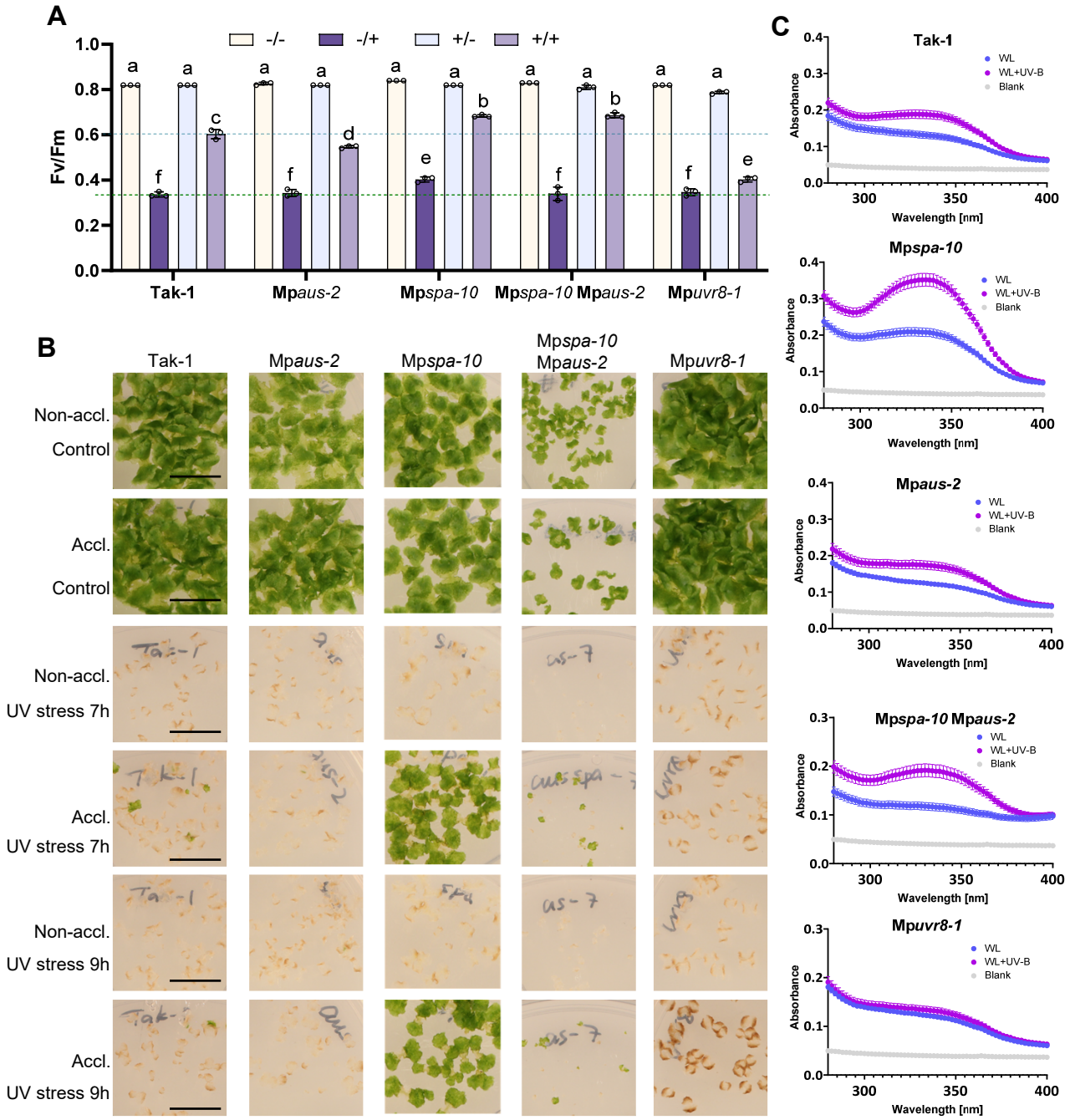

Supplementary Figure S10. MpAUS contributes to protection against UV-B stress.

(**A**) F_v/F_m measurements in wild-type (Tak-1), Mp*aus-2,* Mp*spa-10*, Mp*spa-10* Mp*aus-2*, and Mp*uvr8-1* gemmalings grown for 7 days in white light (non-acclimated) or white light supplemented with UV-B (acclimated), without (not stressed) or with (stressed) additional exposure to broadband UV-B stress for 60 min. -/-, not acclimated, not stressed; -/+, not acclimated, stressed; +/-, acclimated, not stressed; +/+, acclimated, stressed. Individual data points of biological replicates and means ± SD are shown (n = 3). Dashed horizontal lines indicate levels corresponding to Tak-1 not acclimated stressed (green) and acclimated stressed (blue) plants. Letters indicate statistically significant differences between the means ($P < 0.01$) as determined by two-way ANOVA followed by Tukey's post hoc honestly significant difference (HSD) test.

(**B**) UV-B stress survival of Tak-1, Mp*aus-2,* Mp*spa-10*, Mp*spa-10* Mp*aus-2*, and Mp*uvr8-1* plants grown for 7 days in white light supplemented (acclimated) or not (non-acclimated) with UV-B, then exposed to 7 h or 9 h of broadband UV-B or not. Pictures were taken after recovery for another 7 days in white light. Bars = 1 cm.

(**C**) Absorbance spectra (280–400 nm) of methanolic extracts from 9-day-old Tak-1, Mp*spa-10*, Mp*aus-2,* Mp*spa-10* Mp*aus-2*, and Mp*uvr8-1* gemmalings grown for 7 days in white light and exposed (WL+UV-B, purple lines) or not (WL, blue lines) to supplemental UV-B for 2 days. The gray lines show absorbance of the buffer (blank). Values of independent measurements and means ± SEM are shown (n = 3).

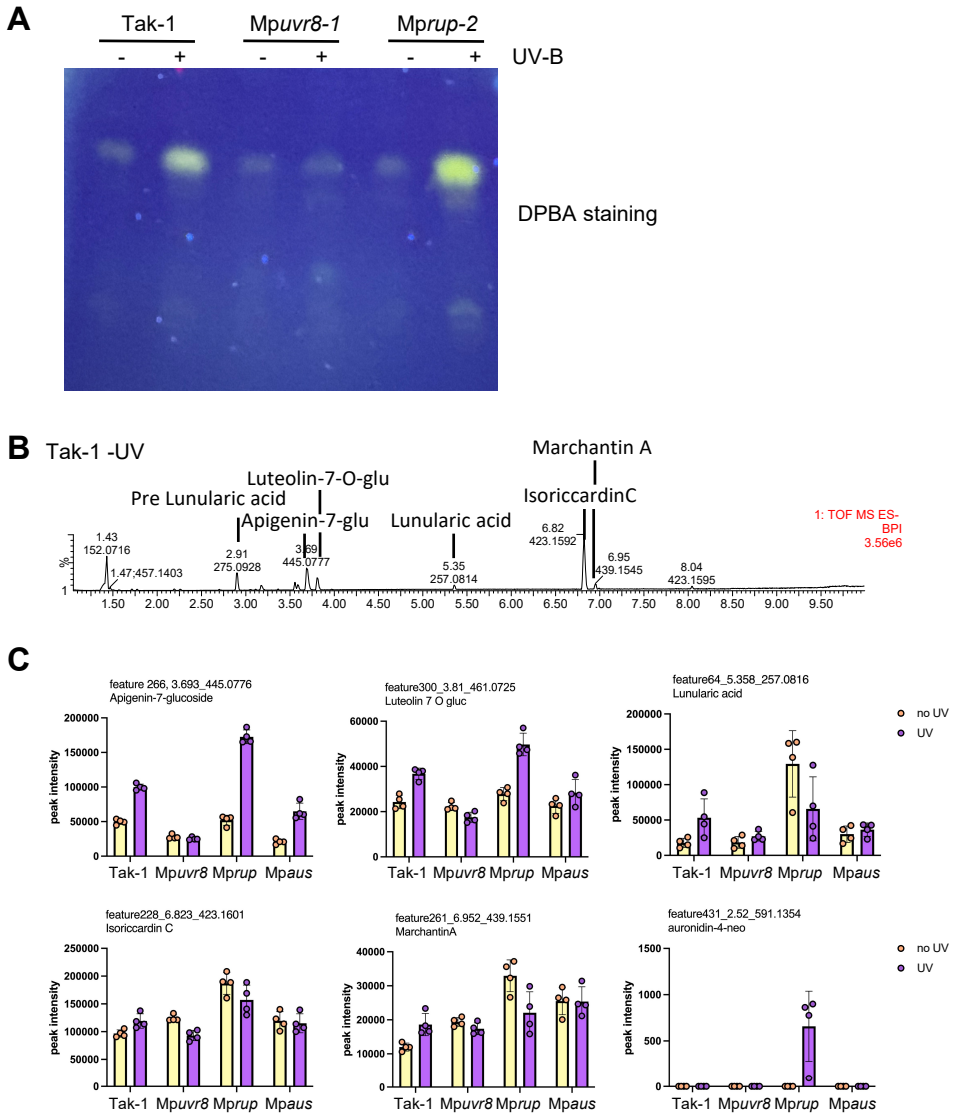

Supplementary Figure S11. MpUVR8- and MpAUS-dependent regulation of metabolite accumulation upon UV-B exposure.
(**A**) High-performance thin-layer chromatography (HPTLC) analysis of flavonol glycoside levels in 7-d-old gemmalings of wild type (Tak-1), Mp*uvr8-1*, and Mp*rup-2* grown for 7 days in white light and exposed, or not, to supplemental UV-B for 2 days. DPBA, diphenylboric acid 2-aminoethylester.
(**B-C)** Metabolomic analysis of 9-day-old plants of Tak-1, Mp*uvr8-1*, Mp*rup-2*, and Mp*aus-2* grown for 7 days in white light and exposed (+) or not (-) to supplemental UV-B (1.5 µmol m^{-2} s^{-1}) for 2 days (*n* = 5, 12 plants per replicate). (B) UHPLC-MS chromatogram from -UV-B Tak-1 sample. Metabolites corresponding to major peaks are annotated based on their accurate mass and MS2 spectra. (C) Relative quantifications of compounds in Tak-1, Mp*uvr8-1* (*uvr8*), Mp*rup-2* (*rup*), and Mp*aus-2* (*aus*) methanolic extracts from plants exposed to UV-B (purple, right bar, UV) or not (yellow, left bar, no UV). Individual data points of biological replicates and means ± SD are shown (*n* = 4).